



NTNU – Trondheim
Norwegian University of
Science and Technology

MODELLING WIND FARM WITH FREQUENCY RESPONSE FOR POWER SYSTEM DYNAMIC STUDIES

Hasala Indika
Dharmawardena

Master of Science in Electric Power Engineering

Submission date: July 2015

Supervisor: Kjetil Uhlen, ELKRAFT

Norwegian University of Science and Technology
Department of Electric Power Engineering



NTNU – Trondheim
Norwegian University of
Science and Technology

MODELLING WIND FARM WITH FREQUENCY RESPONSE FOR POWER SYSTEM DYNAMIC STUDIES

Hasala Dharmawardena

July 2015

MSc Dissertation

Department of Electric Power Engineering

Norwegian University of Science and Technology

Supervisor 1: Professor Kjetil Uhlen, Norwegian University of Science and Technology

Supervisor 2: Dr. Sverre Gjerde, Statkraft AS

Supervisor 3: Professor Olimpo Anaya-Lara, University of Strathclyde

Problem Description

The increasing electricity demand coupled with decreasing fossil fuel reserves has created a paradigm shift in the electricity generation mix moving it away from fossil fuels towards wind and solar sources. Wind energy is forecasted to be a major energy source of the future power system due to its cost competitiveness. Integration of this emerging technology to the future smart grid is a challenge for the power system operators since the features of this emerging technology is markedly different from the classical generator technology which has remained relatively unchanged for more than a century.

In the future smart grid, the system is expected to operate in islanded mode and still provide a reasonable power quality. This requirement coupled with the expected rise of wind energy creates the need to investigate the dynamic response of a wind farm with high wind penetration ratio operating in a small power system. Further this scenario motivates investigating the possibility of enhancing system frequency control and small signal stability.

With this intention the first part of this work is to find the different modelling possibilities for a suitable wind turbine technology for power system dynamic studies. An ideal model should have minimum modelling complexity yet provide accurate representation of a real system. The second part of this work is to find the possibility for increasing the frequency quality of the system. The response of the wind turbine generator models with frequency support is to be compared and a more suitable model for wind farm representation is to be identified.

The future grid requires to be highly reliable and robust. Therefore it is important to understand the effect on system stability with high wind penetration in a small power system. The last part of this work is to investigate the effect of wind energy integration on system stability.

Assignment given: Trondheim, 2015-01-22

Supervisor: Professor Kjetil Uhlen

Abstract

This dissertation presents an analytical study on *modelling wind farm with frequency response for power system dynamic studies*. Recent trends indicate that wind energy penetration in the power system will keep on increasing. This study models a permanent magnet synchronous generator fully rated converter based wind farm, since this is one of the state of art technologies that services this growing demand. Due to the variability in the wind resource, a high demand will be placed on the frequency stability of the power system. This necessitates the requirement of providing both inertial and governor support by the wind farm to the power system. High wind penetration will have a significant impact on the power system stability. These impacts needs to be investigated by conducting power system dynamic studies.

The main challenge is in identifying an appropriate level of complexity of the models to represent power system electro-mechanical dynamics, while keeping the models as simple as possible, to reduce the computational requirements. Taking this into consideration, the main contribution of the modelling work, is identifying a full order model and a reduced order model of a wind farm with frequency response. The dissertation presents the dynamic models of the main components of a wind turbine and shows how the component models are combined to generate a full order and reduced order model.

The wind farm is interfaced to the utility grid by a back to back voltage source converter. Therefore selection of robust control structures and identification of control parameters constitutes an important study element. Both, generator converter controller and grid converter controller is given special attention. Auxiliary control loop for implementing frequency response is identified and integrated to the models.

The power system under study is the Kundur's two area network. One synchronous generator is substituted by the wind farm and contributes to 25% of the system capacity. The dynamic system study investigates aspects of both frequency and small signal response.

The full order and reduced order model dynamic response, for a variable wind speed sequence, shows a high degree of correspondence, both with and without frequency control. Therefore the results of this work indicate that a reduced order model is sufficient to model power system electro-mechanical dynamics without significant loss in accuracy.

The full order and reduced order model small signal response, for constant wind speed and without frequency control shows a high degree of correspondence. However the full order and reduced order model response shows deviation, when the wind farm is supported with frequency control. Therefore the full order model provides a more accurate small signal response for wind farms with frequency control. The studied network reveals a poorly damped inter area mode. Substitution of a synchronous generator by the wind farm, increases the damping of this mode, decreasing inter area oscillations and enhancing system small signal stability.

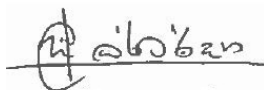
The simulations of an over frequency event, in a system with a wind farm supporting frequency control, clearly shows superior frequency response, in comparison to a wind farm without frequency control. The salient performance is reflected in rate of change of frequency, temporary maximum frequency, steady state frequency and settling time of the frequency response.

Preface

In partial fulfillment of the Master of Science degree in electrical power engineering in Norwegian University of Science and Technology (NTNU), this master thesis has been carried out in the spring of 2015. The subject of wind power in power systems, is a multi disciplinary area of study, requiring a high level of competence, in the full spectrum of electrical engineering disciplines, spanning from electrical machines, power system analysis, aerodynamics to control theory. This has been a remarkable period of intensive studies and challenged my problem solving skills like never before.

The specialization project topic was provided by Statkraft AS and supported by a generous summer job opportunity. I express my sincere gratitude to Leon Notkevich, Anders Borgli, Karstein Brekke and Geir Asker of the Wind Offshore Technology Electrical - Statkraft AS, for the unstinting support and advise freely shared. The ideas and feedback provided by Professor Olimpo Anaya-Lara is greatly appreciated. When the work slowed down to a crawl due to problems with simulation program, Professor Trond Toftevaag was kind enough to give me advanced user manuals of the software. My deepest gratitude goes to him. Many thanks goes to Dr. Sverre Gjerde of Statkraft for providing many practical tips, advises and judicious feedback. Thanks goes to Phd student Traian Preda, who I have bumped on for quick fixes regarding the simulation tool.

Much appreciation goes to my supervisor Professor Kjetil Uhlen for providing this opportunity, supporting me throughout a period of one year and helping me in many numerous ways. This work would not have been possible if not for the support provided by my father financing the two years of master studies in Norway. The unlimited love and support given to me by my parents and sister was my source of strength. In conclusion, it has been a journey of delight and enlightenment, where I discovered taht it's the journey that matters more than the destination. With the intention of looking forward to the next life challenge, I wish you happy reading!



Hasala Dharmawardena

Trondheim, 2015.07.06

Contents

Problem Description	i
Abstract	ii
Preface	iv
1 Introduction	1
1.1 Background and Motivation	1
1.2 System Overview	3
1.3 Scope of Work	3
1.4 Limitations	4
1.5 Sequence of work	5
1.6 Literature Review	5
1.7 Outline of the Thesis	6
2 Theoretical Background and State of the Art	8
2.1 Power system stability classification	8
2.2 Frequency stability	10
2.2.1 Stage I	11
2.2.2 Stage II	11
2.2.3 Stage III	12
2.3 Small Signal stability	13
2.3.1 System model	13
2.4 State of the Art	15
2.4.1 Speed Control	15
2.4.2 Generator Technology	15

2.4.3	Grid Interface	16
2.4.4	Wind Turbine Generator Technologies	16
2.4.5	Wind Turbine Power Electronic topology	17
2.4.6	DC/DC Boost interfaced PMSG wind turbine	17
2.4.7	Back to Back VSC interfaced wind farm	18
2.4.8	Wind Plant control structure	19
3	Power system modelling	20
3.1	Synchronous Generator	20
3.2	Power frequency Converter	22
3.2.1	Introduction	23
3.2.2	Mathematical model	23
3.3	Power Transformers	25
3.4	Transmission lines	25
3.5	Power System Loads	26
3.6	Hydro Governor	26
3.7	Automatic Voltage regulator	27
3.7.1	Reference frame conversion	27
4	Wind Turbine Modelling	29
4.1	Introduction	29
4.1.1	Generic Structure	30
4.1.2	Full Order Model	31
4.1.3	Reduced Order Model	32
4.2	Wind Turbine Mechanical System	32
4.2.1	Wind Aerodynamics	32
4.2.2	Maximum point tracking scheme	35
4.2.3	Pitch Controller	36
4.2.4	Wind turbine drive train	37
4.3	Wind Turbine Energy Conversion System	38
4.3.1	Converter reference frame	38

4.3.2	Full Order Model Electrical System	40
4.3.3	Reduced Order Model Electrical System	60
4.4	Wind Turbine Frequency Control	61
5	Simulation Study	63
5.1	Power System under study	63
5.2	Power System Simulations	64
5.3	Model Validation	65
5.3.1	Full Order Model	65
5.3.2	Reduced Model	67
5.3.3	Comparison of Model Dynamic Response	68
5.3.4	Comparison of Small Signal Response (without frequency control)	71
5.4	Case Study : Governor action and inertia emulation	72
5.4.1	Introduction	72
5.4.2	Over frequency event	77
5.4.3	Under frequency event	79
5.5	Small signal stability with frequency control	81
5.5.1	Effect of synthetic inertia constant on the poorly damped mode	81
5.5.2	Comparison of small signal response for reduced model	81
5.5.3	Comparison of small signal response for full model	81
5.5.4	Modelling of small signal response	83
5.6	Discussion	83
6	Summary	85
6.1	Summary and Conclusions	85
6.1.1	System Modelling	85
6.1.2	Controller Design	86
6.1.3	Simulation Results	86
6.2	Recommendations for Further Work	87
6.2.1	Modelling	87
6.2.2	Controllers	88

<i>CONTENTS</i>	viii
6.2.3 Frequency Response	88
Nomenclature	89
Bibliography	91
List of Figures	100
List of Tables	100
A Power System Model - Parameters	107
A.1 Synchronous generators	107
A.2 Transformer	107
A.3 Transmission line	107
A.4 Capacitor	108
A.5 Turbine Governor	108
A.6 Automatic voltage regulator	108
B WTG parameters	110
B.1 Generator Model	110
B.2 Wind turbine Model	111
B.3 Pitch Model	111
B.4 Per Unit System	112

Chapter 1

Introduction

1.1 Background and Motivation

Providing an affordable and reliable electricity supply has become a key need for the modern society. The world electricity demand is increasing year by year but the conventional energy sources are not increasing (hydro power) or are declining (fossil fuels). The conversion from the current energy mix to an energy mix dominated by renewable energy is inevitable. At present this conversion is supported by government policy such as the 20% target for renewable sources in the energy mix by 2020 set by the European Union in 2008 [1].

Wind energy is the fastest growing energy source in Europe[2]. Offshore wind is expected to have the largest growth gradient in the coming decades [3]. In 2012 the total offshore wind installations amounted to 3.5 GW and is expected to reach 60-80 GW by 2030 [4]. Due to these reasons offshore wind technology is gaining increasing attention from both industrial and academic circles.

With increasing penetration in the energy mix, it is inevitable that the wind power technology be cost competitive and financially feasible. It is not feasible to provide a mass scale solution of wind power when it requires subsidies for financial sustainability. Typical wind turbines do not have the operational flexibility of classical synchronous generators. This is a further deterrent to integration of more wind power. Much research has been conducted to find methods to use a wind turbine as virtual synchronous generator [5].

Wind is a variable energy source and integrating wind power in large amount to the system

needs careful planning. The power system operators need to understand how integrating wind power affects the power system. Thus the need to have accurate models for wind farms. The characteristic response of a wind farm is markedly different from the conventional generators.

The modern power system is slowly but surely being converted from the passive classical system to an active system popularly known as the smart grid. The smart grid concept calls for the possibility of system being able to operate in islanded mode disconnected from the main grid. If a system operating with a high wind penetration is forced to operate in islanded mode, it should still be able to operate and provide electric power with sufficient power quality and robustness. Maintaining stable operation under these conditions has become more challenging than ever.

Power system stability was considered a key problem for system operation starting from 1920's [6]. This thesis focuses on frequency control and small signal stability of a power system with high amount of wind penetration. It is challenging to control frequency in a small power system with high wind penetration due to variability in wind speed [7]. It is important to model wind farms with appropriate models and conduct relevant simulation studies to understand the dynamic interaction between the power system and the wind farms.

At present, frequency control is offered by all major wind turbine manufacturers [8][9]. Further, some transmission system operators have made frequency control a mandatory grid code requirement [10]. This strongly suggest that frequency control will be a mandatory ancillary service required from wind turbines in the near future. The requirement for providing frequency control becomes critical when the wind penetration is high. Therefore it is natural to include this feature in the wind turbine. It is important to understand the power system dynamics in a power system, with wind farms offering frequency control. This is a main motivation for this study.

The main contribution of the modelling work is, identifying a full order model and a reduced order model of a wind farm with frequency response. The dissertation presents the dynamic models of the main components of a wind turbine and shows how the component models are combined to generate a full order and a reduced order model.

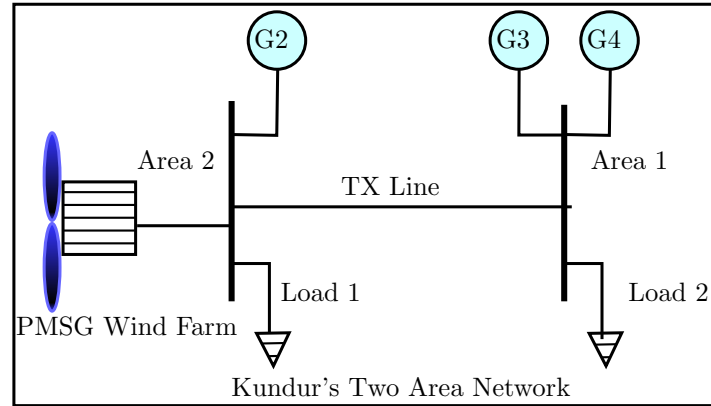


Figure 1.1: Power system under study - Kundur's two area network [11]

1.2 System Overview

The Kundur's two area network as presented in figure 1.1 is the system under study. The system consists of four synchronous generators of equal capacity and type, with two generators connected to each area. The system was originally used to represent the existence of electro mechanical modes in a power system [12]. The system total capacity is 3 GW. The wind farm consists of 240 numbers of 1.5 MW wind turbines. An aggregate model is used to represent the wind farm. High wind power penetration creates noticeable frequency variations in the system. This system is used since it will illustrate the extreme effects, and have observable phenomenon which are analysed in this study.

1.3 Scope of Work

The scope of work for the thesis is as follows;

- Modelling of permanent magnet synchronous generator (PMSG) based fully rated converter (FRC) wind turbine generator with different level of complexity (reduced order model and full order model)
- Modelling of power system network and classical synchronous generators
- Simulation for model validation in normal operation with variable wind speed and comparison of model response

- The implementation of frequency control in the wind turbine model
- Simulation for both over frequency and under frequency events, for different models, and comparison of response
- Modal analysis of the different models and comparison of response for small perturbations
- Analysis of effect on frequency quality by implementing frequency support

1.4 Limitations

The limitations of this work is as follows;

- The modelling is only valid for stability studies involving slow power system dynamics in the range of 0.2 Hz to 10 Hz
- The focus of this work is power system frequency. Voltage stability is not considered.
- The model uses, only one of the many possible control strategies for wind turbine control. The results are only valid for this particular control scheme and should not be generalized without analysis.
- The system under study is a hypothetical system and the results are derived with an academic inclination. It is not intended for the parameters (eg: frequency) to be compared with a grid code. The system controllers are chosen with inclination to project a worse case scenario for frequency control.
- The wind turbine governor action is only valid for over frequency events. In all other conditions the output power follows the maximum point tracking scheme. This is the only economic limitation that has been considered. Economics for wind power plant is not included nor considered in this study.

1.5 Sequence of work

The sequence of work is as follows;

1. Conduct literature survey covering state of art for PMSG modelling and controls, frequency control and related research
2. Choose control strategy and topology for full model
3. Choose possible approximations to the full model and generate reduced model
4. Choose strategy to implement primary response
5. Model system in the power system simulation tool
6. Validate models with variable wind speed sequence and compare response for different models
7. Model primary response and integrate it into wind turbine models
8. Simulate system with and without inertial model and illustrate the effect on system frequency
9. Simulate system with frequency control and compare system response for over frequency and under frequency events
10. Conduct modal analysis, compare results for different models
11. Propose suitable model for stability studies from the different models considered in the study

1.6 Literature Review

The work done in this simulation study builds up and uses the research done in the related work summarized in this section.

The benefits of using a PMSG for variable speed wind turbines is presented and experimentally validated in [13]. A structure for modelling any generic converter interfaced wind turbine

system is presented in [14]. Specific implementations of PMSG based FRC WTGs are presented in [15, 16, 17, 18, 19, 20, 21]. Reference [22] includes both WTG modelling as well as a method for aggregating and representing wind farms. Reference [23] presents models for all the main types of WTG technologies while [24] also includes a comparison between simulated response and real response. Reference [25] presents a method for model reduction and aggregation of wind farms for dynamic studies.

A wealth of options and control strategies for PMSG FRC WTGs are presented in [26, 27, 28, 29, 30]. Highly efficient vector control strategy for PMSG FRC WTGS is presented in [31]. A vector control strategy applied to PMSG based FRC WTG's with the simulations experimentally validated, is presented in [32]. Reference [33] covers many of the key topologies and control strategies and provides a comparison of the generator controller response. Modelling and controls for PMSG WTG systems with the generator side PWM rectifier is analysed in detail in [34, 35, 36, 37, 38, 39].

A complete study of frequency response by wind farms in small power systems, with high wind power penetration, is presented in [40]. This study analyses both inertial as well as governor response in detail. However the wind farm model used is a highly reduced model which represent any VSWT technology. The possibility of emulating and supporting primary frequency response by wind turbines is illustrated in [41]. The effects of emulated inertia on frequency disturbance with different values for inertia emulation constant is compared and presented in [42]. A method to implement not just primary frequency control but also secondary frequency control is presented in [43]. Design considerations for selecting a inertia emulation scheme is described in [44]. Reference [44] also proposes a novel inertia emulation scheme.

A recent survey of grid codes required for wind power integration is presented in [10, 45, 46]. A review of the power converter topology used with PMSG based WTGs is presented in [47]. A complete small signal stability analysis for a PMSG FRC is presented in [48].

1.7 Outline of the Thesis

Chapter 1 gives an overall introduction to the thesis. The research motivation, scope of work and methodology is presented in this chapter.

Chapter 2 consists of two parts. The first part presents an introduction to the power system theory required for reading the thesis. The second part presents the state of art for the wind turbine technology that is used in this work and gives the basis for selection the wind turbine that has been modelled in this work.

Chapter 3 presents in detail, the models and approach used for power system modelling. This includes all power system components except components of the wind turbine generator system.

Chapter 4 presents detail modelling wind turbines including mechanical, electrical components as well as the control system. The problem of selection as well tuning of the controllers are addressed in this chapter.

Chapter 5 presents the simulations study. It includes the validation of the models, case study presenting the benefit of applying primary frequency control in a over frequency event, comparison of model response for both over frequency and under frequency events as well as a modal analysis to to model response to a small signal disturbance. This chapter includes the discussion of the results.

Chapter 6 summarises the work done, provides suggestions for further work and presents outcomes of the thesis.

Chapter 2

Theoretical Background and State of the Art

The first section of this chapter presents an introduction to the topic of power system stability. The second section provides an introduction to the state of art for wind turbines. The third section introduces some basic theory required to understand some of the analysis conducted in latter chapters.

2.1 Power system stability classification

According to [49], *"power system stability is the ability of an electric power system, for a given initial operating condition, to regain a state of operating equilibrium after being subjected to a physical disturbance, with most system variables bounded so that practically the entire system remains intact"*. The instability can occur in different ways. A single machine can become instable and lose synchronism while the rest of the system is stable. A cluster of generators in a single area can lose stability without cascaded failure of the whole power system. Similar to the generators, loads can become unstable where the instability occurs without cascaded system failure. On the other hand the instability starting at one point can cascade and cause the complete power system to fail. The physical disturbance that effects stability can be large or small. Ideally, the power system should be robust enough, to be stable after being subjected to disturbances, that have a high probability of occurrence. Instability of the power system, can be viewed as one or more system variables having unbounded response after a disturbance. Power system variables are interlinked and therefore system stability is one single interconnected problem. In order to

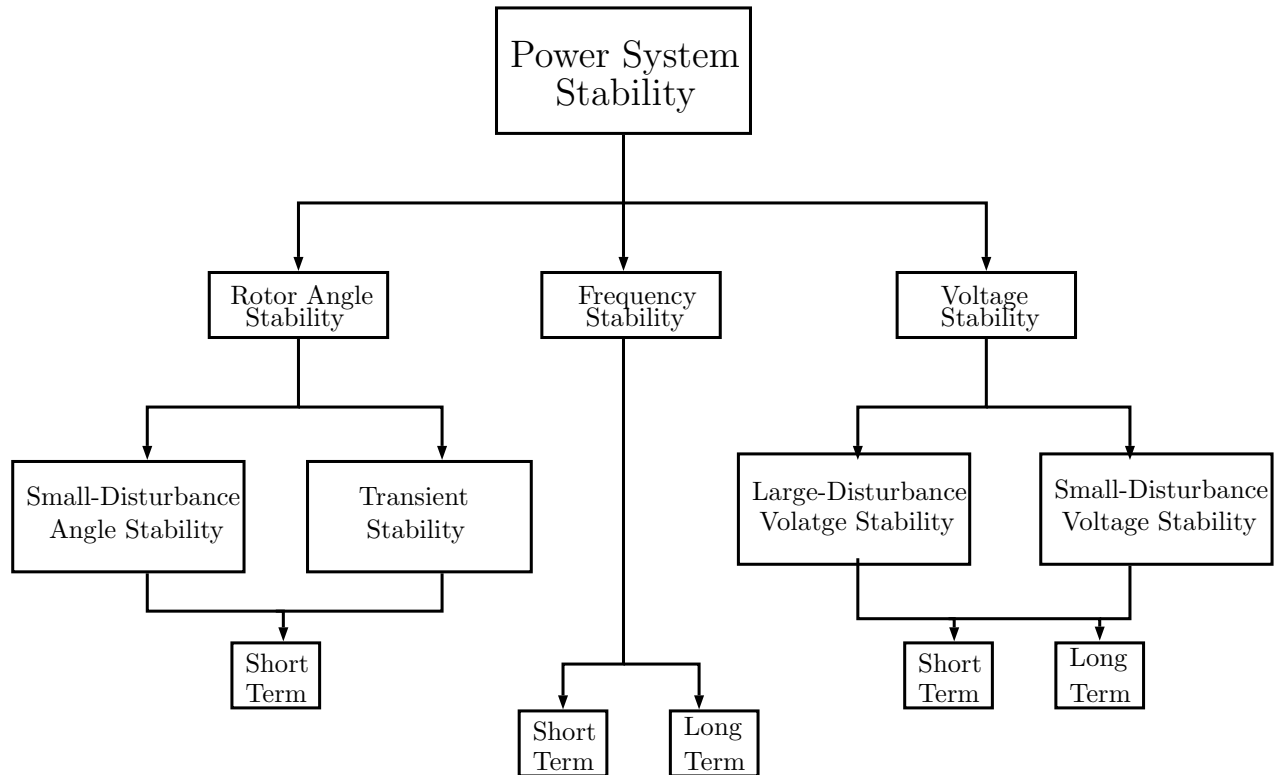


Figure 2.1: Power system stability classification [49]

simplify the analysis of power system stability a classification is presented in [49] based on factors that leads to instability and supported by partial stability concept presented in [50]. In this work classification as presented in [49] is used. Power system stability is categorized on three main criteria,

- The system variable in which the instability is observed - e.g. rotor angle, voltage
- The size of the disturbance that is considered in the stability studies. e.g. Large disturbance such as disconnection of generator or small disturbance which occur continuously such as small load variations
- The time interval required to assess stability. e.g. short term, long term

The complete stability classification from [49] is given in figure 2.1. Rotor angle stability refers to the ability of the generators to maintain synchronism after being subject to a disturbance. After a disturbance the generator electromagnetic torque and the mechanical torque will be unbalanced. This in turn will lead to the generator rotor to oscillate. If the rotor angle

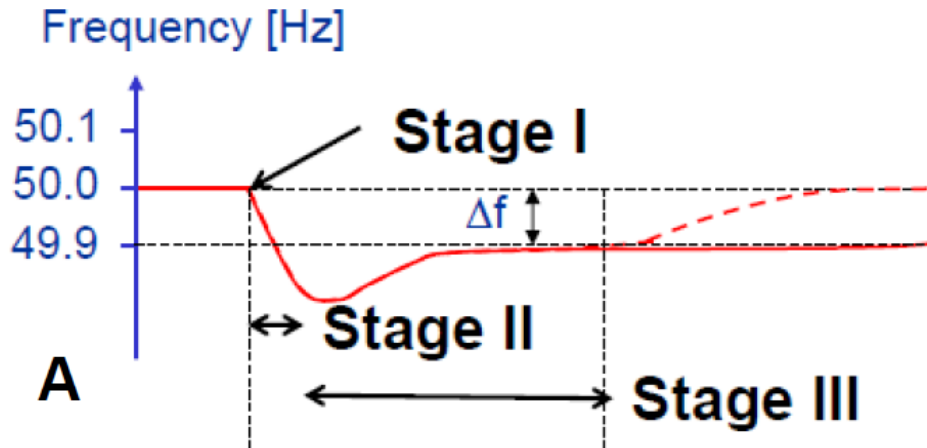


Figure 2.2: Typical frequency response for under frequency event [51]; Frequency (Hz) vs time response for an under frequency event

oscillations are increasing in magnitude it will lead to the machine going out of synchronism and getting disconnected from the system. Frequency stability refers to the ability of the power system to maintain a bounded system frequency when subject to severe disturbances. Instability occurs when frequency swings are sustained causing tripping of generators or loads. This is mainly associated with inadequate generation equipment response, insufficient spinning reserves or weak coordination between the control and protection equipment. The time frame for analysis starts from a few seconds to several minutes. In this study the governors of the synchronous generator and the power controller of the wind turbines are the main factors that determine frequency stability. Voltage stability refers to the ability to maintain a steady voltage in the system nodes after a system disturbance.

The work in this thesis is focused on small signal stability and frequency stability. Voltage stability is not discussed.

2.2 Frequency stability

The frequency response of the power system, due to an under frequency event, caused either by connection of a large loads or the disconnection of generators is given in figure 2.2. As per [27] frequency response can be classified into four main stages depending on the time duration of the associated dynamics. Three of these stages are of interest to this thesis.

2.2.1 Stage I

For the first few seconds after the under frequency event, rotor swings will occur in larger degree with local generators and in lesser degree in other generators of the system. The initial contribution of electrical power is dominated by the local generator. In stage I, contribution to meet load demand is dependent on the electrical distance from the generator to the event node [27]. The speed of the machines will be different in this stage, meaning that the instantaneous frequency at each generator bus will be different.

2.2.2 Stage II

Stage I ends in few seconds when the power deficit starts to slow down all the machines, and the speed of the machines become equal. Starting from the first few seconds to several seconds, stage II will be dominant. All the machines will slow down at approximately the same rate. The system frequency will decrease, with its rate of change of frequency (ROCOF) being determined by the system inertia. The power imbalance is met by converting the stored kinetic energy to electrical energy. In this thesis, this response is presented as inertial response or fast primary response. The drop in system frequency is determined by equation 2.1 [42]. Where H is the inertia time constant in seconds, $p_{m,i}$ is the turbine mechanical power in pu, $p_{e,i}$ is the generator electrical power in pu and f_i is the frequency in Hz. $\frac{df_i}{dt}$ is defined as the Rate Of Change Of Frequency. Power system inertia determines the system response in stage II.

$$2H_i \frac{df_i}{dt} = p_{m,i} - p_{e,i} \quad (2.1)$$

Unlike classical synchronous generators whose frequency is tied to the grid, the new renewable technologies with fully rated converter interface do not contribute to system inertia. Increasing wind penetration has created a requirement for these resources to contribute to system inertia in an artificial manner. The artificially introduced inertia is called synthetic or emulated inertia [42]. Emulating inertia from wind farms is an important feature for the future power system, if they are to support a high wind penetration. The method to emulate inertia is by adding a supplementary control loop to inject power to the grid depending on the value of $\frac{df_i}{dt}$. The supplementary control loop will slow the machine and transfer the stored kinetic energy to the

grid.

Grid code requirements for inertial support

According to European Network of Transmission System Operators for Electricity (ENTSO-E) [52], the requirement of synthetic inertia is handed down to regional TSOs. For example the spanish TSO recommends 5% of the capacity of the plant to be available as contribution for inertia [10].

Industry offerings

Currently many of the top wind turbine manufacturers offer a commercial solution for both inertial and governor response in wind farms. Some examples are Siemens - Netconverter [53] and GE Windinertia [9].

2.2.3 Stage III

Starting from a several seconds, the turbine governor systems will start to respond to the frequency deviation and generation will start to increase. This will halt the frequency drop. Frequency will reach its minimum value and then start to increase due to the effect of primary governor control. Due to this the system frequency will rise from its minimum value and attain a steady state value determined by the system droop. This stage is referred to as as governor response or governor action in this thesis. It is shown in figure 2.2.

In stage III when turbine-governor operates to increase the generator active power, the active power injection follows the frequency - power curve given in figure ???. Where ω_{NL} , ω_{FL} and ω_0 are the generator steady state frequency at no load, full load and rated load respectively. The governor droop R is defined as per equation 2.2.

$$R = \frac{\omega_{NL} - \omega_{FL}}{\omega_0} = \frac{\Delta f}{\Delta P} \quad (2.2)$$

Currently most of the TSOs require high frequency reserve response. Fo example in Ireland, beyond a system frequency of 50.25 Hz, a droop of 4.4% is required from wind farms [54].

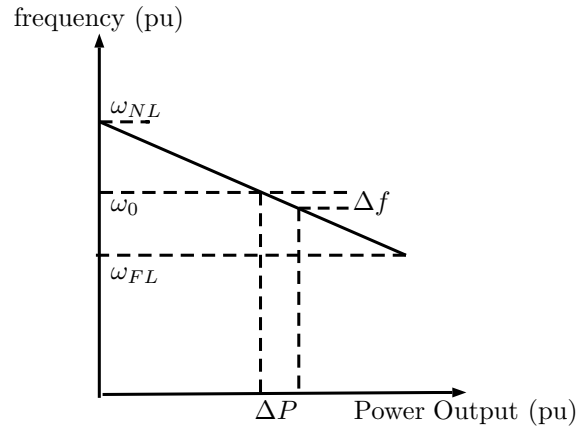


Figure 2.3: Ideal steady state Frequency - power characteristics of governor with speed droop[11]

2.3 Small Signal stability

The intention of this section is to give an introduction to small signal stability theory. It is recommended to refer [27] or [11], for a more rigorous approach to small signal stability theory.

2.3.1 System model

Any dynamic system can be represented in the differential matrix form, given by equation 2.3 [27].

$$\dot{\mathbf{x}} = \mathbf{F}(\mathbf{x}) \quad (2.3)$$

Here column vector \mathbf{x} is the state vector. Each individual element of the state vector, x_i is a state variable. The steady state of the system is given by equation 2.4. When the the steady state operating point of the system is \mathbf{o} , the corresponding values of the state variables are given by the state vector \mathbf{x}_o satisfying equation 2.4.

$$\dot{\mathbf{x}} = \mathbf{F}(\mathbf{x}_o) = \mathbf{0} \quad (2.4)$$

Using the Taylor's series and expanding \mathbf{F} around the equilibrium operation point \mathbf{o} , while neglecting the non-linear terms of expansion, we get the linear state space equation 2.5.

$$\Delta \dot{\mathbf{x}} = \mathbf{A} \Delta \mathbf{x} \quad (2.5)$$

Here $\Delta \mathbf{x} = \mathbf{x} - \mathbf{x}_o$ and $\mathbf{A} = \frac{\partial \mathbf{F}(\mathbf{x})}{\partial \mathbf{x}}$. The square matrix \mathbf{A} is the state matrix. The eigen values of state matrix \mathbf{A} is defined as the values of scalar parameter λ that satisfy the equation 2.6. For each scalar λ_i there is column vector ϕ_i which satisfies equation 2.6.

$$\mathbf{A} \phi = \lambda \phi \quad (2.6)$$

Simplifying equation 2.6 by using matrix algebra, equation 2.6 is converted to equation 2.7.

$$(\mathbf{A} - \lambda \mathbf{I}) \phi = \mathbf{0} \quad (2.7)$$

The characteristics equation with n solutions, λ_1 to λ_n is found by solving equation 2.8. The values λ_1 to λ_n are the eigen values of the system.

$$\det((\mathbf{A} - \lambda \mathbf{I})) = 0 \quad (2.8)$$

The small system stability of the system is determined by the eigen values. For a system to be stable the real part of the eigen value should be negative $\sigma < 0$. The general form for complex eigen value λ_i is given by equation 2.9. Each eigen value represents a mode of the system with certain oscillation frequency and damping.

$$\lambda = \sigma \pm j\omega \quad (2.9)$$

The oscillation frequency of the mode in Hz is given by equation 2.10. The damping ratio of this mode is given by equation 2.11.

$$f = \frac{\omega}{2\pi} \quad (2.10)$$

$$\zeta = \frac{-\sigma}{2\pi} \quad (2.11)$$

The rate of decay of the oscillation is determined by the damping ratio. A decay of $1/e = 37\%$

in the oscillation amplitude will occur in $1/2\pi\zeta$ cycles.

2.4 State of the Art

The most commonly used wind turbine technologies can be categorized according to the pitch control system used, generator technology used or the grid interface technology used.

2.4.1 Speed Control

The pitch control system determines how the turbine speed is controlled. The two main type of pitch control are stall control and pitch control.

1. Stall control is passive where the blade pitch can not be changed. The rotor aerodynamics are designed to stall the wind turbines at adversely high wind speeds. This is the simplest method for rotor speed control. The efficiency of energy extraction is optimum only at rated wind speed.
2. Pitch control is active control of turbine speed, where the pitch angle of the blade is possible to be changed. By changing the pitch angle the output power and the speed of turbine can be controlled. The disadvantage of this method is the requirement for an extra pitch mechanism. However due to high controllability in wind turbine power, granted by the pitch controller, it has become a state of art feature of modern wind turbines.

2.4.2 Generator Technology

Synchronous and asynchronous generators are used in modern wind turbines. Synchronous technology employed include classical electrically excited generators as well as permanent magnet excited generators. Asynchronous technology used include squirrel cage generators and wound rotor generators.

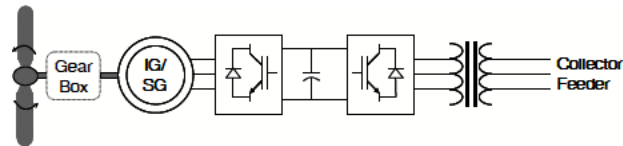


Figure 2.4: Type-4 WTG [55]

2.4.3 Grid Interface

Older wind turbine technology used to be directly connected to the electrical grid. In recent times partial power electronics interface and full power electronics interface has become a popular choice due to the possibilities in providing ancillary services.

2.4.4 Wind Turbine Generator Technologies

The IEEE classification of the wind turbine generators [55] is used in this dissertation. Accordingly, there are four main types of wind turbine generator configurations that are grouped according to the flexibility of speed control and the type of electrical interface to the grid. They are,

1. Type 1 - Fixed speed - Direct connected
2. Type 2 - Limited Variable speed - Direct connected
3. Type 3 - Limited Variable speed - Partial power electronic interface
4. Type 4 - Full Variable speed - Full power electronic interface

Only type 4 includes a full power converter interface. Since this thesis models a FRC based WTG, the state of art is limited to a discussion on type 4 WTG technology.

Type 4 - Variable speed - Full power electronic interface

The Type 4 turbine shown in figure 2.4 completely de-couples the grid side from the generator side. The turbine can ensure maximum energy extraction throughout its operational speed range. Usually it is operated at its optimal aerodynamic speed. Both asynchronous and synchronous generator technologies are used with a full converter interface.

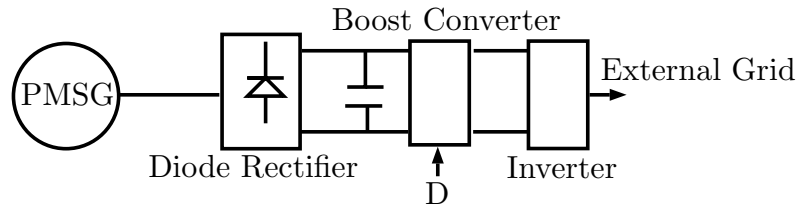


Figure 2.5: DC/DC Boost interfaced PMSG wind turbine

This study models a Type-4 PMSG based variable speed, fully power electronic interfaced WTG. Due to having a large number of permanent magnet pole pairs the generator can be direct driven. Further the generator does not require any external excitation. Due to these advantages one of the most popular choices for offshore wind farms is the direct driven PMSG FRC technology. According to leading manufacturer siemens [8], PMSG FRC design has lower weight , lower number of components, higher reliability, lower infrastructure, installation, operation and maintenance cost when considered as an offshore wind farm solution.

2.4.5 Wind Turbine Power Electronic topology

In a FRC WTG, the grid side power electronic converter is usually Voltage Source Converter. For the generator side, there are two main power electronic topologies that can be used [56]. They are,

1. DC/DC Boost interfaced PMSG wind turbine
2. Back to back VSC interfaced PMSG wind turbine

2.4.6 DC/DC Boost interfaced PMSG wind turbine

This interface consists of an uncontrolled diode rectifier connected at the generator side as shown in 2.7. The grid side is a fully rated voltage source converter. However the DC link voltage needs to be controlled. Therefore a DC/DC Boost converter is needed as an intermediary system to control and provide stable DC link voltage for proper operation of the grid side VSC. The Control signal to control the DC link voltage by boost converter is shown as D in the figure 2.7.

The system is simple in design, low in cost and high in reliability. However the it generates harmonic currents resulting in torque ripples. These might result in both torsional reso-

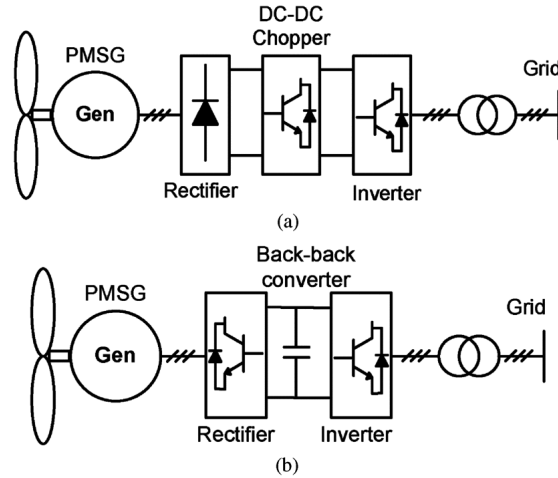


Figure 2.6: DC/DC Boost interfaced PMSG wind turbine [57]

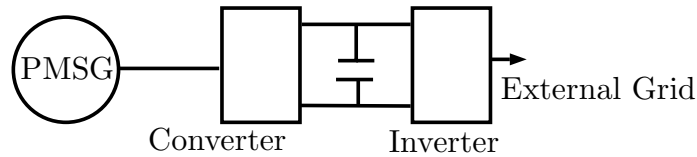


Figure 2.7: Back to back VSC interfaced wind turbine

nances as well as mechanical vibrations [56]. This is the main drawback of this topology. Further output DC voltage needs to be regulated by using the DC-DC converter. The design, modelling, controlling and inertia support implementation for this topology has been conducted in [34][35][36][37][38][39].

2.4.7 Back to Back VSC interfaced wind farm

In this type, the generator side power interface is also a VSC. Therefore both generator as well as the grid side, active power and reactive power transfer is controllable and operation is highly flexible. The PMSG can be operated at its maximum efficiency. Therefore this topology is the most popular choice in the industry [58]. It is the most used turbine and constitutes of the state of art for Type 4 wind turbine generators [59]. In this dissertation, it is the chosen system topology for modelling.

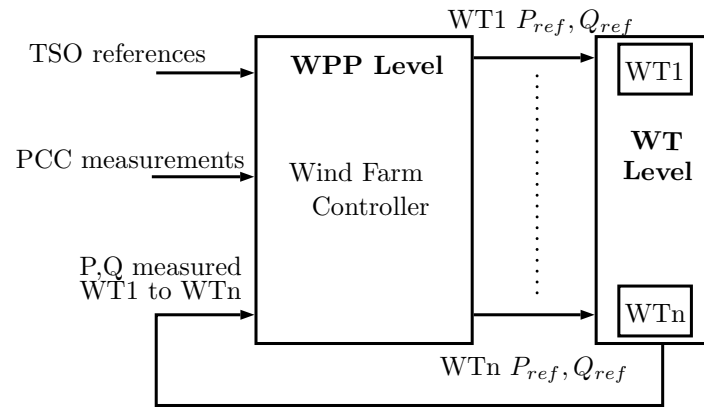


Figure 2.8: Overview of Wind farm controller

2.4.8 Wind Plant control structure

A wind farm [60] consists of many wind turbine generators interconnected together. In real system operation the TSO requires the wind farm to adhere to its requirements. Therefore there is a requirement to control the wind farm from system level while providing a simple system level interface to the TSO as shown in figure 2.8. Depending on the TSO requirements and taking into account the operating condition of the individual wind turbines, the wind farm controller will control the individual wind turbines to collectively adhere to the TSO requirements. This study does not take into account the plant level controller but uses an aggregate model which represents all the wind turbines in the wind farm by one single lumped wind turbine model.

Chapter 3

Power system modelling

This chapter presents the models used for simulation of classical power system components in for the simulation study. Rigorous derivation of these models can be referred in classical power system analysis texts such as [61].

3.1 Synchronous Generator

The sixth order model given in [27] is used for modelling the classical electrically excited synchronous generators. There are three synchronous generators, G2 in area 1 and G3 and G4 in area 2. All generators have identical parameters except for the inertia constant which is slightly different for area 1 and area 2. The system parameters are given in appendix A. A detail derivation of the mathematical model is addressed in [27]. The model is presented, with the objective of highlighting the aspects, that will be having an impact on the work carried out.

The model is given in dq rotor reference frame. By applying space vector theory [62], the 3-phase system in stationary coordinates is transformed into a two-phase system in rotating coordinates. This transformation is commonly known as the modified park transformation [63]. It is extensively used in this dissertation. The transformation is described in section 3.7.1.

The assumptions made to develop the mathematical model of the synchronous generator are that,

- The flux distribution is sinusoidal

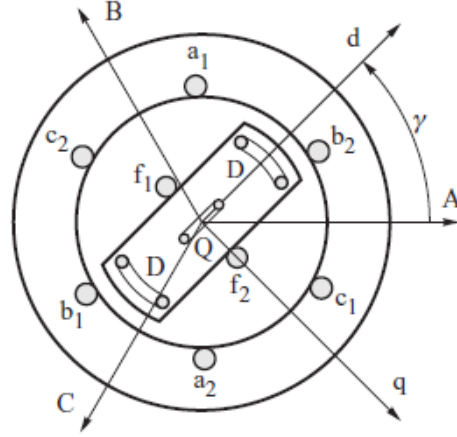


Figure 3.1: Synchronous generator cross section

- The winding capacitance is negligible
- Hysteresis losses are negligible
- The rotor speed in the transient and sub-transient state is approximately equal to the synchronous speed
- Linear magnetic circuits and independence of the inductance values are independent from the current (saturation is negligible)

The cross section of the synchronous generator model from [27], given in figure 3.7, includes rotor field winding f_1f_2 , stator armature winding ABC , d-axis damper winding D and q-axis damper winding Q . The mathematical model in $dq0$ rotor reference frame is given below.

$$T''_{do} \dot{E}''_q = E'_q - E''_q + I_d(X'_d - X''_d) \quad (3.1)$$

$$T''_{qo} \dot{E}''_d = E'_d - E''_d - I_q(X'_q - X''_q) \quad (3.2)$$

$$T'_{do} \dot{E}'_q = E_f - E'_q + I_d(X_d - X'_d) \quad (3.3)$$

$$T'_{qo} \dot{E}'_d = -E'_d - I_q(X_q - X'_q) \quad (3.4)$$

$$T'_{qo} \dot{E}'_d = -E'_d - I_q(X_q - X'_q) \quad (3.5)$$

$$2H\dot{\Delta\omega} = P_m - P_e \quad (3.6)$$

$$\dot{\delta} = \Delta\omega \quad (3.7)$$

The variables and parameters are,

T''_{do} = d-axis subtransient open-circuit time constant

T'_{do} = d-axis transient open-circuit time constant

T''_{qo} = q-axis subtransient open-circuit time constant

T'_{qo} = q-axis transient open-circuit time constant

E''_q = q-axis subtransient emf

E'_q = q-axis transient emf

E''_d = d-axis subtransient emf

E'_d = d-axis transient emf

E'_f = field emf

X''_q = q-axis subtransient reactance

X'_q = q-axis transient reactance

X''_d = d-axis subtransient reactance

X'_d = d-axis transient reactance

X_d = d-axis reactance

X_q = q-axis reactance

H = generator inertia time constant

$\Delta\omega$ = rotor speed deviation

δ = rotor angle

All quantities are in per unit except for H which is in seconds. Equations 3.1 to 3.6 model the electrical dynamics of the synchronous generator. Equations 3.6 and 3.7 model the mechanical dynamics of the generator. The state variables for the sixth order model consists of the six variables $E''_q, E'_q, E''_d, E'_d, \Delta\omega$ and δ .

3.2 Power frequency Converter

This chapter addresses the system design concepts for power converters including concepts required for the system controls presented in later chapters.

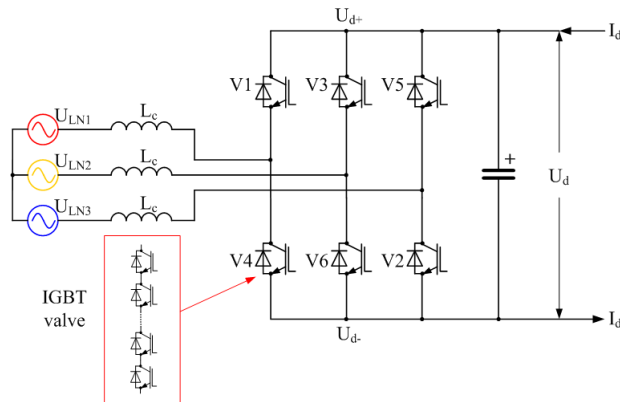


Figure 3.2: Physical scheme for voltage source converter

3.2.1 Introduction

A power converter is the component that converts AC to DC or vice-versa. The two kinds of converter technologies that are currently used are Line Commutated Converters which use thyristors for switching and Voltage Source Converters which use Insulated Gate Bipolar Transistors for switching. In the wind farms with fully rated converter systems, voltage source converters can provide the required flexibility in control and operation. Therefore they are the state of art in the wind industry. The IGBT voltage source converter consists of six IGBTs and six anti-parallel diodes connected in a bridge structure as presented in figure 3.2 .

In a variable speed, fully rated converter wind turbine electrical system, the generator side converter converts the low frequency AC to DC while the grid side converter converts the DC voltage to grid AC voltage. Therefore, in this thesis, the generator side power converter is referred to as the rectifier and the grid side converter is referred to as the inverter.

3.2.2 Mathematical model

The IGBTs are switched using Pulse width modulation. The switching frequency is in the Khz range. Since this frequency is much higher than the frequency of the studied phenomena, which is usually in the range from 0.2 Hz to 20 Hz [11], a fundamental frequency model of the power converters can be used for power system stability studies. This choice also maintains the consistency in accuracy across all the models.

Given an ideal DC voltage with magnitude V_{dc} , when sinusoidal PWM is being employed,

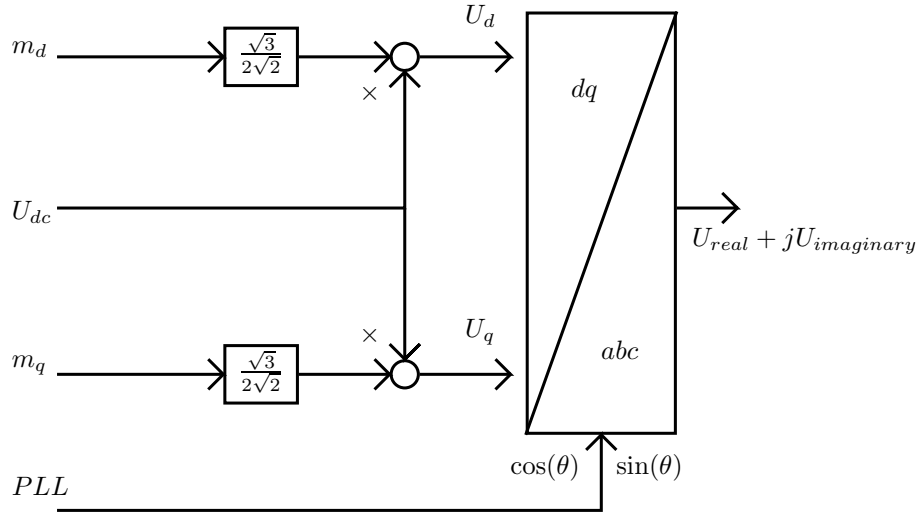


Figure 3.3: block diagram for voltage source converter [30]

rms AC voltage is given by equation 3.8, [64] where converter is assumed to be ideal.

$$|V_{ac}| = \frac{\sqrt{3}}{2\sqrt{2}} m V_{dc} \quad (3.8)$$

The phase of the AC voltage can be controlled by the converter to any value required.

The converter voltage V_{ac} in grid voltage oriented reference frame is given by,

$$V_{acr} = \frac{\sqrt{3}}{2\sqrt{2}} m_r V_{dc} \quad (3.9)$$

$$V_{aci} = \frac{\sqrt{3}}{2\sqrt{2}} m_i V_{dc} \quad (3.10)$$

$$V_{ac} \angle \phi = V_{acr} + jV_{aci} \quad (3.11)$$

Where, V_{acr} , V_{aci} , ϕ , m_r and m_i represent the real component of the ac voltage, the imaginary component of the ac voltage, voltage angle, real component of the pulse width modulation index and the imaginary part of the pulse width modulation index.

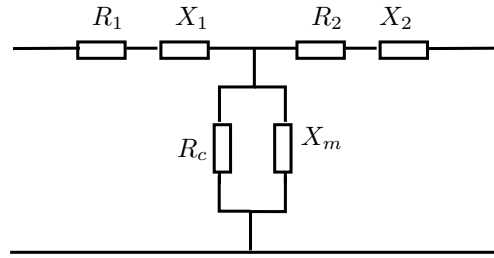


Figure 3.4: Equivalent circuit of a transformer

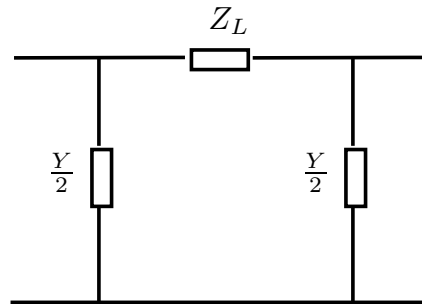


Figure 3.5: Equivalent circuit of a transmission line

3.3 Power Transformers

The equivalent model of the transformer (referred to the primary side) applied [61] in this thesis, is given in figure 3.4. Where,

R_1, R_2 = Primary and secondary winding resistance

X_1, X_2 = Primary and secondary winding leakage reactance

R_c = core loss resistance

X_m = Magnetising reactance

In the studied Kundr's two area network both both core loss resistance and magnetizing reactance are neglected to simplify the system model. Therefore the transformer is modelled by an impedance Z_T .

3.4 Transmission lines

This study uses the π - model of a transmission line given in figure 3.5.

Z_L = Total series impedance per phase

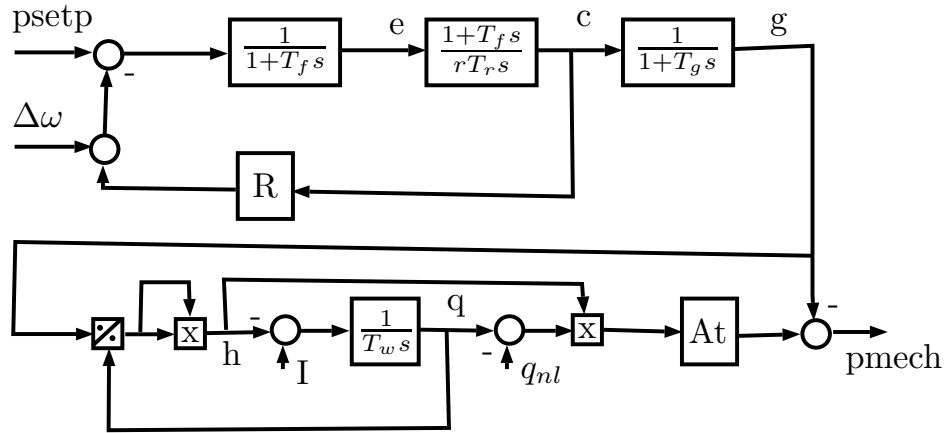


Figure 3.6: Control Block Diagram for the Hydro Governor

Y = Total shunt admittance per phase

In the simulation model the short line assumptions is applied. Therefore Y is assumed to be negligible and the model reduces to a simple series impedance given by Z_L .

3.5 Power System Loads

The power system complex loads as well as capacitor banks are modelled as constant impedance loads. The load voltage is assumed to be stiff since voltage variations in the simulation study is negligible.

3.6 Hydro Governor

In the modelled power system, 75% of the penetration is still from classical generation. In order to highlight the frequency variations, slow hydro governors are used for the generators. The hydro governor presented in [65], is used for this study. The parameters of the hydro governor model are given below. All time constants are in seconds.

R = Permanent Droop in pu

r = Temporary Droop in pu

T_r = Governor Time Constant

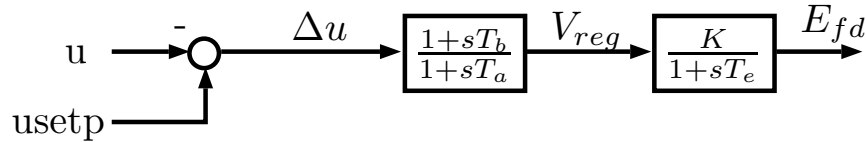


Figure 3.7: Control Block Diagram for the AVR

T_f = Filter Time Constant

T_g = Servo Time Constant

T_w = Water Starting Time

A_t = Turbine Gain in pu

D_{turb} = frictional losses factor in pu

q_{nl} = No Load Flow in pu

3.7 Automatic Voltage regulator

The simplified excitation system (AVR SEXS) given in [66], is used in this study. The control block diagram of the AVR is given in figure 3.7. The model parameters are,

T_a = Filter derivative time constant in seconds

T_b = Filter delay time in seconds

K = Controller gain in pu

T_e = Exciter time constant in seconds

3.7.1 Reference frame conversion

The rotor reference frame relates to system reference frame by a rotation of axis equal to the rotor angle. The conversion matrix to the system reference frame from the local rotor reference frame is given by equation 3.12. The synchronous machine model when presented in a rotor oriented reference frame is known as the park model. Figure 3.8 presents the relative position of the two coordinate systems. Any system with similar rotational displacement of axis can be transformed using this transformation.

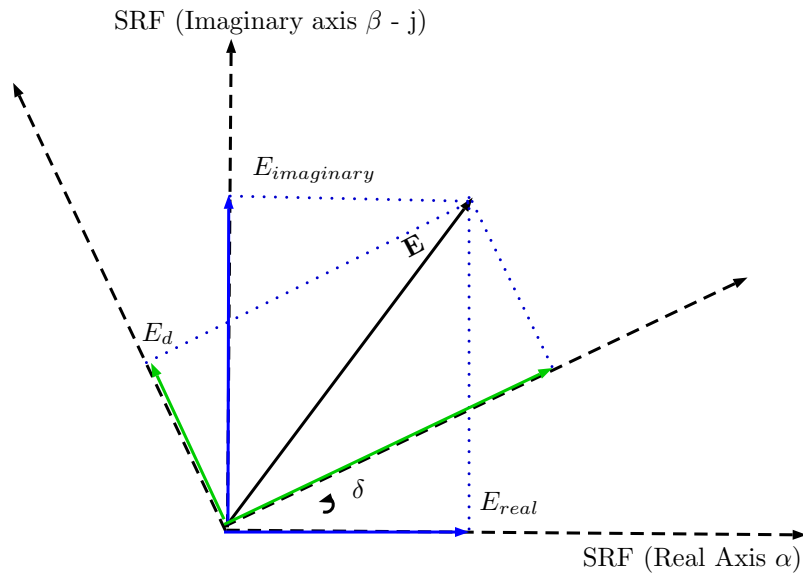


Figure 3.8: Coordinate transformation from local rotor reference frame to system reference frame

$$\begin{bmatrix} E_r \\ E_i \end{bmatrix} = \begin{bmatrix} \cos\delta & -\sin\delta \\ \sin\delta & \cos\delta \end{bmatrix} \begin{bmatrix} E_q \\ E_d \end{bmatrix} \quad (3.12)$$

E_q and E_d are the d-axis and q-axis components of emf in the local rotor reference frame and E_r and E_i are the d-axis and q-axis components of emf in the system reference frame. δ is the rotor angle. Figure 3.8 presents the relative position of the two coordinate systems.

Chapter 4

Wind Turbine Modelling

This chapter establishes the mathematical model of a wind turbine generator applicable for power system dynamic studies. The first section describes the generic structural representation of the system. The second section presents how the component models are combined to give a full order and reduced order model. The rest of the chapter will describe the detail models of the individual components.

4.1 Introduction

A main objective of this thesis is to model a wind turbine generator with least effort and computational requirements while providing a sufficiently accurate response. There are three complexity levels of modelling [67] that can be applied in a power system simulation study. The first is the low resolution approach, which only considers the mechanical dynamics (the electrical dynamics are neglected). The reduced order model used in this work belongs to this category. The second is the medium resolution approach, where the electrical dynamics are simplified by modelling the electrical machines, using a fundamental frequency (phasor) approximation. The models provide sufficient accuracy to analyse system electro-mechanical transients. The full order model used in this work belongs to this category. The third category is a high resolution approach, which models all dynamics, including high frequency switching and DC transients. The scope of interest in a power system stability study, is limited to electro-mechanical dynamics. Therefore modelling complexity of this study is limited at most to the second level.

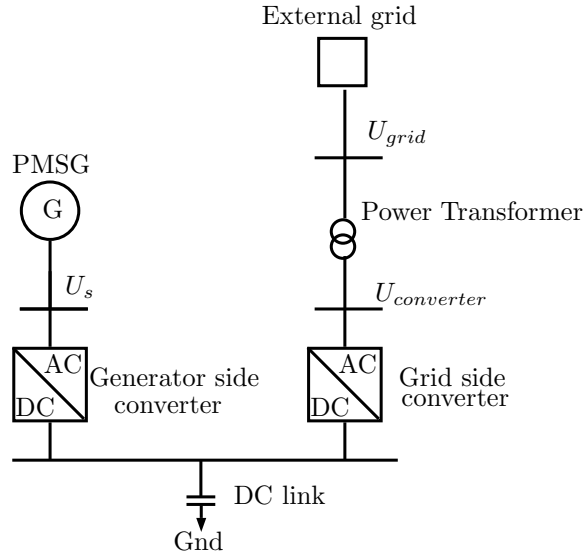


Figure 4.1: Wind farm single line diagram

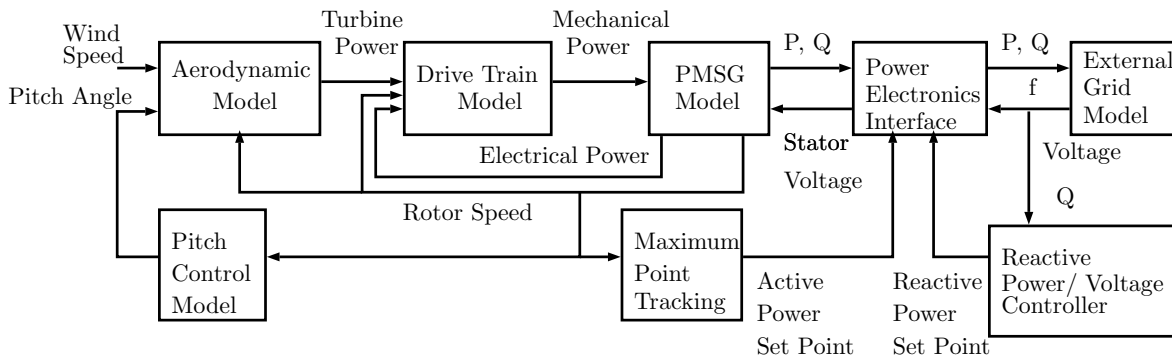


Figure 4.2: Functional structure of wind turbine

4.1.1 Generic Structure

The single line diagram of the modelled wind turbine generator is given in figure 4.1. The wind farm electrical system consists of PMSG, generator side converter, DC link, grid side converter and step up power transformer. The generator side converter controls the PMSG. The DC link provides the interface between the two converters. The grid side converter provides the grid interface. The lower generator voltage, is stepped up to the higher utility grid voltage by the power transformer.

This system can be represented by the generic functional diagram shown in figure 4.2. The mechanical subsystem consist of the aerodynamic model, pitch control model, drive train model

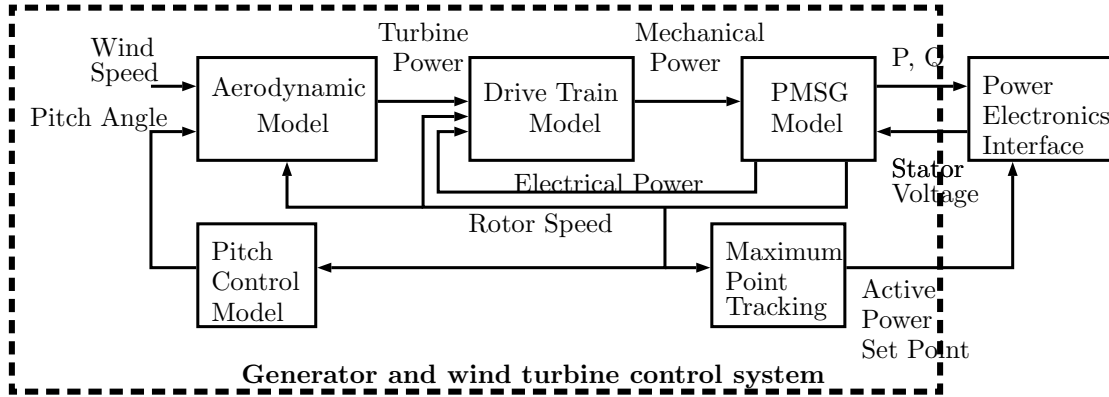


Figure 4.3: Full Model : Full order model functional structure of mechanical system

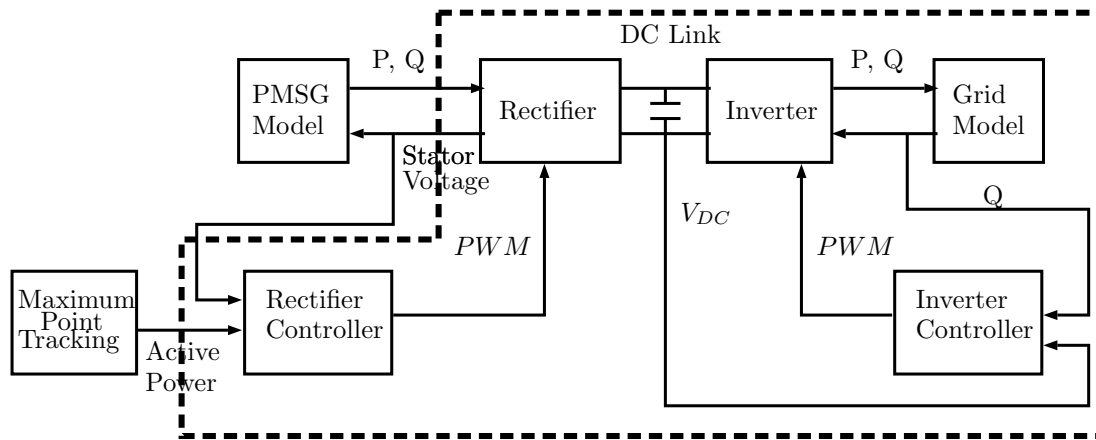


Figure 4.4: Full Model : Electrical system structure

and the maximum point tracking model. The drive shaft of the generator is directly connected to the wind turbine. The pitch control mechanism controls the wind turbine power output.

4.1.2 Full Order Model

The full order model, represents both mechanical and electrical dynamics. The structure of this model can be presented using two subsystems. The first given in figure 4.3, shows how the mechanical component models are combined, to create the mechanical subsystem. The second given in figure 4.4, shows how the electrical component models are combined to create the electrical subsystem.

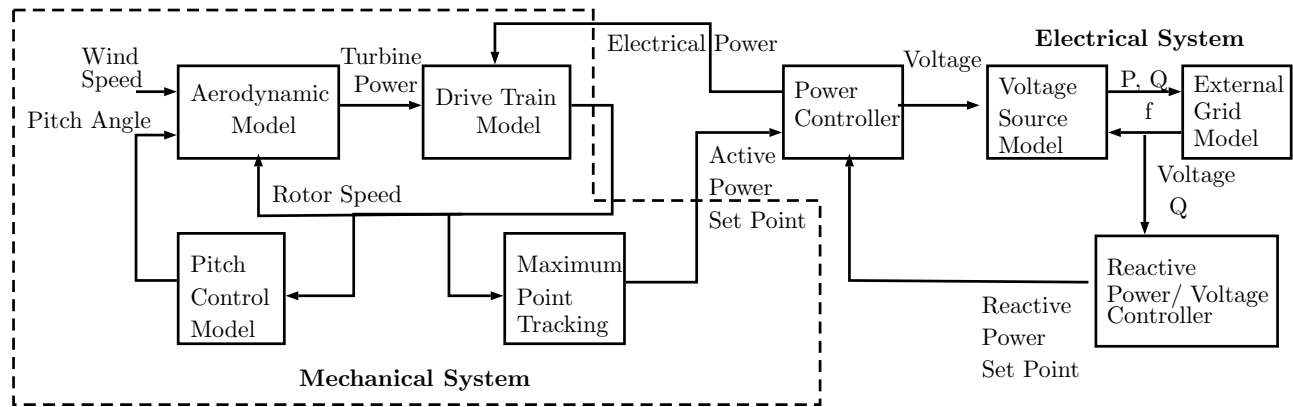


Figure 4.5: Reduced order model functional structure

4.1.3 Reduced Order Model

The structure of the reduced order model is given in figure 4.5. This is an approximate model which neglects the generator, generator side controls and DC link dynamics. The wind turbine mechanical dynamics are however represented.

4.2 Wind Turbine Mechanical System

The mechanical subsystem is common for both full order and reduced order model. This can be observed by comparing figure 4.3 and figure 4.5. The wind speed, pitch angle and rotor speed determines the wind power extracted by the wind turbine. This phenomenon is modelled in the aerodynamic model. The extracted mechanical power generates torque on the wind turbine shaft, driving the electrical generator. The generator converts the mechanical energy to electrical energy. The resulting rotor speed determines the power reference to the power electronic interface, using the maximum point tracking scheme.

4.2.1 Wind Aerodynamics

The source of energy that drives a wind turbine, is the kinetic energy in the wind. When the wind mass strikes the blades of the turbine, the speed of the air mass decreases, causing a change of momentum resulting a loss in energy. This loss in energy of the wind mass, is converted by the turbine and reflected as rotational kinetic energy. In itself modelling wind turbine aerodynamics

is a highly researched [68], advanced field of study. Sophisticated models for wind aerodynamics are available in literature. However this work will use a simple empirical method presented in [69], for modelling this energy conversion process.

Either a real wind speed sequence or a modelled wind speed sequence can be used to simulate wind dynamics. Reference [70] uses a simple wind turbulence model. Reference [22] presents a wind speed model which also includes tower shadow effect. In general, a theoretical wind speed model will include a combination of mean, ramp, gust and noise components [71]. Instead of using a theoretical model, this work follows the approach of [24], where a real wind speed sequence is applied. A measured wind speed sequence, from a wind farm in Gansu province, China which is given in [72], is used in this work.

The total wind power P_w , available for extraction by the turbine, is given by equation 4.1. Here A is the turbine cross section area, V is the mean wind speed over the turbine surface and ρ is the air density.

$$P_w = \frac{1}{2} \rho A V^3 \quad (4.1)$$

The fraction of power extracted from the available power in the wind formula by practical turbines is expressed by the performance coefficient [69], C_p . The power extracted is given by equation 4.2. A turbine cannot extract more than 59% [73][58] of the total available power. This maximum theoretical limit of the performance coefficient, is known as the betz limit [74]. The extracted mechanical power P_m , from wind, is given by equation 4.3.

$$P_m = C_p P_w \quad (4.2)$$

$$P_m = \frac{1}{2} \rho A V_w^3 C_p \quad (4.3)$$

C_p is a function of pitch angle, β and the tip speed ratio, λ . The tip speed ratio is defined by equation 4.4, where ω_m is the rotational speed of the turbine, R is the radius of the turbine and V_w is the wind speed.

$$\lambda = \frac{\omega_m R}{V_w} \quad (4.4)$$

According to [24], C_p characteristics for different wind turbines types are alike. This gives

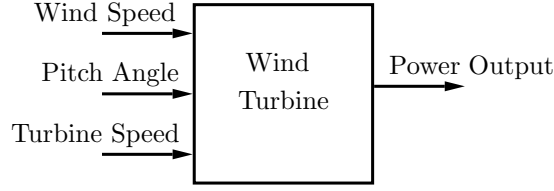
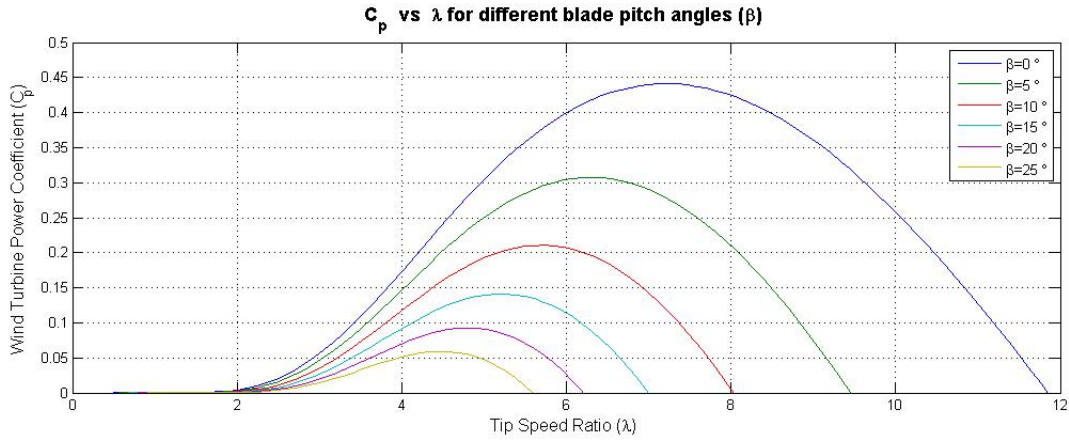


Figure 4.6: Wind aerodynamic block diagram

Figure 4.7: C_p as function of λ for different pitch angles

rise to the possibility of using a generic equation to represent C_p . This work uses an empirical formulae from [69], in the form presented in equation 4.5. The values for constants C_1 to C_9 as applicable to variable speed wind turbines are extracted from [24]. The equations 4.3 and 4.5 gives the wind aerodynamic model presented in figure 4.6. λ_i is given by equation 4.6.

$$C_p(\lambda, \beta) = c_1 \left(\frac{c_2}{\lambda_i} - c_3\beta - c_4\beta^{c_5} - c_6 \right) e^{-\frac{c_7}{\lambda_i}} \quad (4.5)$$

$$\lambda_i = \frac{1}{\frac{1}{\lambda + c_8\beta} - \frac{c_9}{\beta^3 + 1}} \quad (4.6)$$

The variation of C_p as a function of λ for different values of β , derived using equation 4.5 is given in figure 4.7. It shows that the highest C_p values are obtained, when operating with β at 0 degrees. This highlights the fact that by increasing β , the wind turbine power can be decreased.

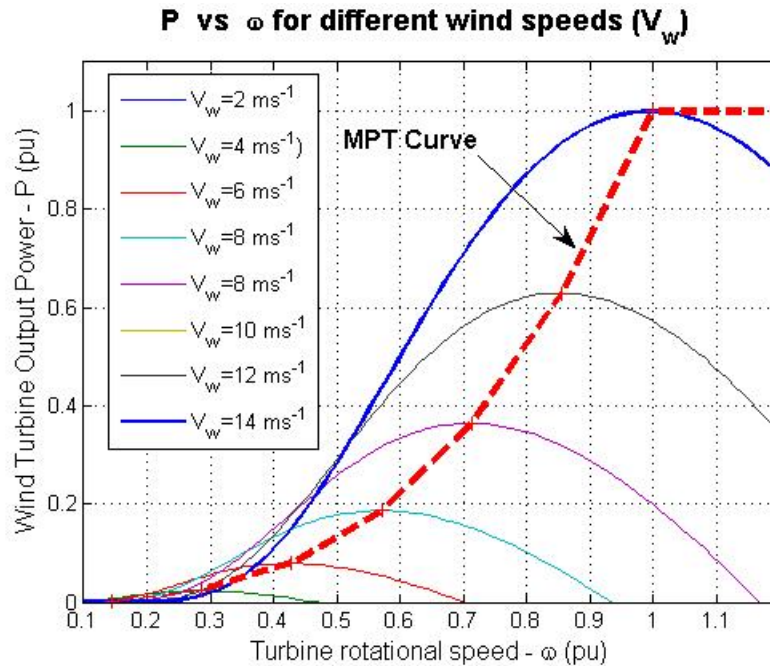


Figure 4.8: Wind turbine output power variation as a function of turbine rotational speed

4.2.2 Maximum point tracking scheme

The variable speed operation of a wind turbine is motivated by the requirement to operate at maximum efficiency, in order to extract the maximum possible power available in the wind. When the wind speed is high, causing the turbine speed to increase, the power needs to be limited to the maximum safe limit for the turbine. The wind turbine output power, as a function of turbine speed, is derived using equations 4.3, 4.4 and 4.6, is given figure 4.8. This figure shows that for each wind speed, output power can be maximised by operating at a specific rotational speed. The operating points for maximum power output, for each wind speed point, combines to create the MPT characteristics for this turbine. Therefore by operating the wind turbine, power - speed characteristics, following the red MPT curve in figure 4.8, maximum efficiency at lower wind speed and safe operation at higher wind speeds is realised. In this model, maximum point tracking scheme is implemented, by generating the output power reference, using the turbine rotational speed as input to the MPT scheme given in figure 4.9.



Figure 4.9: MPT scheme block diagram

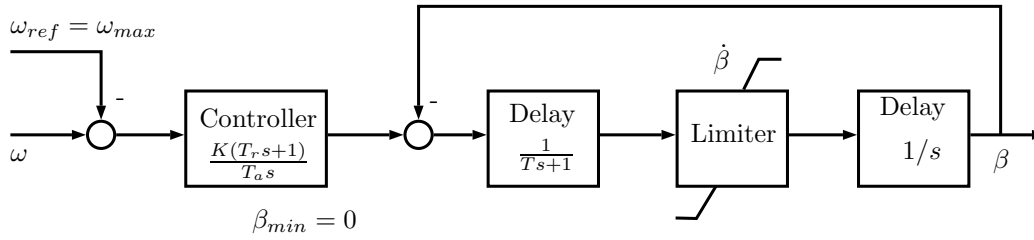


Figure 4.10: Pitch angle Controller block diagram

4.2.3 Pitch Controller

The turbine power output is controlled by the pitch mechanism shown in 4.11. The general control objective of the pitch angle controller is to control the turbine speed to the reference value. Different models for pitch system are available in literature [69][24]. The simple pitch controller model given in [15] is used for this study. Control block diagram for the implemented pitch controller is given in figure 4.10. The turbine speed error generates the reference pitch angle by using a PI controller. The actuating mechanism is a servo motor. The pitch controller operates to limit the turbine output power to its rated value in high wind speed conditions. This functionality is implemented by fixing the reference wind turbine speed to a constant value (rated value), while setting the pitch angle reference minimum limit to 0 degrees. The variables used in the model are,

K_a = blade angle controller gain

T_r = lead time constant (s)

T_a = blade angle controller time constant (s)

T = servo time constant (s)

ω_{ref} = maximum speed (pu)

$\dot{\beta}$ = blade positioning speed (degrees/second)

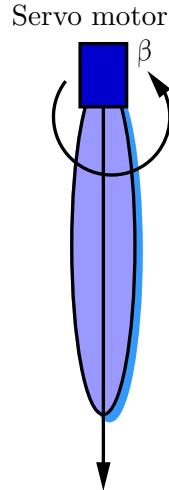


Figure 4.11: Output power control by blade pitch control

4.2.4 Wind turbine drive train

The wind power extracted by the turbine rotor, drives the wind turbine drive train. The turbine in turn, drives the PMSG and converts the mechanical power into electrical power. The mechanical drive train is direct driven. Therefore, assuming a perfectly stiff shaft, turbine speed is equal to the generator speed. In order to generate the rated output power, for a low speed machine, (larger number of pole pairs) a high torque will be required, as per the mechanical relationship given in equation 4.7. Therefore, the relative shaft stiffness values will decrease. For a system with low rotational speed, a significant shaft twist will occur, resulting in a significant dynamic change of the generator electric angle [28]. In order to model this effect, at least a two mass system will be required. However this work considers a system with 13 pole pairs. According to [28], the drive train for this WTG can modelled using a the single mass model, given in equation 4.8. The control block diagram for the drive train model is given in figure 4.12. Where P , T , J and ω is given by mechanical power in W, shaft torque in Nm, rotor inertia in Kgm and rotor speed in rad/s, respectively.

$$P = T \times \omega \quad (4.7)$$

$$\frac{\Delta P}{\omega} = \Delta T = J_{eq} \cdot \frac{d\omega}{dt} \quad (4.8)$$

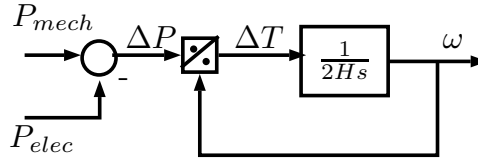


Figure 4.12: Mechanical drive train block diagram

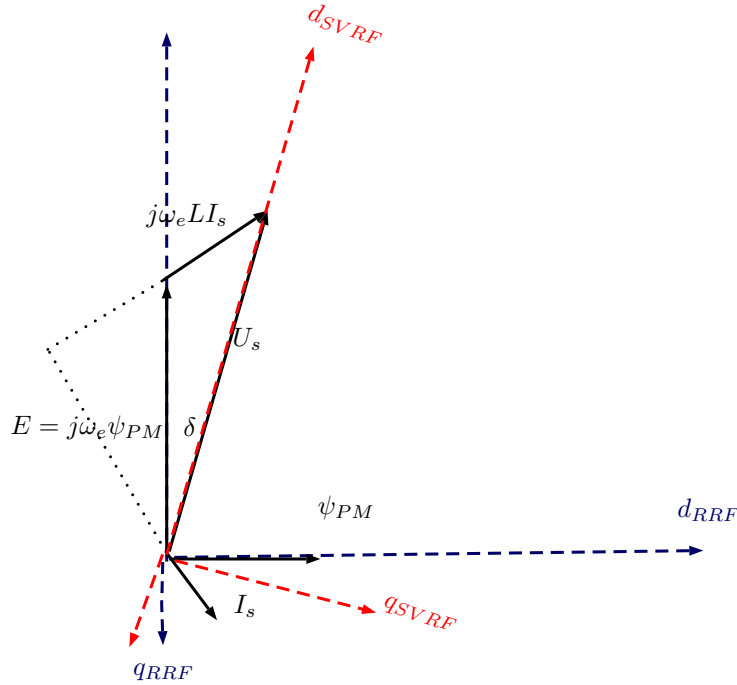


Figure 4.13: Rectifier controller reference frame

4.3 Wind Turbine Energy Conversion System

At the start of this chapter the general structure of the models were introduced. Next the mechanical system structure and models were described in detail. This section focuses on the detail modelling of the wind turbine energy conversion system. The control of the energy conversion process, is based on controlling the two back to back power converters.

4.3.1 Converter reference frame

The control strategy for rectifier controller, is implemented in stator voltage oriented reference frame, where the d-axis is aligned to the stator voltage vector ($u_{sd} = u_{stator}$), as illustrated in figure 4.13. The control strategy for the inverter controller, is implemented in grid voltage oriented

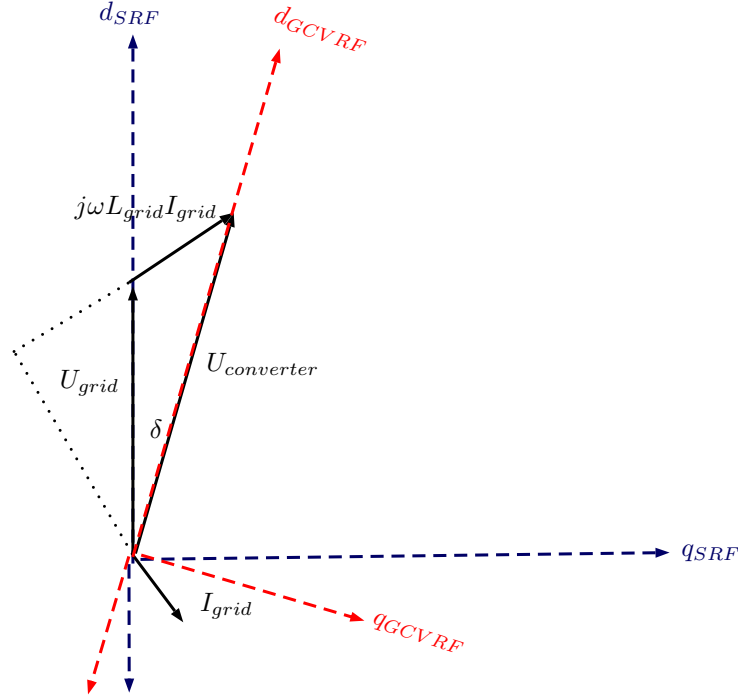


Figure 4.14: Inverter controller reference frame

reference frame, where the d-axis is aligned to the grid voltage vector $u_{sd} = u_{grid}$, as illustrated in figure 4.14. The stator q-axis voltage is zero. Therefore the generator active and reactive power can be given [32] by,

$$P = \frac{3}{2} u_{sd} i_{sd} \quad (4.9)$$

$$Q = -\frac{3}{2} u_{sd} i_{sq} \quad (4.10)$$

Where u_{sd} is the direct axis voltage and i_{sd} and i_{sq} are direct and quadrature axis current components in the stator voltage reference frame. All quantities are in per unit. It is evident from these two expressions that generator active power can be controlled, by independently controlling the d-axis current while the generator reactive power can be controlled, by independently controlling the q-axis current. The conversion between the reference frames is carried out by using the modified park transformation given in section 3.7.1. A phase locked loop (PLL) is used to calculate the phase angle of the voltage phasor.

4.3.2 Full Order Model Electrical System

The functional structure of the wind turbine energy conversion system is given in figure 4.4. Referring this diagram, the two main controllers are given as rectifier controller (generator/machine side controller - MSC) and the inverter controller (grid side controller - GSC).

PMSG Controller

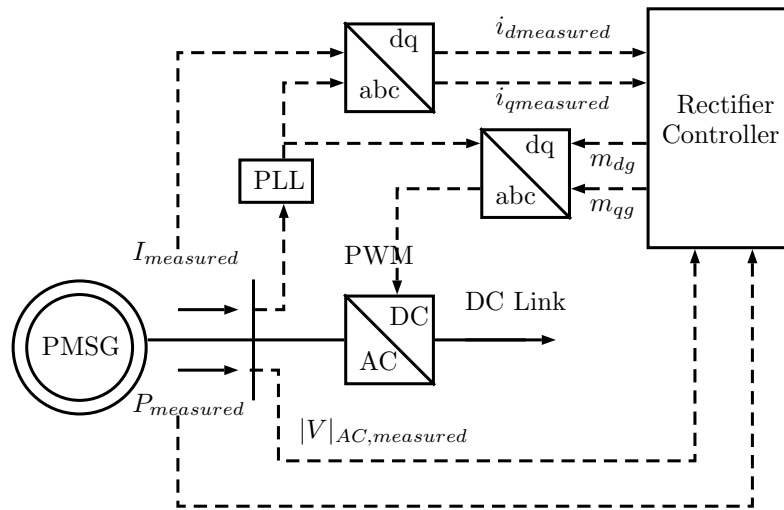


Figure 4.15: Rectifier controller configuration diagram

The PMSG is controlled by the rectifier controller. There are different vector control schemes that can be used for controlling a PMSG. Widely used vector control schemes include zero d axis current control (ZDC), maximum torque control (MTPA), unity power factor control and constant voltage control [56][75][26]. In this thesis, constant voltage control described in [26] is used. The control objective is, control of the generator stator voltage to its rated value. The advantage of this scheme is that the generator and rectifier can operate at rated voltage. However the generator will have a reactive power demand, when operating in low wind speeds. The control objective is two fold.

- Extraction of the generator power as per active power set point generated by the maximum point tracking scheme
- Control of generator stator voltage magnitude to its rated value

As per equations 4.9, it can be observed that generator active power can be controlled, by controlling the d-axis current. As per equation 4.10, it can be observed, that the generator reactive power can be controlled by using the q-axis current. The generator side converter active power set point is a function of the rotor speed and follows the maximum power point. The generator side stator voltage controller, controls the stator voltage magnitude to its rated value.

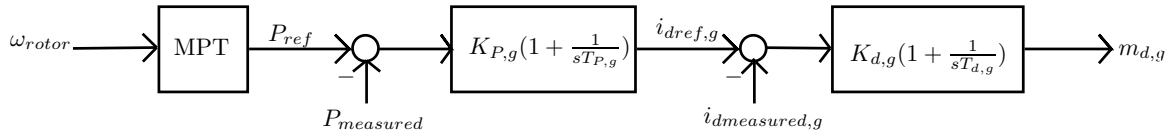


Figure 4.16: Rectifier controller active power control loop

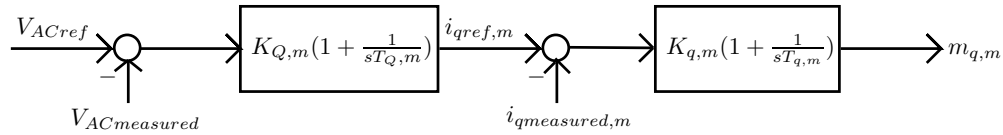


Figure 4.17: Rectifier Controller reactive power control loop

The control structure in figure 4.16, is implemented in this work to achieve the first control objective. It consists of an outer active power control loop and an inner d-axis current control loop. The control structure presented in figure 4.17 is used to achieve the second control objective. It consists of an outer stator voltage magnitude control loop and an inner q-axis current control loop. According to the controller physical implementation given in figure 4.15, the generator stator voltage magnitude, voltage angle and the generator current are the input signals to the controller. The controller output is the PWM index of the rectifier.

Rectifier Controller Inner Current Loop Tuning

Inner current loop tuning

In a rotor oriented dq reference frame, with direct axis aligned with rotor flux vector, the equations for the PMSG is given by [26],

$$\lambda_{sd} = L_s i_{sd} + \lambda_{PM} \quad (4.11)$$

$$\lambda_{sq} = L_s i_{sq} \quad (4.12)$$

$$v_{sd} = R_s i_{sd} + \frac{d}{dt} \lambda_{sd} - \omega_m \lambda_{sq} \quad (4.13)$$

Where λ_{sd} , λ_{sq} , v_{sd} , v_{sq} , L_s , i_{sd} , i_{sq} , R_s , ω_m , λ_{PM} is given by d and q axis flux linkage, d and q axis stator voltage, stator inductance, d and q axis current, stator resistance, generator speed and field flux linkage respectively. The field flux linkage (permanent magnet excitation) is time invariant. Substituting to equation 4.13 from equations 4.11 and 4.12, gives v_{sd} .

$$v_{sd} = R_s i_{sd} + \frac{d}{dt} (L_s i_{sd} + \lambda_{fd}) - \omega_m (L_s i_{sq}) \quad (4.14)$$

$$v_{sq} = R_s i_{sq} + \frac{d}{dt} \lambda_{sq} + \omega_m \lambda_{sd} \quad (4.15)$$

Substituting to equation 4.15 from equations 4.11 and 4.12, gives v_{sq} .

$$v_{sq} = R_s i_{sq} + \frac{d}{dt} (L_s i_{sq}) + \omega_m (L_s i_{sd} + \lambda_{fd}) \quad (4.16)$$

Since this PMSG is a non salient pole machine, stator d-axis inductance and q-axis inductance is considered equal [76] ($L_s = L_d = L_q$). Therefore the electro magnetic torque (T_e) of the generator is given by [26],

$$T_e = \frac{3}{2} \lambda_{PM} i_{sq} \quad (4.17)$$

The modelling assumption for the PMSG are,

- Stator transients are neglected since the study is focused on fundamental frequency simulations [11]
- A single mass model is assumed for the mechanical drive

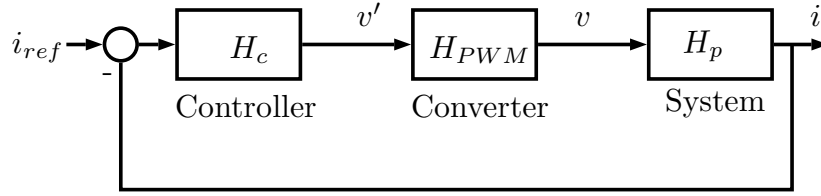


Figure 4.18: Block diagram for rectifier inner current control loop

- Magnetic saturation in the machine is neglected and flux distribution is assumed to be sinusoidal
- The only active power losses are stator copper losses
- The synchronous generator doesn't have damper windings [26]

Converting the voltages to laplace domain for controller design with the cross coupling terms viewed as a disturbance from control point of view, the system transfer function H_p is given by,

$$H_p = \frac{i_{sd}}{v_{sd}} = \frac{1}{R_s + sL_s} \quad (4.18)$$

$$H_p = \frac{1}{R_s(1 + \tau_s)} \quad (4.19)$$

Here τ is given by L_s/R_s . The same transfer function is valid for the q-axis current loop, since the parameters are identical. The control block diagram for generator side control inner current loop is given in figure 4.18.

Controller

A proportional integral (PI) controller, in the form given in equation 4.20 is used throughout this dissertation. Here K_p is the proportional gain, and T_i is the integral gain.

$$H_c = K_p \frac{(1 + T_i s)}{T_i s} \quad (4.20)$$

Converter

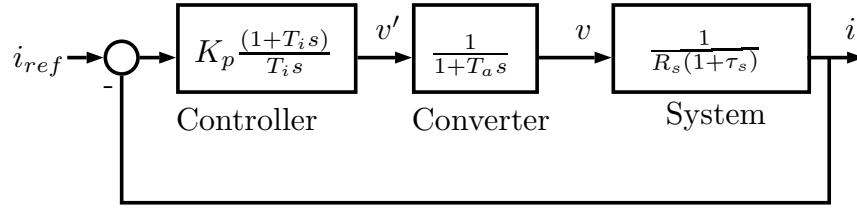


Figure 4.19: Transfer function for inner current control loop

Parameter	Value
Stator resistance R_S	0.0001 pu
Synchronous reactance X_s	1.5 pu
Switching frequency	1 kHz
Measurement delay	2 ms

Table 4.1: Generator Parameters for controller tuning

Converter is modelled as a delay of T_a , where the delay time is approximated by half the switching time period.

$$H_{PWM} = \frac{1}{1 + T_a s} \quad (4.21)$$

System

The control system needs to modulate the current value to its reference value dictated by the outer control loop. The open loop transfer function (H_{OL}) for this system would be, $H_c H_{PWM} H_p$ and is given by equation 4.22.

$$H_{OL} = \frac{K_p(1 + T_i s)}{T_i s(1 + T_a s)R_s(1 + \tau)} \quad (4.22)$$

Using the modulus optimum tuning criteria given in [77], controller parameters are chosen as,

$$T_i = \tau \text{ and } K_p = \frac{\tau R}{2T_a} \quad (4.23)$$

The calculated parameters for the inner current controller is given in table 4.2. The bode plot for the open loop transfer function given in figure 4.20 confirms stable operation with a cross

Parameter	value (pu)
K_p	0.96
$T_i(\tau)$	47.8 s
T_a	2.5 ms

Table 4.2: Rectifier inner current controller parameters

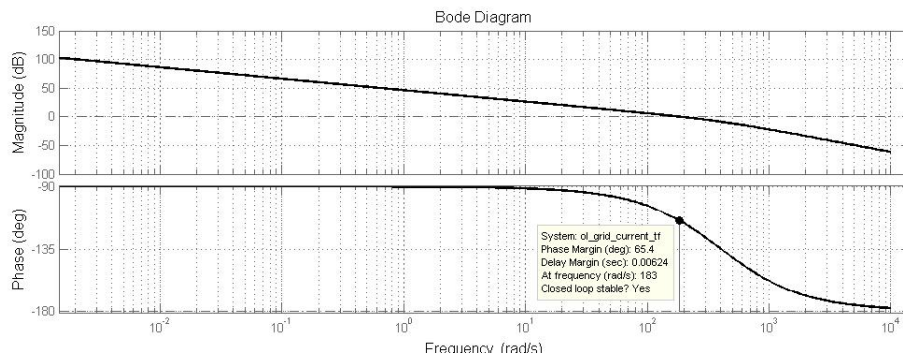


Figure 4.20: Generator current controller open loop bode plot

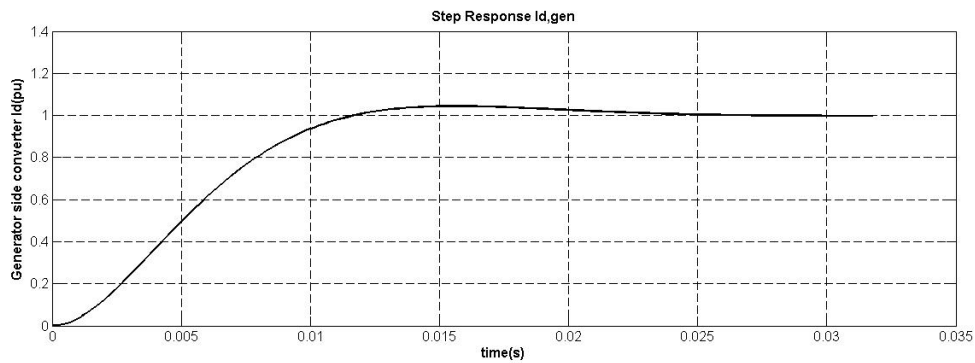


Figure 4.21: Generator current controller step response plot

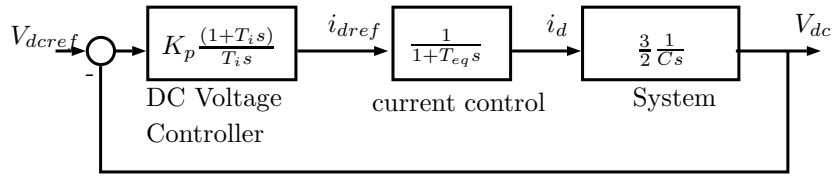


Figure 4.22: Rectifier controller outer active power loop

Parameter	value (pu)
K_p	0.1
$T_i(\tau)$	47.8 s
T_{eq}	5 ms

Table 4.3: Rectifier active power loop controller parameters

over frequency of 180 rad/s and phase margin of 65 degrees. The time response of the controller, to a step in current input, given in figure 4.21 shows a settling time of 15 ms.

Rectifier Controller active power loop tuning

In the converter control reference frame, active power is given by [32],

$$P = \frac{3}{2} u_{sd} i_{sd} \quad (4.24)$$

As per [77], the inner current loop transfer function is replaced by a simple first order function with $T_{eq} = 2T_a$, resulting in control block diagram given in figure 4.22. The control requirement for outer loop is for its response to be approximately 10 times slower than the inner control loop. K_p is chosen such that the open loop cross over frequency is (180/10) 10 rad/s, while T_i is chosen to cancel the pole of the transfer function. The bode plot for the open loop transfer function given in figure 4.23, confirms stable operation with an inherently stable system and cross over frequency of 20 rad/s. The time response of the controller to a step in current input given in figure 4.24 shows a settling time of 250 ms.

Cross over frequency of 20 rad/s and an inherently stable system is observed for calculated parameters given in table 4.3. The settling time for power controller being 250 ms and settling time for inner current being 20 ms, the design objectives are realized.

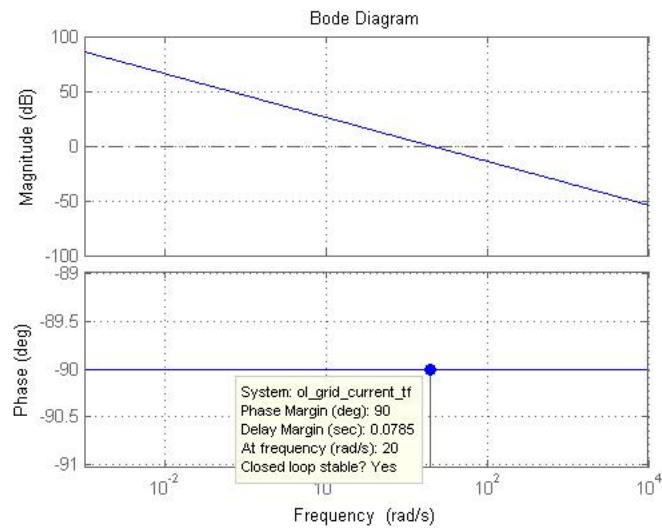


Figure 4.23: Generator current controller open loop bode plot

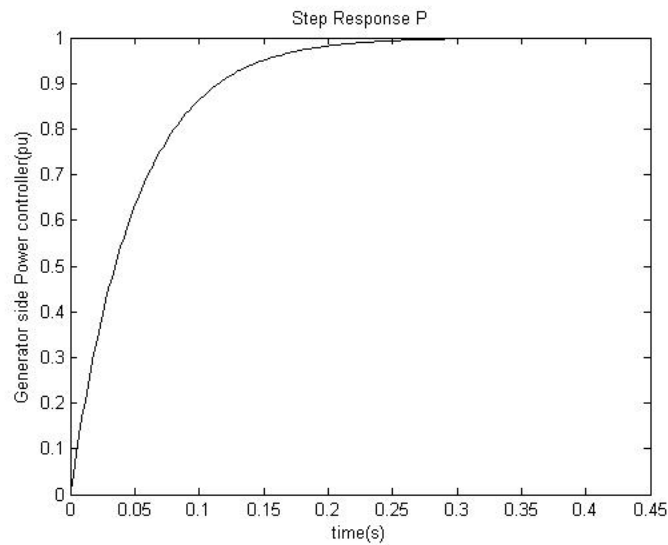


Figure 4.24: Generator current controller step response plot

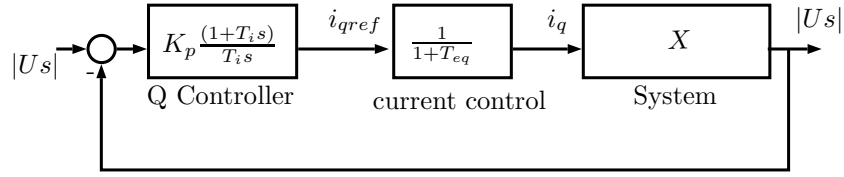


Figure 4.25: Stator voltage control loop block diagram

Outer loop stator voltage controller

In the converter control reference frame phasor diagram, given in figure 4.13, the stator voltage magnitude is given by;

$$|u| = E \cos \delta + X i_q \quad (4.25)$$

Since the P and Q control is decoupled, δ is dictated by the active power transfer while internal emf, E is dictated by the rotor speed. Therefore both E and δ are constants. The only possibility of controlling the stator voltage is by controlling i_q . Linearising equation 4.25, results in equation 4.26, which defines the system transfer function. Here X is the synchronous reactance of the PMSG.

$$\Delta |u| = x \Delta i_q \quad (4.26)$$

As per [77], the inner current transfer function is replaced by a simple time delay of $T_{eq} = 2T_a$. The resulting control block diagram for the stator voltage control loop is given in figure 4.25. The control requirement for outer loop, is for its response to be approximately 10 times slower than the inner control loop. K_p is chosen such that the open loop cross over frequency is $(180/10) = 18$ rad/s. T_i is chosen to cancel the pole of the transfer function. The bode plot for the open loop transfer function given in figure 4.26, confirms inherently stable system with cross over frequency of 15 rad/s. The time response of the system to a step in current input, illustrated in figure 4.27, shows a settling time of 400 ms. The settling time for power controller being 250 ms and settling time for inner current being 20 ms, the design objectives are realized. The calculated controller parameters are given in table 4.4.

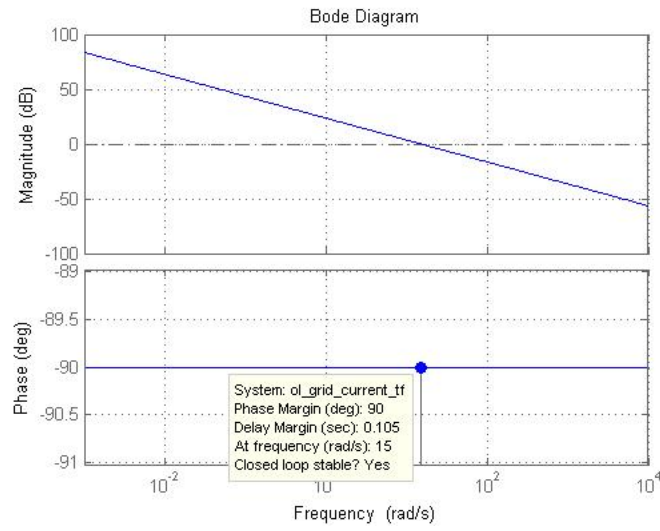


Figure 4.26: Generator stator voltage controller open loop bode plot

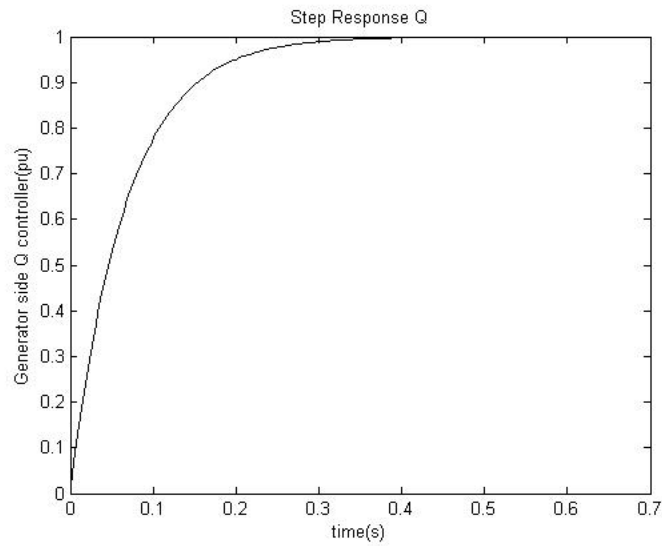


Figure 4.27: Generator stator voltage controller step response plot

Parameter	value (pu)
K_p	0.05
$T_i(\tau)$	47.8 s
T_{eq}	5 ms

Table 4.4: Calculated parameters of the outer loop controller

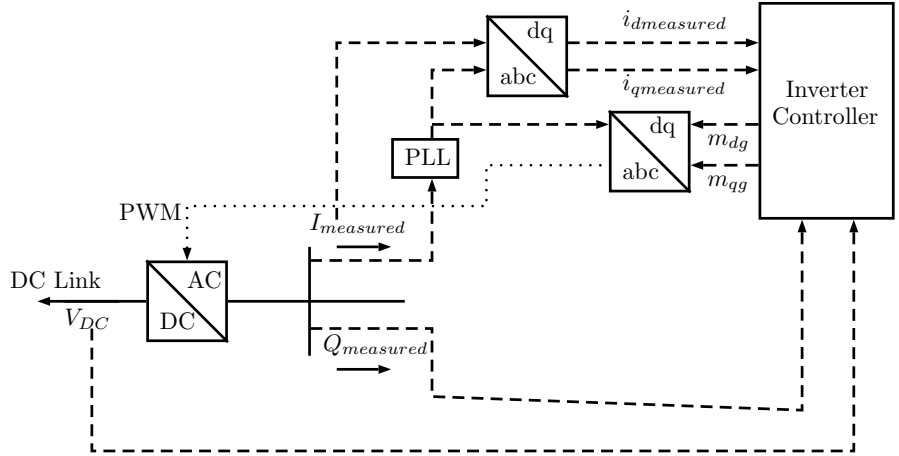


Figure 4.28: Inverter controller configuration diagram

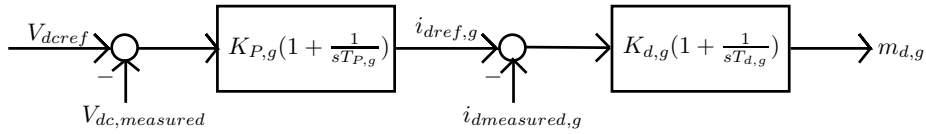


Figure 4.29: Inverter DC voltage control loop

Inverter Controller

As shown in figure 4.4 the inverter controller controls the grid side power frequency converter. The control objective of this controller is two fold.

- Control of DC bus voltage to its reference (rated) value
- Control of reactive power exchange with grid to its reference value (initial value)

The figure 4.28 shows a detailed configuration diagram, illustrating the structure of the inverter control system. As per equations 4.9 and 4.10 the inverter active power can be controlled by controlling the d-axis current while the inverter reactive power can be controlled by controlling the q-axis current.

The block diagram in figure 4.29 is implemented to achieve the first control objective. It consists of an outer DC voltage control loop and an inner d-axis current control loop. The block diagram in figure 4.30, is used to achieve the second control objective. It consists of an outer reactive power control loop and an inner q-axis current control loop. As illustrated by the inverter

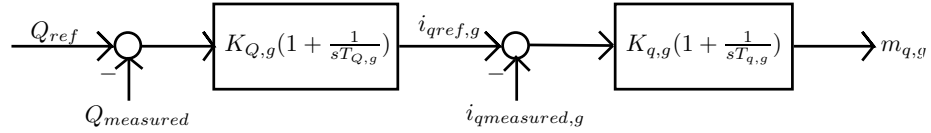


Figure 4.30: Inverter reactive power control loop

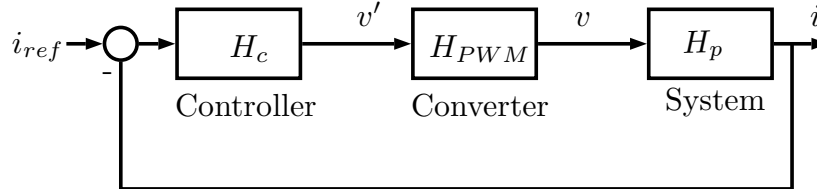


Figure 4.31: Control block diagram for inner current control loop

controller configuration diagram, the required inputs to the controller are, grid reactive power, DC bus voltage, inverter current and the voltage angle.

Inner current loop tuning

The control block diagram for grid side control inner current loop is given in figure 4.31. The single line diagram given in figure 4.32, explains the notations used for derivation of the transfer functions. For the above grid side converter scheme in dq grid voltage oriented reference frame, the converter voltages are derived by writing the voltage balance equations across the filter impedance. Converter d-axis and q-axis voltage is given by equations 4.27 and 4.28 [32].

$$v_{d1} = (Ri_d + L \frac{d}{dt} i_d) - \omega_s L i_q + v_d \tag{4.27}$$

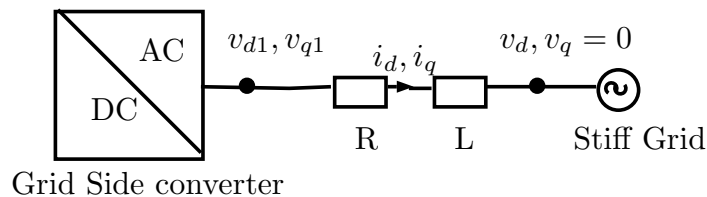


Figure 4.32: SLD for grid side converter interface

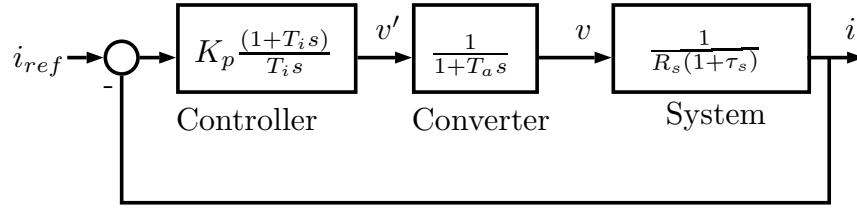


Figure 4.33: Transfer function for inner current control loop

$$v_{q1} = (Ri_q + L \frac{d}{dt} i_q) + \omega_s L i_d \quad (4.28)$$

$$H_p = \frac{i_d}{v_d} = \frac{1}{r(1 + \tau s)} \quad (4.29)$$

Converting the voltages from time domain to laplace domain, with the cross coupling terms viewed as a disturbance from control point of view, the system transfer function is given by equation 4.29. Here $\tau = L/R$. The same transfer function applies for the q-axis controller, since the parameters are identical.

Controller

Conventional design techniques are used to calculate the controller parameters. The form of the PI controller given in equation 4.30 is applied.

$$H_c = K_p \frac{(1 + T_i s)}{T_i s} \quad (4.30)$$

Converter

Converter is modelled as a delay of T_a , with its transfer functions given by equation 4.31.

$$H_{PWM} = \frac{1}{1 + T_a s} \quad (4.31)$$

System

The system open loop transfer function $H_{OL} = H_c H_{PWM} H_p$ is given by equation 4.32.

Parameter	Value
Filter resistance r	0.01 pu
Filter reactance X_s	0.1 pu
Switching frequency	1 kHz
Measurement delay	2 ms

Table 4.5: Grid Parameters for controller tuning

Parameter	value (pu)
K_p	0.2
$T_i(\tau)$	0.1 s
T_a	2.5 ms

Table 4.6: Parameters for inverter current controller

$$H_{OL} = \frac{K_p(1 + T_i s)}{T_i s(1 + T_a s)R_s(1 + \tau)} \quad (4.32)$$

The controller is tuned using the modulus optimum criteria [77] given in equation 4.33. The grid parameters and switching delay of the converter is given in table 4.5. The controller parameters are calculated and presented in table 4.6.

$$T_i = \tau \text{ and } K_p = \frac{\tau R}{2T_a} \quad (4.33)$$

The bode plot for the open loop transfer function given in figure 4.34 confirms stable operation with a cross over frequency of 180 rad/s and phase margin of 65 degrees. The time response of the controller, to a step in current input illustrated in figure 4.35, shows a settling time of 20 ms.

DC voltage controller

For stable operation of converter, the DC link voltage is required to be held constant. Further this ensures the power balance. The power balance assuming negligible power losses is presented in equation 4.34. According to this equation, grid side converter d-axis current component, is directly proportional to the active power transfer, when DC link voltage is held constant. Balance

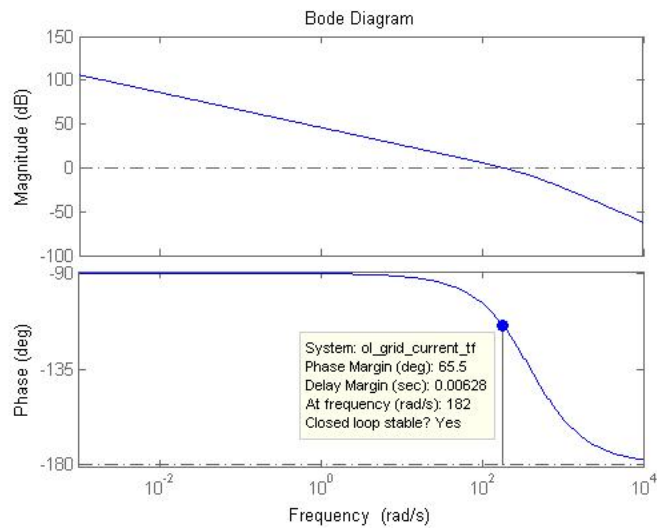


Figure 4.34: Inverter current controller open loop bode plot

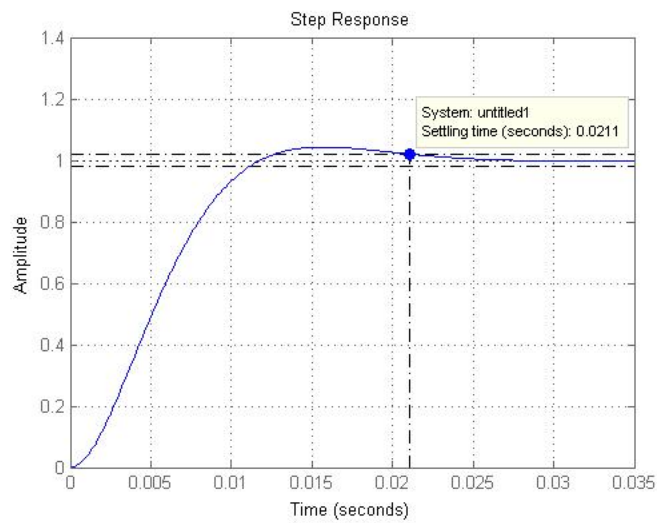


Figure 4.35: Inverter current controller step response plot

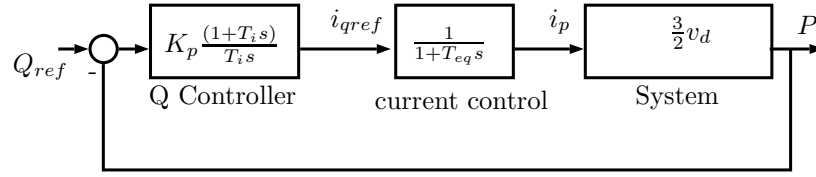


Figure 4.36: DC voltage control loop block diagram

of power transfer from DC link to AC grid is given by equation 4.34.

$$P = v_{dc} i_{dc} = \frac{3}{2} u_d i_d \quad (4.34)$$

Applying Kirchoffs current law to the capacitor node gives equation 4.35. Where v_{dc} , i_{dc} and C denotes DC link voltage, DC current and the DC link capacitance.

$$i_{dc} - i_L = C \frac{d}{dt} v_{dc} \quad (4.35)$$

Substituting for the value of i_{dc} from equation 4.34 to equation 4.35, gives equation 4.36.

$$\frac{3}{2} \frac{u_d i_d}{v_{dc}} - i_L = C \frac{d}{dt} v_{dc} \quad (4.36)$$

Equation 4.37, derived by linearising equation 4.36 around the rated point of operation, results in equation 4.37. Here Δi_L is a disturbance in the control point of interest.

$$C \frac{d}{dt} \Delta v_{dc} = \frac{3}{2} \frac{v_{d,0} \Delta i_d}{v_{dc,ref}} \quad (4.37)$$

The value of v_d and v_{dc} at point of linearising is $v_{d,0}$ and $v_{dc,ref}$. The transfer function from v_{dc} to i_d is given by equation 4.38.

$$\frac{\Delta v_{dc}}{\Delta i_d} = \frac{3}{2} \frac{v_{d,0}}{v_{dc,ref} C s} \quad (4.38)$$

The DC voltage control outer loop is given in figure 4.36. The inner current loop is replaced by a first order transfer function [77] ($T_{eq} = 2T_a$). Using symmetric optimum tuning criteria [77], ($a = 3$ and $T_c = X_c$) results in equations 4.39, 4.40 and 4.41.

Parameter	value (pu)
K_p	6.67
$T_i(\tau)$	0.045 s
T_{eq}	5 ms

Table 4.7: DC voltage control loop parameters

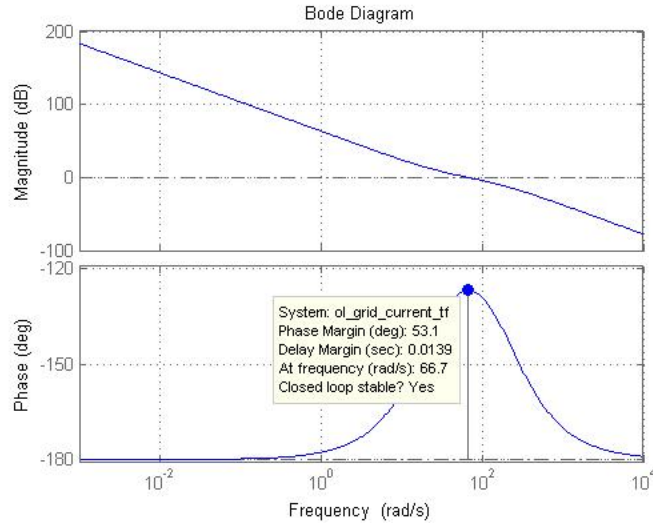


Figure 4.37: DC voltage outer control open loop bode plot

$$T_i = a^2 T_{eq} \quad (4.39)$$

$$K_p = \frac{T_c}{aKT_{eq}} \quad (4.40)$$

$$H_{OL} = \frac{K_p K (1 + T_i s)}{T_i s (1 + T_{eq} s)} \frac{3}{2Cs} \quad (4.41)$$

The open loop transfer function for this system is given by equation 4.41. The calculated controller parameters are given in table 4.7. The bode plot for the open loop transfer function, given in figure 4.37, confirms stable operation with a cross over frequency of 67 rad/s and phase margin of 53 degrees. The time response of the system to a step in current input, presented in figure 4.38 shows a settling time of 200 ms. The outer loop is approximately 10 times slower

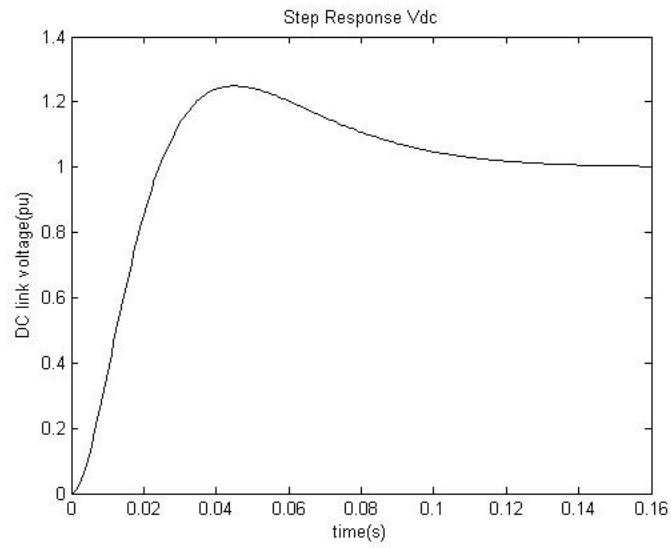


Figure 4.38: DC voltage outer control loop step response plot

compared to the inner current loop.

Parameter	value (pu)
K_p	0.1
T_i	5 ms

Table 4.8: Grid reactive power controller parameters

Reactive power controller

In the converter control reference frame reactive power is given by [32] equation 4.42.

$$Q = \frac{3}{2} u_{sd} i_{sq} \quad (4.42)$$

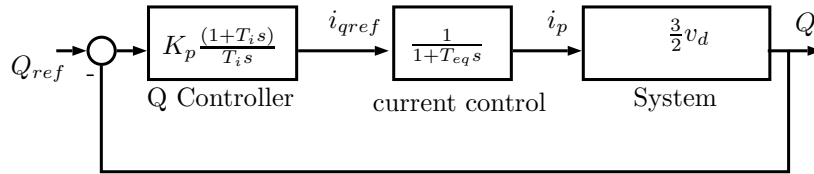


Figure 4.39: Reactive power control block diagram

As per [77], the inner current transfer function is replaced by a simple time delay of $2T_a$. The resulting control block diagram for the reactive power control loop is given in figure 4.39.

The control objective for the reactive power controller is to be 10 times slower than the inner control loop. K_p is chosen such that the open loop cross over frequency of the power loop is 10 rad/s. T_i is chosen to cancel the pole of the transfer function. The calculated controller parameters using this method are given in table 4.8. The bode plot for the open loop transfer function given in figure 4.40, confirms stable operation with a cross over frequency of 67 rad/s and phase margin of 53 degrees. The time response of the system to a step current input presented in figure 4.41, shows a settling time of 500 ms, giving a satisfactory 10 times slower response compared to the inner current loop.

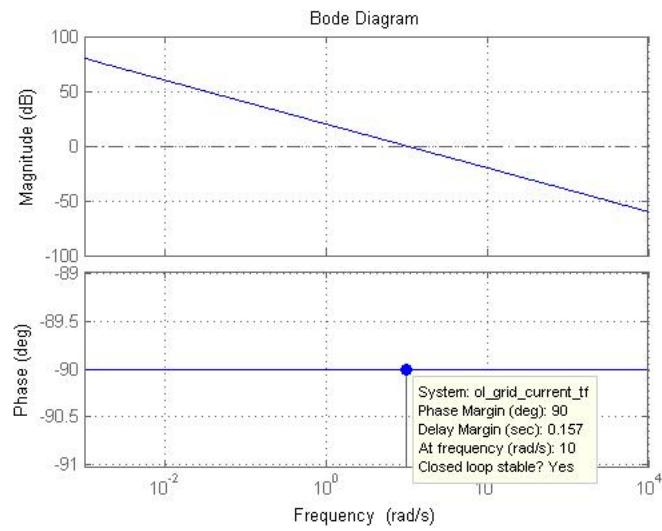


Figure 4.40: Grid reactive power open loop bode plot

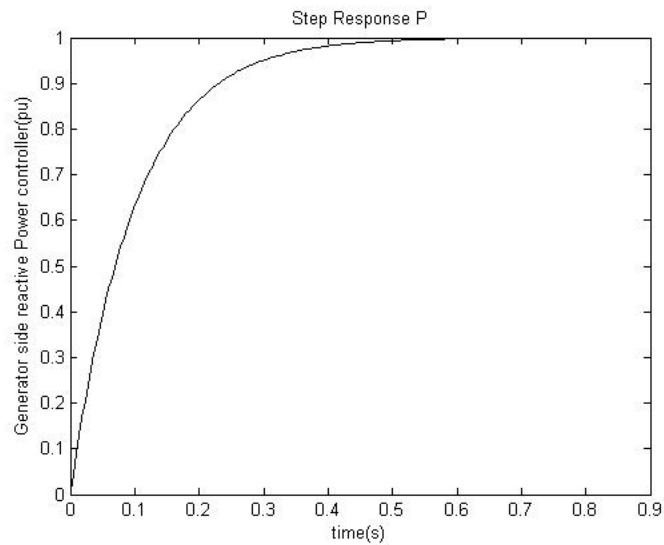


Figure 4.41: Grid reactive power step response

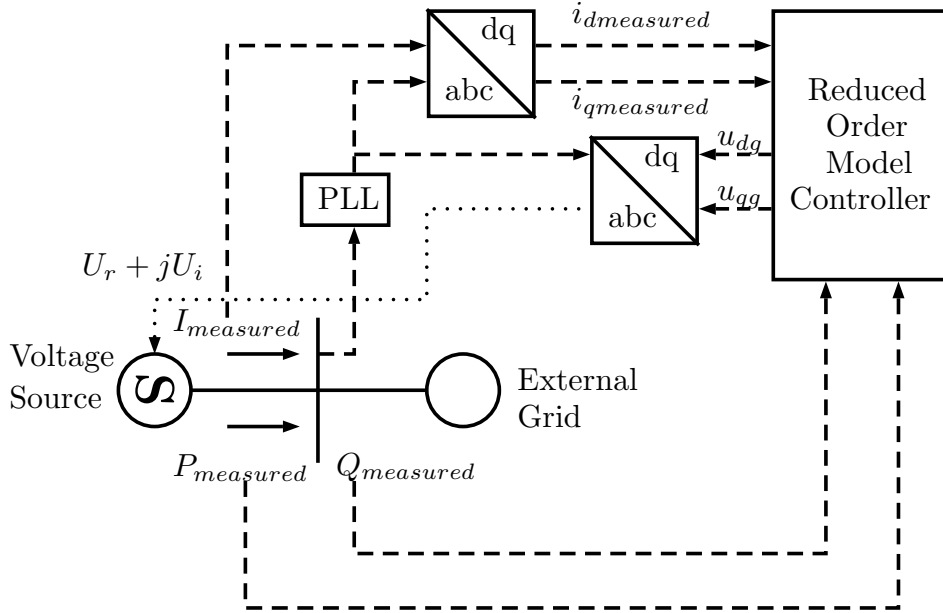


Figure 4.42: Reduced Model Electrical control structure

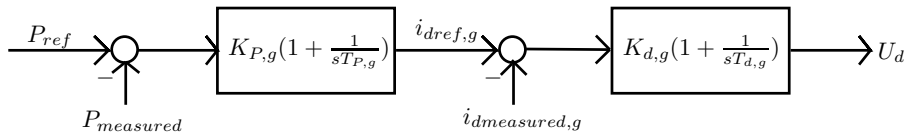


Figure 4.43: Reduced order model active power control loop

4.3.3 Reduced Order Model Electrical System

The reduced order model structure is given in figure 4.5. This figure illustrates the interface and the interaction between the mechanical system and the electrical system. A more detailed structure of the electrical system including input output signals is given in figure 4.42. The PMSG, generator side converter and DC link, is replaced by a thevenin equivalent voltage source. Since the DC-link fully decouples the PMSG from the grid, this is a valid assumption. As shown in figure 4.42, the controlled parameter is the thevenin equivalent voltage ($U_r + jU_i$).

The inner current loop controller and its parameters are identical to the full order model inverter current controller, which was addressed in detail in the section 4.3.2. Therefore it will not be repeated in this section. The reactive power outer loop is similarly identical to the full model inverter reactive power loop which was addressed in the section 4.3.2. The only control loop yet to be analysed and controller parameters calculated, is the active power control outer

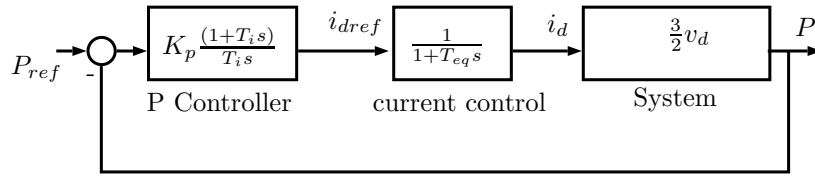


Figure 4.44: Reduced order model active power loop block diagram

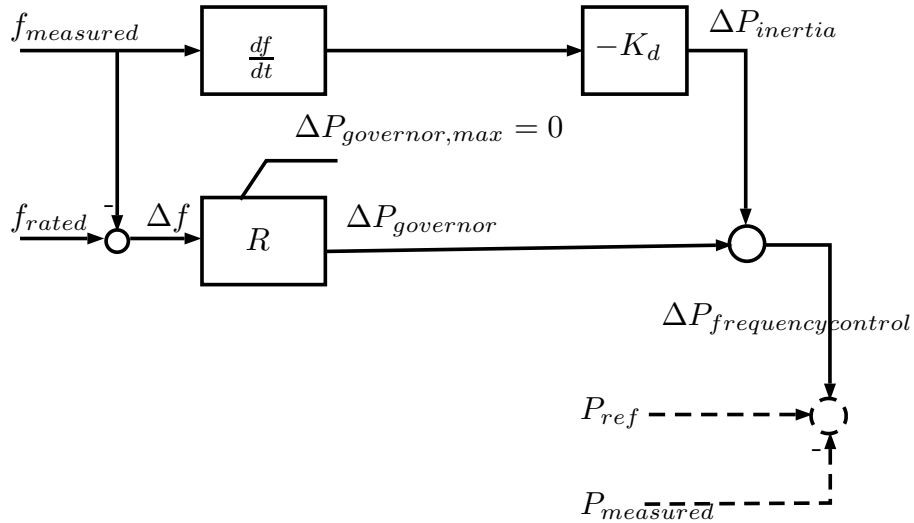


Figure 4.45: Auxiliary control loop for frequency control

loop. However, the structure of this control loop is similar to the full model inverter reactive power outer loop analysed in the section 4.3.2, when the reactive power is replaced by active power and q-axis current by the d-axis current. The reduced model active power outer loop is presented in 4.43. The control block diagram for the outer active power loop is given in figure 4.44. The controller parameters are identical to the parameters of the inverter reactive power controller.

4.4 Wind Turbine Frequency Control

Unlike classical synchronous generators, fully rated converter interfaced wind turbines do not naturally provide inertial or governor support. The simplest way to provide frequency control [41] is to add an auxiliary control loop to the active power controller. Since governor action follows a droop characteristic it can be modelled as a deduction of active power, proportional

to the frequency deviation. Since the wind farm is already assumed to be operating at maximum power, it only responds to over frequency events and supports the grid by decreasing its production. System inertia is emulated by injecting active power proportional to the rate of change of frequency. The auxiliary control loop for frequency control used in this work is given in figure 4.45. The existing parts of the active power control loop is given in dash lines while the added auxiliary control loop is given in solid line. The governor action constant R , is referred to as the wind farm governor droop while the inertial action constant K_d , is referred to as the wind farm (synthetic) inertia (emulation) constant. The frequency control auxiliary loop $\Delta P_{frequencycontrol}$, is augmented to the active power control loop to provide the wind farm with frequency support. In the reduced order model, it is inserted to the grid active power control loop, while in the full order model, it is inserted to the generator side converter active power control loop.

Chapter 5

Simulation Study

5.1 Power System under study

The Kundur's two area network [12] given in figure 1.1 is the power system used for this study. The single line diagram of this system is given in figure 5.1. The numbers in the power system component name describes the nodes they are connected to or connected between. The base system is symmetric across bus 8 and consists of two areas connected with a weak tie line. Synchronous generators G1 and G2 consists of the area 1 and G3 and G4 consists of the area 2. G1 and G2 have identical parameters to G3 and G4. The generator voltage is converted to transmission voltage by the generator transformers given as T1-5, T2-6. A 25 km length transmission lines given by L5-6, connects the generators in the same area. Bus 6 is connected to bus 7 via a 10 km transmission line. At bus 7, load L7 and capacitor bank C7 is connected. The capacitor bank is connected to the bus 7 to ensure appropriate system voltage profile. Bus 7 is connected

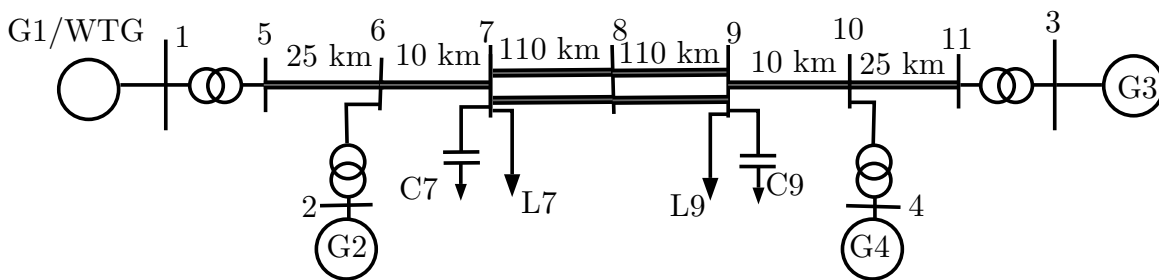


Figure 5.1: Single line diagram of power system under study - Kundur's two area network [12]

Table 5.1: Initial state of the power system

Component	Active Power(MW)	Reactive Power (MVar)
G1/WTG	360	-19
G2	360	-42
G3	378	-16
G4	360	-160
L7	-720	100
L9	-720	100

to bus 9 via double transmission lines. All transmission lines in this study are of similar type. Area 2 is of similar structure to area 1. The parameters of these power system components are given in the appendix A.

If a large system is used, it would be difficult to understand and examine the factors that influence system dynamics. Though this power system is small it uses realistic parameters. Further the base system has one inter area mode and two local area modes. The local area modes are not investigated in this study. The inter area oscillations will however be investigated. The 3 GW system with a low value of machine inertia and slow turbine governors creates significant frequency variations in the system. This supports the system frequency control studies that are executed. Being less complex and realistic while providing a similar dynamic behaviour as a complex system motivated the use of Kundur's two area network for this study.

The variations to the study case consists of replacing Generator 1 with a full order model of a wind farm and replacing Generator 1 with a reduced order model of a wind farm. The system is operated at approximately 50% of capacity, in order to be able to change system loads by wide margins. The same parameters for the hydro-governor (HYGOV) and AVR (SEXS) is applied on the synchronous generator and kept unchanged throughout the simulation study. A summary of the steady state condition, from which the dynamic simulation is initialised, is given in table 5.1.

5.2 Power System Simulations

The Digsilent powerfactory power system simulation program [78] is used for carrying out the simulations. The first step in a dynamic simulation is to find the initial condition for the system.

A power flow calculation is conducted to find the initial values of most of the system variables. G3 is modelled as the slack bus while the other synchronous generators are modelled as PV busses. The wind farm operates as a PQ bus. The initial values for the mechanical models are manually entered, while ensuring that the mechanical steady state values match with the electrical steady state values obtained from the load flow calculations. The small signal stability study is carried out using the modal analysis package of Digsilent powerfactory. The calculation algorithm used is the QR method [79]. The dynamic studies are conducted with a time step of 10 ms.

Initial simulations are conducted for a system consisting only of synchronous generators, to set up the base case for comparison. Next, simulations are done with wind farm full order model and reduced order model with out frequency control. It is followed by simulations, where wind farm is supported by frequency control. The final set of simulations, are focused on modal analysis, to gauge the system small signal stability for these different scenarios.

5.3 Model Validation

According to the control objectives, the expected operation of the wind farm with increasing wind speed and decreasing wind speed is as follows. As wind speed increases, the turbine speed increases, following the maximum point tracking algorithm. Once the turbine speed has increased to its maximum, the pitch controller activates to curtail the turbine speed to its maximum limit. When the wind speed decreases from this high value, the pitch angle is reduced till zero and the wind farm power output starts following the maximum point tracking curve.

The model is validated by testing the simulation response for a measured wind speed sequence for 300 seconds time duration from [72]. The term validation, in this context refers to observing if the model's actual response matches with the expected response. In this simulation case, frequency control is disabled ($K_d = 0$, $R=0$).

5.3.1 Full Order Model

The figure 5.2 validates, successful operation of the pitch controller to limit the wind farm maximum power output and speed by controlling the pitch angle. The figure 5.3 shows that the active

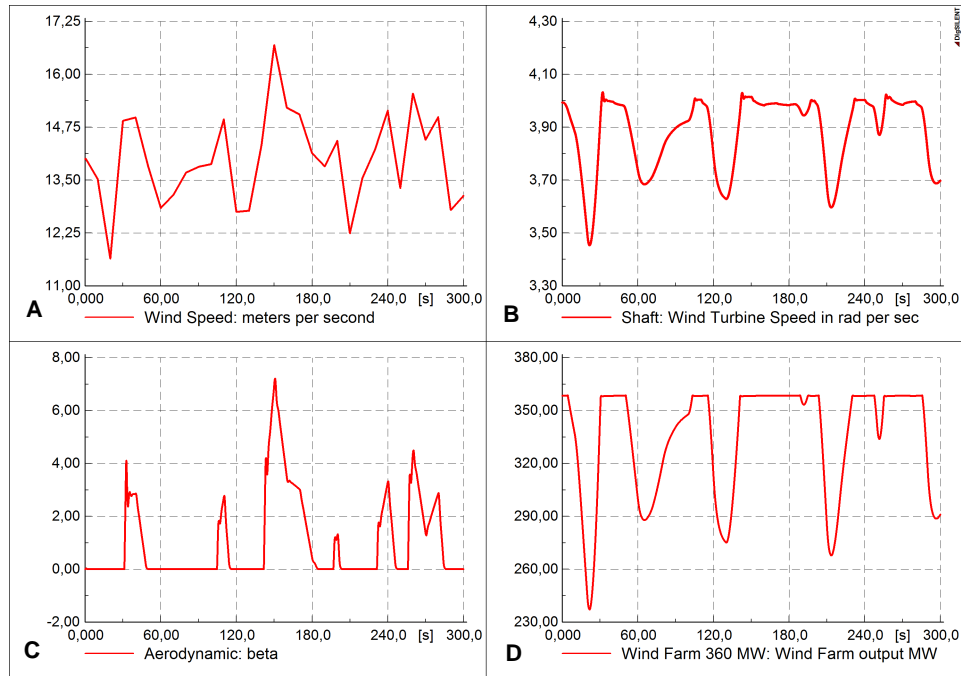


Figure 5.2: Validation of the full model mechanical system response, subplot A - wind speed(ms^{-1}) variation, subplot B - wind turbine speed (rads^{-1}) variation, subplot C - pitch angle (β - degrees) variation, subplot D - wind farm electrical output (MW) variation

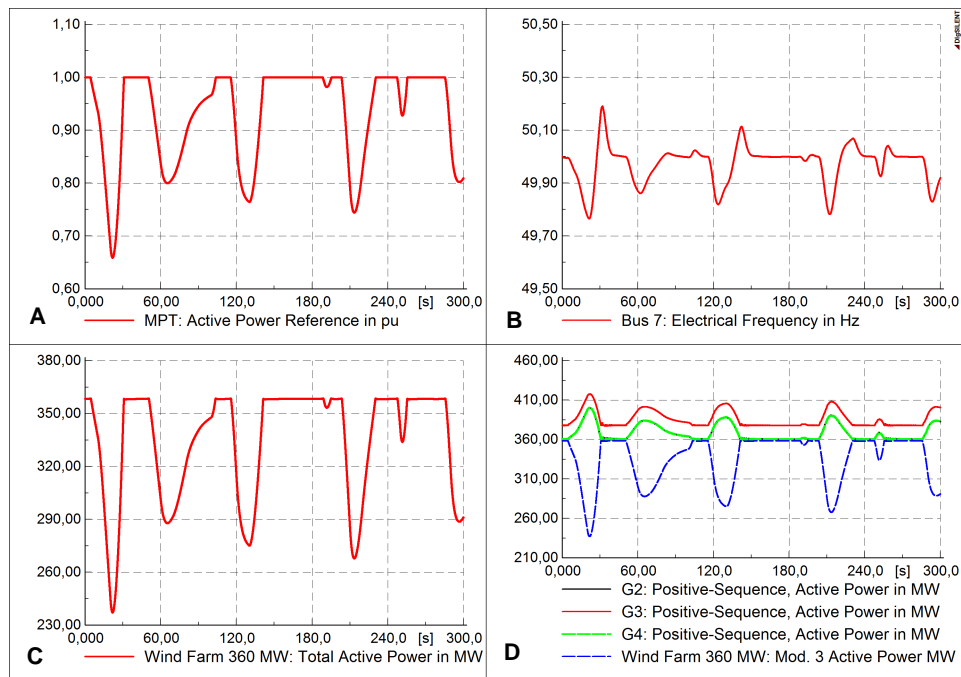


Figure 5.3: Validation of the reduced model electrical system response, subplot A - reference power set point (MW) generated by the maximum power point tracking scheme, subplot B - system frequency measured at bus 7 in Hz, subplot C - wind farm electrical output (MW), subplot D - all generator active power output (MW) variation

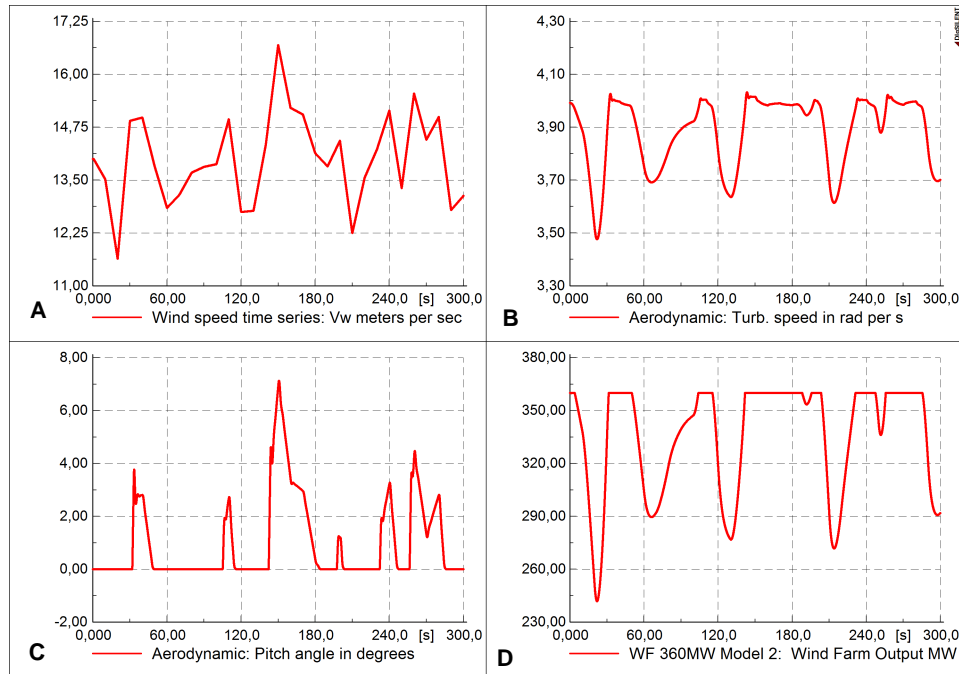


Figure 5.4: Validation of the reduced model mechanical system response, subplot A - wind speed ($m s^{-1}$) variation, subplot B - wind turbine speed ($rad s^{-1}$) variation, subplot C - pitch angle (β - degrees) variation, subplot D - wind farm electrical output (MW) variation

power reference follows the MPT scheme while the actual active power output strongly follows its reference value. Therefore, the full order model is validated.

5.3.2 Reduced Model

The figure 5.4, validates successful operation of the pitch controller to limit the wind farm maximum power output and speed by controlling the pitch angle. The figure 5.5, validates successful operation of the maximum point tracking scheme. Since the system response matches the expected response and the full order model response, the reduced order model for is validated.

Observations

The operation of the synchronous generator's turbine governor system to control system frequency is evident from figure 5.5. The reason for the significant variations in frequency is the variable power output from the wind farm. The system requires much faster turbine governor systems than the very slow hydro governor systems that are installed, to reduce the effect of

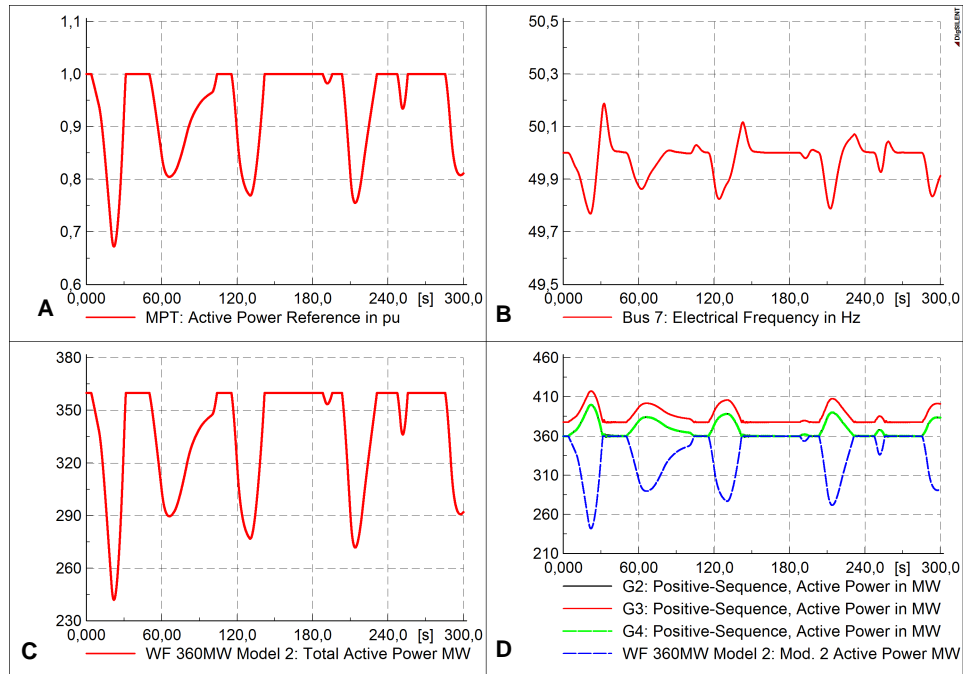


Figure 5.5: Validation of the reduced model electrical system response, subplot A - reference power set point (pu) generated by the maximum power point tracking scheme, subplot B - system frequency measured at bus 7 in Hz, subplot C - wind farm electrical output (MW), subplot D - all generator active power output (MW) variation

connecting this wind farm.

5.3.3 Comparison of Model Dynamic Response

A comparison of the active power response with same wind sequence between the full model and reduced model is given in figure 5.6. The turbine speed response, pitch controller response and power response compare and match against each other as observed in figure 5.7. The plots show that the response from the two models are similar.

The effect of each of the models on the other generators is compared in figure 5.8. The system generators power response and system frequency response, compare and overlap against each other as observed in figures 5.8 and 5.9.

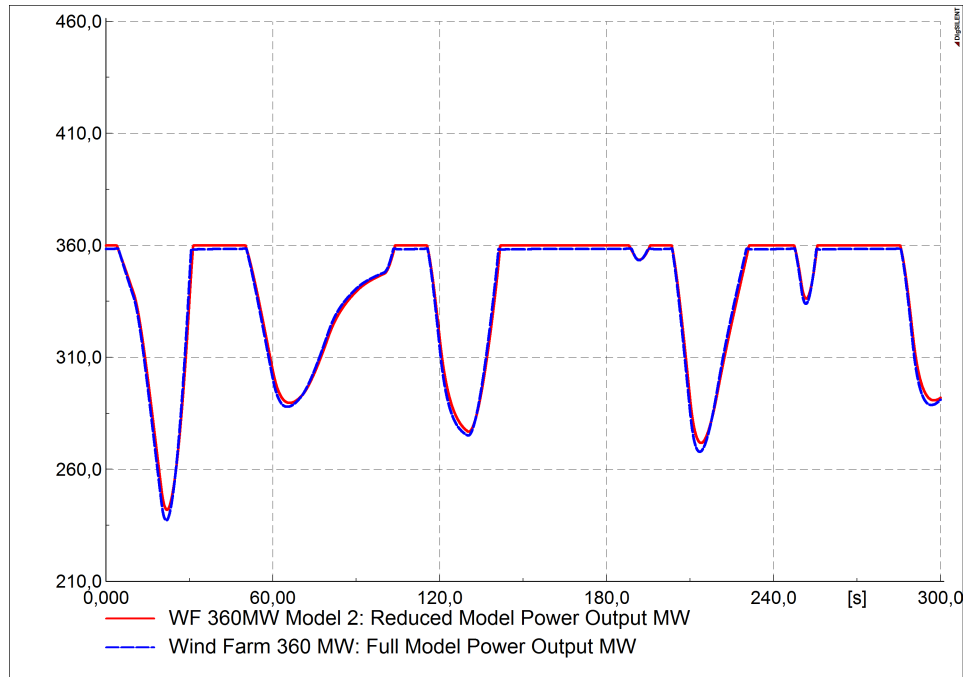


Figure 5.6: Reduced Model and full model output power comparison

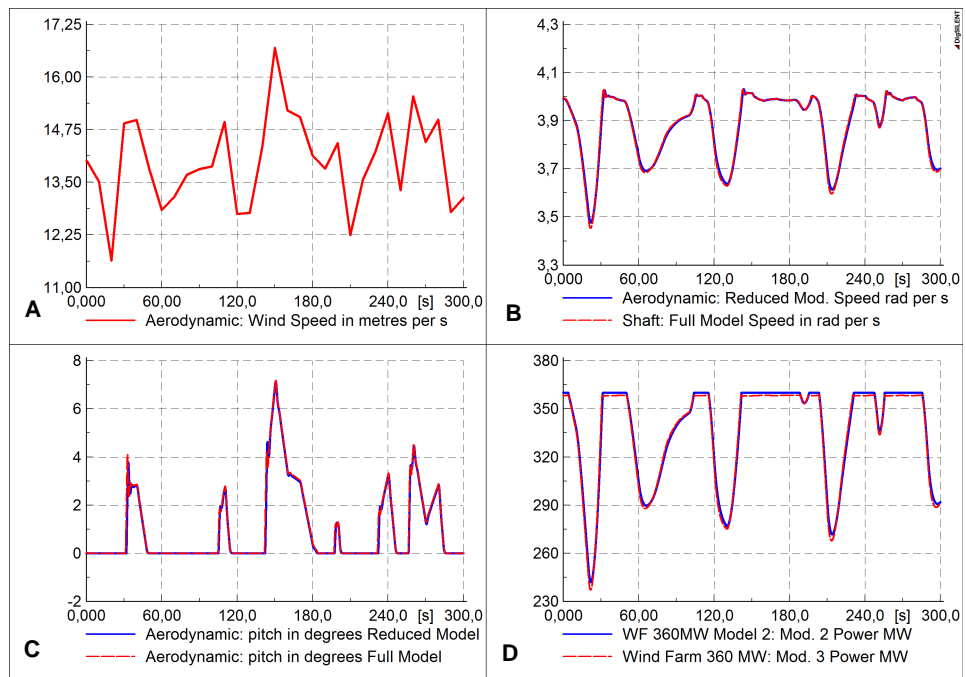


Figure 5.7: Comparison of Mechanical response between full model and the reduced model, subplot A - wind speed(ms^{-1}) variation, subplot B - wind turbine speed ($rads^{-1}$) variation, subplot C - pitch angle (β - degrees) variation, subplot D - wind farm electrical output (MW) variation

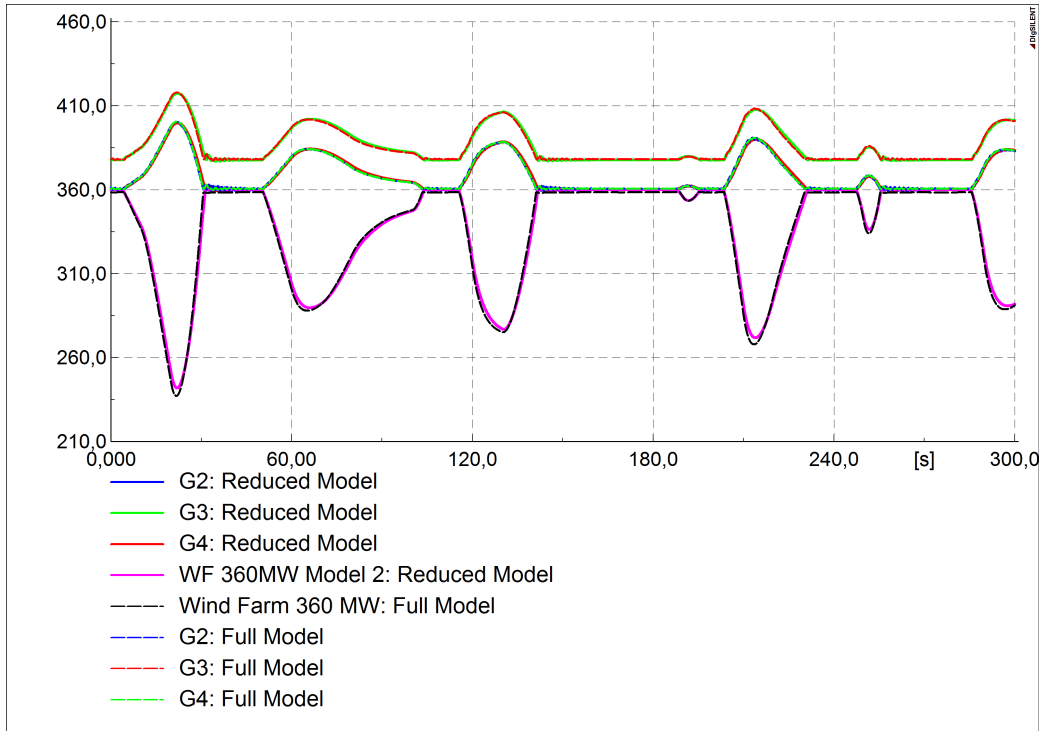


Figure 5.8: Reduced Model and full model generator active power (MW) comparison

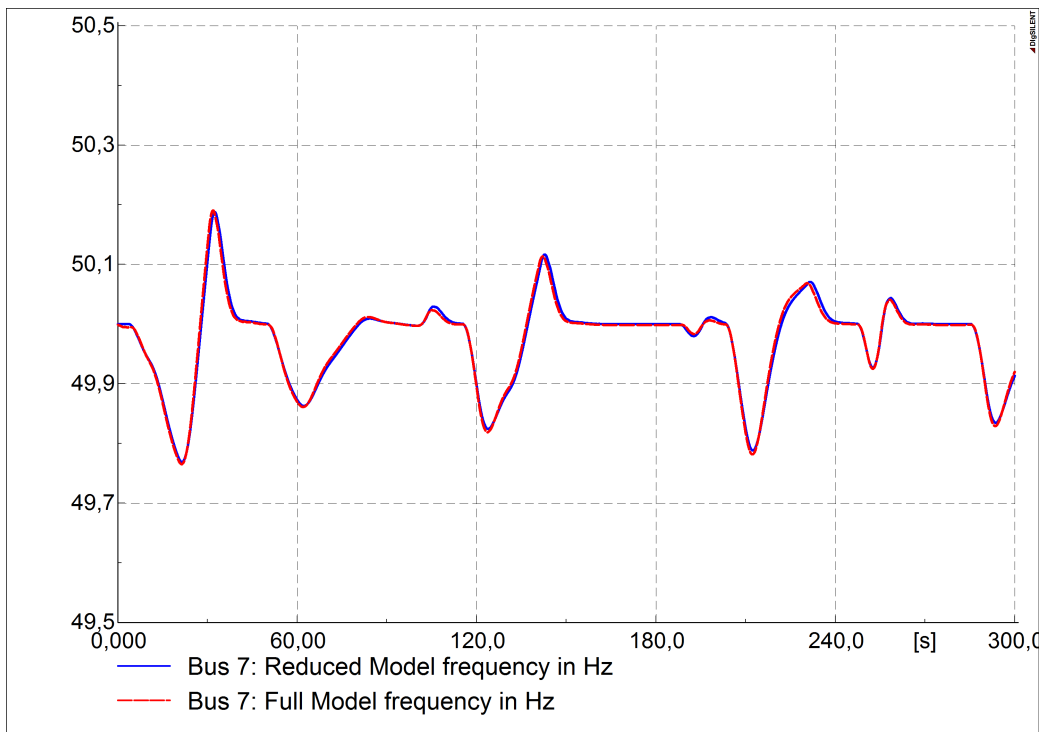


Figure 5.9: Reduced Model and full model system frequency (Hz) response comparison

Table 5.2: Comparison of poorly damped eigen values (without frequency control)

Name	Real Part (1/s)	Im. Part (rad/s)	Damped Frequency (Hz)	Damping Ratio
Sync. Gen Model : λ_{17}	-0.054	3.69	0.59	0.015
Red. Model : λ_{20}	-0.10	3.97	0.63	0.026
Full Model : λ_{34}	-0.11	4.23	0.67	0.025

5.3.4 Comparison of Small Signal Response (without frequency control)

The poorly damped eigen values, extracted from the modal analysis conducted separately, with the results for synchronous generator, wind farm full order model and wind farm reduced model, is given in table 5.2. All eigen values have negative real values. Therefore the system is small signal stable. In this simulation the wind farm is without frequency control. Only one eigen value is poorly damped. It represents an inter area mode as observed from the time domain response. The first important observation is that, the eigen modes are identical for both wind farm models. The second important observation is that substituting the wind farm for the synchronous generator G1, has almost doubled the of the damping ratio of the inter-area mode. The system small signal stability is enhanced with the wind farm.

The time domain response to a small perturbation applied to the system with reduced model and full model is given in figure 5.10. Inspection shows a clear inter area mode with G2 oscillating against G3 and G4. The slight difference in the time domain response can be explained by observing the difference in the poorly damped eigen values. The full model response is slightly less damped and has a slightly higher oscillation frequency. In this system by using the reduced model, more optimistic results are obtained.

However the deviations are minor and can be considered negligible. Since transient response and small signal response for both models are identical, it is safe to use a reduced order model without sacrificing a significant level of model accuracy in a power system transient study. However, the analysed wind farms in this case, do not have frequency control.

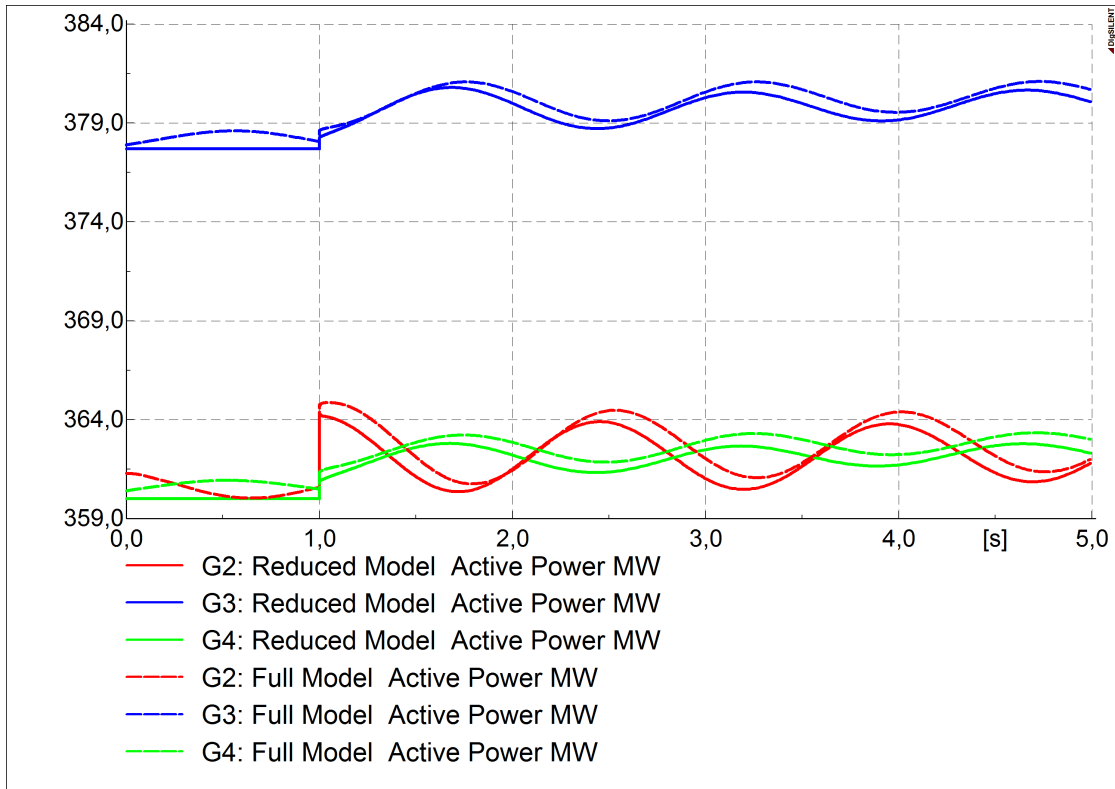


Figure 5.10: Comparison of Small Signal Response

5.4 Case Study : Governor action and inertia emulation

5.4.1 Introduction

This section provides an insight in to how a wind turbine generator can provide frequency support to a small network. This simulation is not a general case and is meant to *highlight* and explain the benefits of providing frequency control (inertial and primary support services) from the interconnected wind farm to the small grid. The reduced model is used for the simulations.

In this case study, wind farm inertia constant, K_d is set at 100 and wind farm governor droop constant, R is set at 50. An over frequency event is simulated by decreasing the active power of the load L7 by a step of 360 MW. According to the mechanical system response for this event given in figure 5.11, a transient oscillation in the wind turbine speed is observed. This is a stress on the turbine mechanical system. Further, since the drive train is a single mass model this effect will be larger in a real system. The stress impulse on the drive shaft due to providing inertial response is needed to be studied in more detail before implementing inertial response

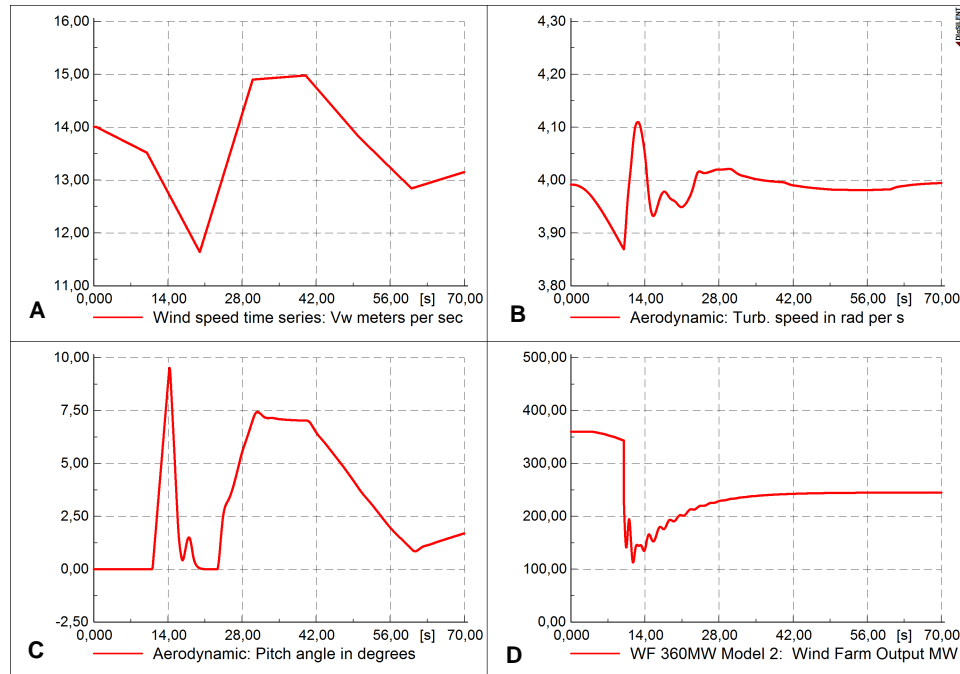


Figure 5.11: Wind farm mechanical system response for over frequency event : Case Study; subplot A - wind speed(ms^{-1}) variation, subplot B - wind turbine speed (rads^{-1}) variation, subplot C - pitch angle (β - degrees) variation, subplot D - wind farm electrical output (MW) variation

in an actual WTG. The wind farm output drops down by 115 MW from 360 MW to 245 MW, 35 seconds after the load event and settles down at that value. The wind farm is now operating in droop mode and contributing to frequency support of the system. All machines have dropped production to 245 MW except the reference machine.

The response from the frequency control control loop is given in figure 5.12. The sub plot A is the Bus 7 frequency variation in Hz, sub plot B is the output of the inertial control loop in pu, sub plot C is the output from the governor response control loop in pu and sub plot D is the summation of sub plot C and B. Sub plot D gives the total contribution from the supplementary controller. Maximum contribution of the inertia controller is -0.517 pu and it decays to 0 in 10 seconds. The governor response has a maximum value of -0.532 pu and decays to 0 at -0.321 pu. The maximum power de-rated, due to primary response is -0.617 pu. The system regains steady state approximately 35 seconds after occurrence of the event. The power of the generators (except reference machine), and wind farm settles at 245 MW dropping down to 115 MW from the initial 360 MW.

In order to highlight the benefit of integrating primary support services to the wind farm, the

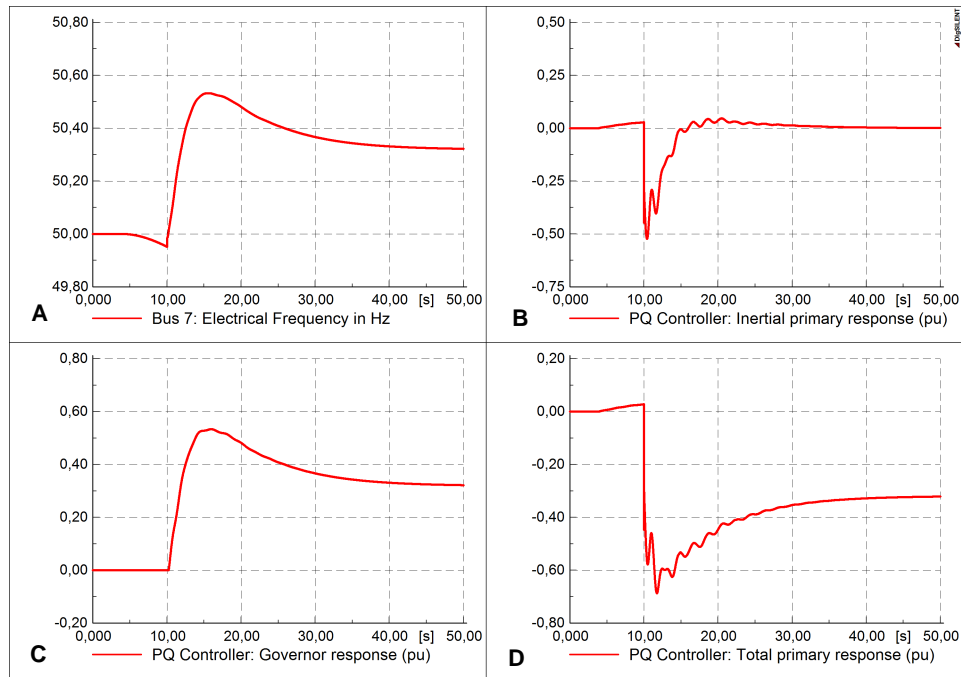


Figure 5.12: Primary response emulation control loop for over frequency event : Case Study

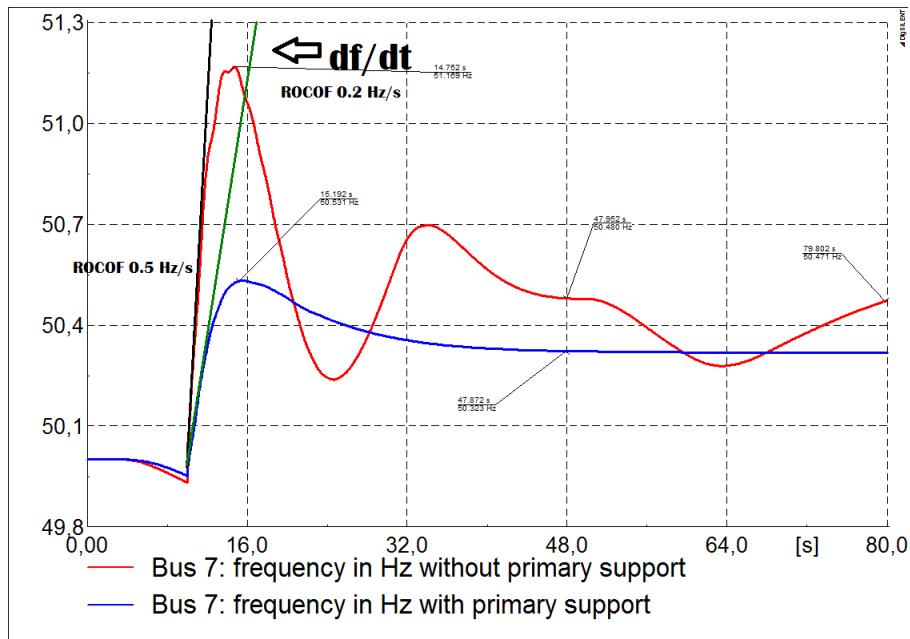


Figure 5.13: System frequency comparison

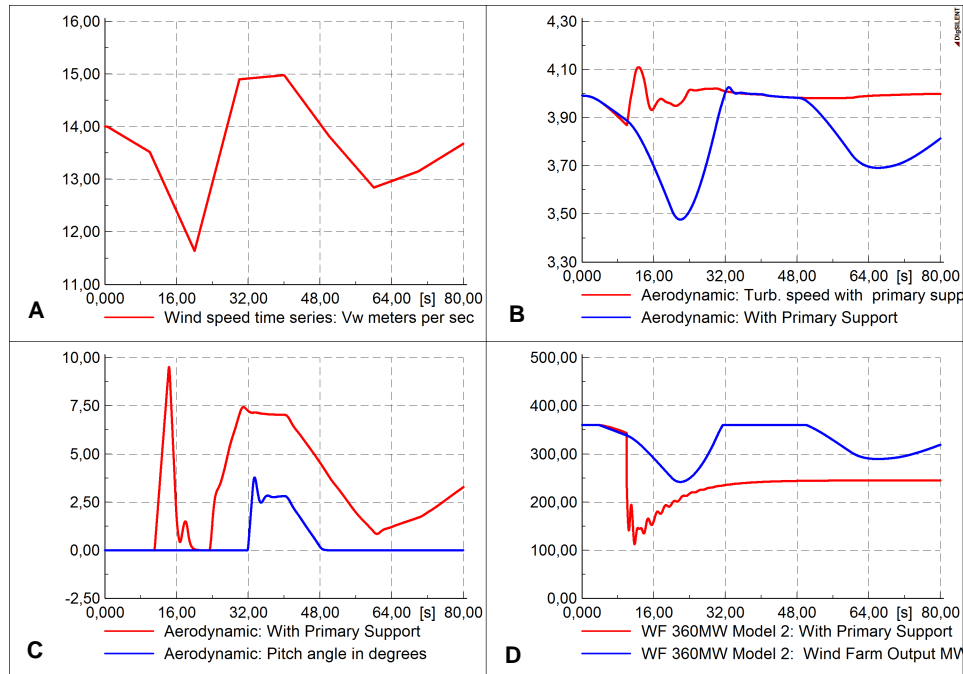


Figure 5.14: Comparison of Mechanical response between reduced model with primary support and without primary support, subplot A - wind speed ($m s^{-1}$) variation, subplot B - wind turbine speed ($rads^{-1}$) variation, subplot C - pitch angle (β - degrees) variation, subplot D - wind farm electrical output (MW) variation

frequency response for the case with frequency control and without frequency control is compared in figure 5.13. The red graph presents the instance without primary support and the blue graph with primary support. Tangents to the two curves are drawn at $t=10s$ in black and green, to present the difference in the rate of change of frequency (ROCOF). Without frequency control, ROCOF is 0.5 Hz/s . It decreases to 0.2 Hz/s when frequency control is provided. The maximum transient frequency for the case without primary support is 51.17 Hz . It decreases to 50.53 Hz when the primary support is provided. The frequency response without primary support is oscillatory and decays to a high 50.48 Hz in approximately 70 seconds after the fault. With primary support the response is smooth and damped. The system frequency settles to 50.32 Hz in approximately 40 seconds after the fault. Therefore, the system with frequency control provides much higher quality frequency response.

Figure 5.14 is a comparison of the response of the mechanical system. From sub plot C it is evident that the stress on the pitching mechanism is much higher when frequency control is implemented. Therefore, it is important to consider the possibility of the pitching system to

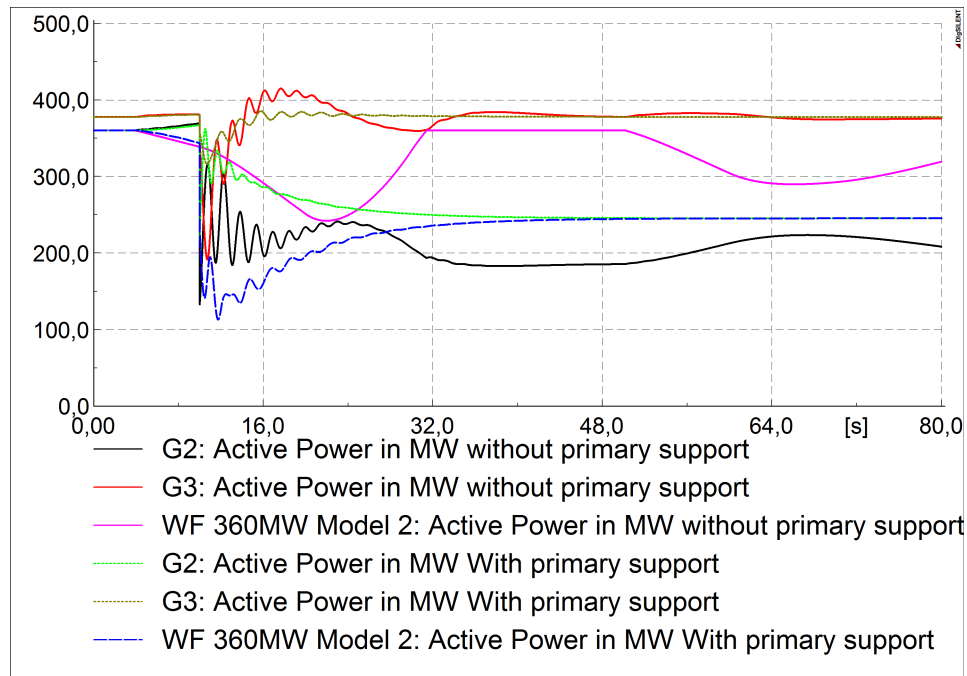


Figure 5.15: Comparison of generator active power response with and without frequency control withstand this extra stress. According to the sub plot D the wind farm operator will be operating in a de-rated mode. The area between the blue and red curves represents the total energy loss of energy due to providing frequency control. This will have financial implications which will need to be analysed in more detail.

Figure 5.15 is a comparison of the active power response of all the generators in the system. The power swings without inertia is much higher than the power swings with inertia, for all the synchronous generators. When frequency control is applied, the generators's rotor angle stability is greater and contributes to a system with better stability and well as frequency quality. This is due to the df/dt term in the primary response control loop, which acts to damp the power system oscillations. Implementing primary support in this wind farms helps to damp the power system oscillations.

It should be noted that the wind speed, in this scenario is on the high side and also that the system is chosen to magnify the benefit of integrating primary support to a wind farm. The primary response power rejection, is a significantly large 200 MW. This is however not a general case. It is a demonstration of how primary control in a wind farm operates to compensate for wind speed and load variations in a small system with wind contribution (WPR) of 25%.

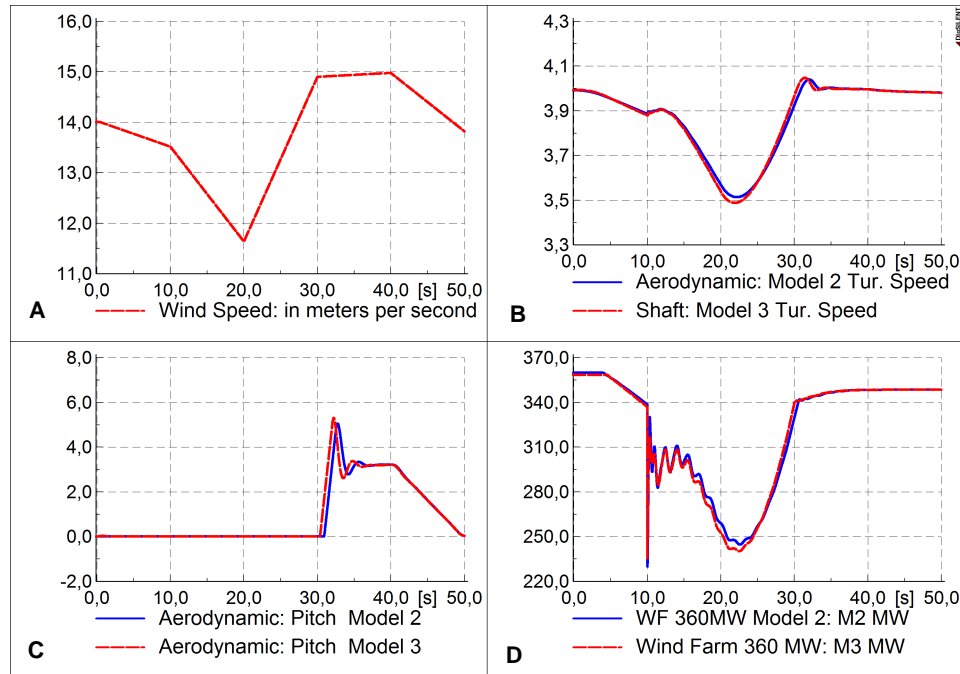


Figure 5.16: Over frequency event - Comparison of Mechanical response between reduced order model and full order model, subplot A - wind speed (ms^{-1}) variation, subplot B - wind turbine speed ($rads^{-1}$) variation, subplot C - pitch angle (β - degrees) variation, subplot D - wind farm electrical output (MW) variation

5.4.2 Over frequency event

The previous section focused on showing the benefit of having primary support using the reduced model and an over frequency event. This section compares the response of the full order model and reduced order model when primary support is applied and the system subjected to an over frequency event. The over frequency event is simulated by decreasing the load 7 active power by a step of 360 MW at $t=10$. Parameter values used for the frequency control loop are $K_d=10$ and $R=5$. The response for the two different models are examined and compared against each other.

The turbine speed response, pitch controller response and power response, compare and match with each other for both models as observed in figure 5.16. The system generator power response compare and match against each other as observed in figure 5.17. The system frequency response compare and match against each other as observed in figure 5.18. The response of both models are identical. Therefore, the reduced order model is sufficient to model the system transient response.

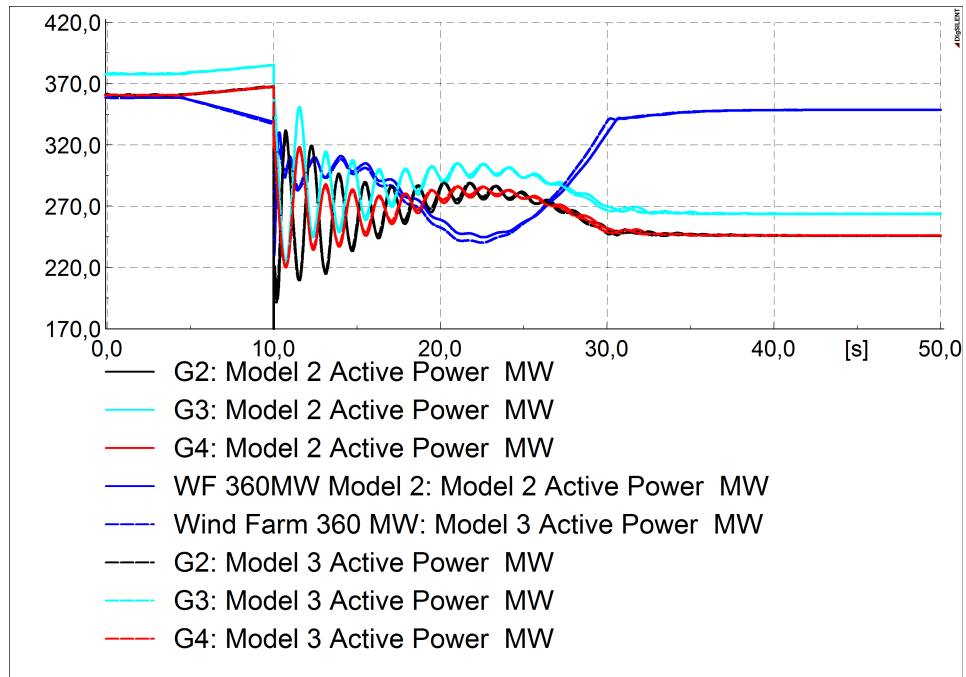


Figure 5.17: Over frequency event - Comparison of reduced order model and full order model generator active power

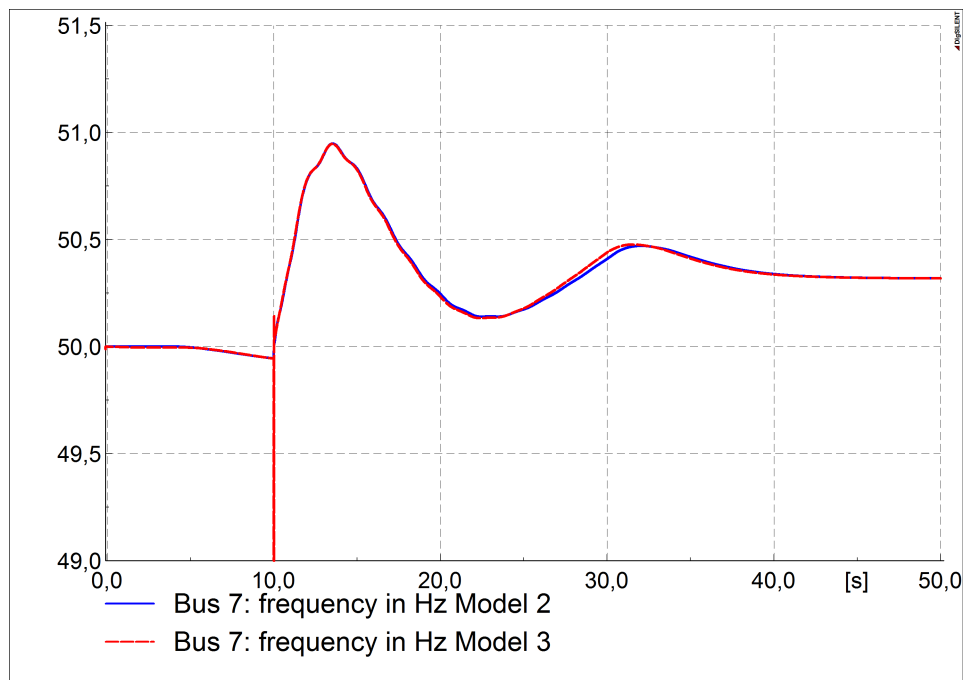


Figure 5.18: Over frequency event - Comparison of reduced order model and full order model system frequency response

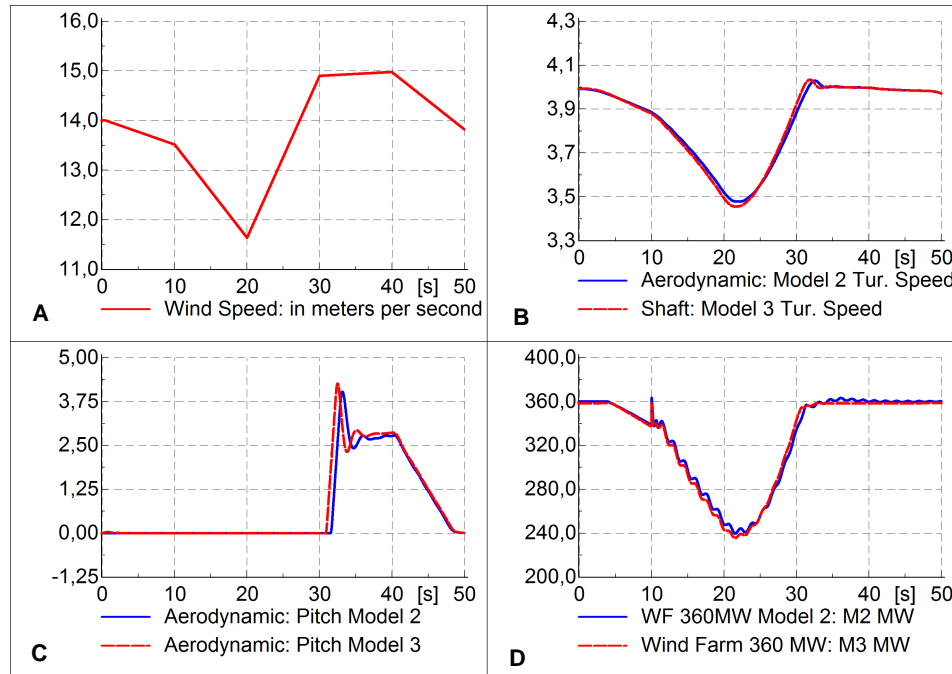


Figure 5.19: Under frequency event - Comparison of Mechanical response between reduced model and full, subplot A - wind speed (ms^{-1}) variation, subplot B - wind turbine speed ($rads^{-1}$) variation, subplot C - pitch angle (β - degrees) variation, subplot D - wind farm electrical output (MW) variation

5.4.3 Under frequency event

The previous section compares the response of the full model and primary model when primary support is applied and the system subjected to an over frequency event. This section compares the system response for an under frequency event. The under frequency event is simulated by increasing the load 7 active power by a step of 100 MW at $t=10$. Parameter values used for the primary support control loop are $K_d=10$ and $R=5$. Note that primary support strategy for under frequency event does not include governor support and R is in effect 0. The response for the two different models are examined and compared against each other.

The turbine speed response, pitch controller response and power response compare and match with each other for both models as observed in figure 5.19. The system generator power response compare and match against each other as observed in figure 5.20. The system frequency response compare and match against each other as observed in figure 5.21. The response of both models are identical. Therefore the reduced order model is sufficient to model the system dynamics.

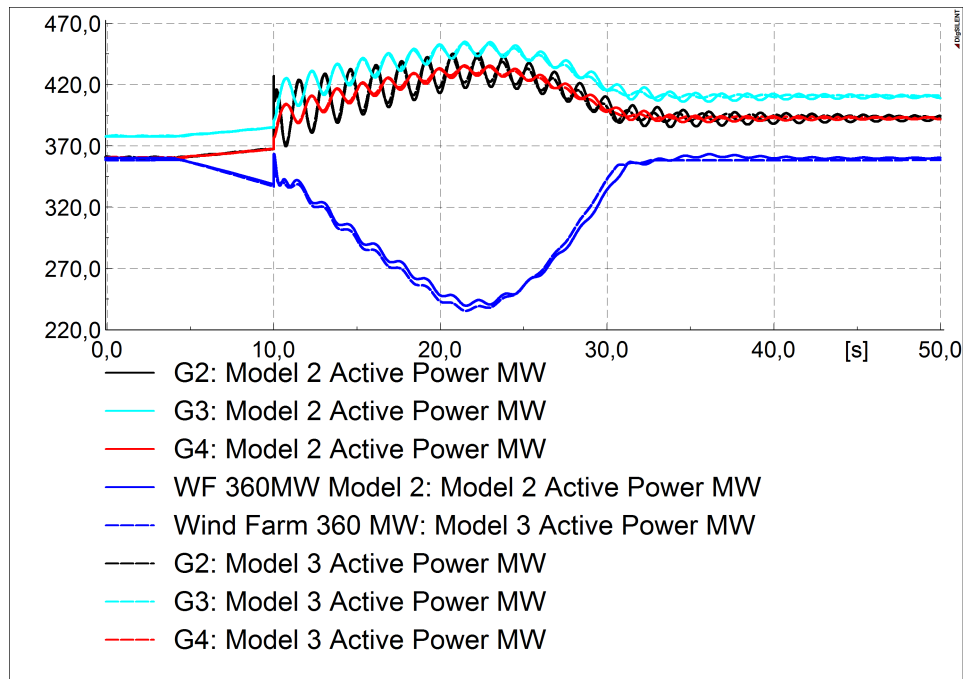


Figure 5.20: Under frequency event - Comparison of reduced model and full model generator active power

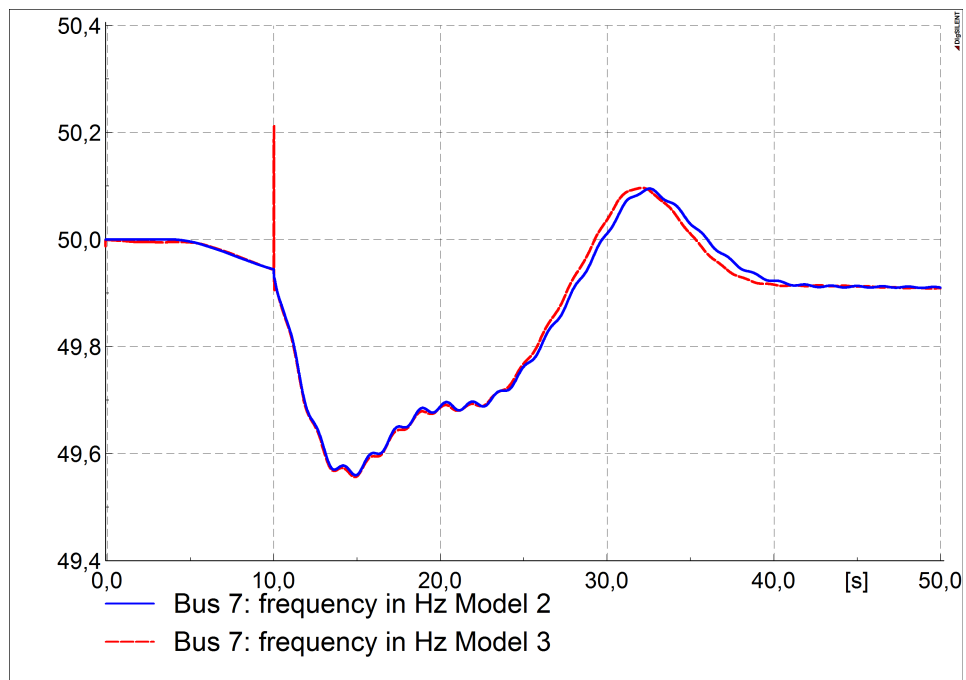


Figure 5.21: Under frequency event - Comparison of reduced model and full model system frequency response

Table 5.3: Comparison of poorly damped eigen values : changing k_d from 1 to 15

Name	Real Part (1/s)	Im. Part (rad/s)	Damped Frequency (Hz)	Damping Ratio
Red. Model : λ_{20}	-0.1029	3.973	0.632	0.0259
Full Model : λ_{34}	-0.1078	4.228	0.672	0.0254

5.5 Small signal stability with frequency control

The response to a small disturbance, for the models without frequency control was examined and simulated in the section 5.3.4. In this section, the effect of emulating inertia, on small signal stability is investigated. In the first subsection the effect of K_d on the poorly damped inter area mode is investigated. In the next subsections small signal response with reduced model and full model for different values of K_d is investigated.

5.5.1 Effect of synthetic inertia constant on the poorly damped mode

In order to investigate the influence of emulated inertia, K_d is changed from 1 to 15, modal analysis is conducted and the resulting poorly damped eigen values are extracted. The calculated eigen values given in table 5.3, remain unchanged. This shows that, either the reduced model nor the full model, has any influence on the dominant inter-area mode.

5.5.2 Comparison of small signal response for reduced model

The power oscillations observed due to a small load disturbance is given in figure 5.22. The response for $K_d = 1$ is slightly different from the response for $K_d = 15$, even if the poorly damped mode is still unchanged. This points to the fact that the other eigen values are being influenced by the change in K_d , which in turn influences the overall time domain response.

5.5.3 Comparison of small signal response for full model

The power oscillations observed due to a small load disturbance is given in figure 5.23. The response for $K_d = 1$ is identical to the response for $K_d = 15$. This points to the fact that K_d is not influencing the overall time domain response. Since, in this model, active power reference for frequency control loop is applied to the generator side converter, with the generator side being

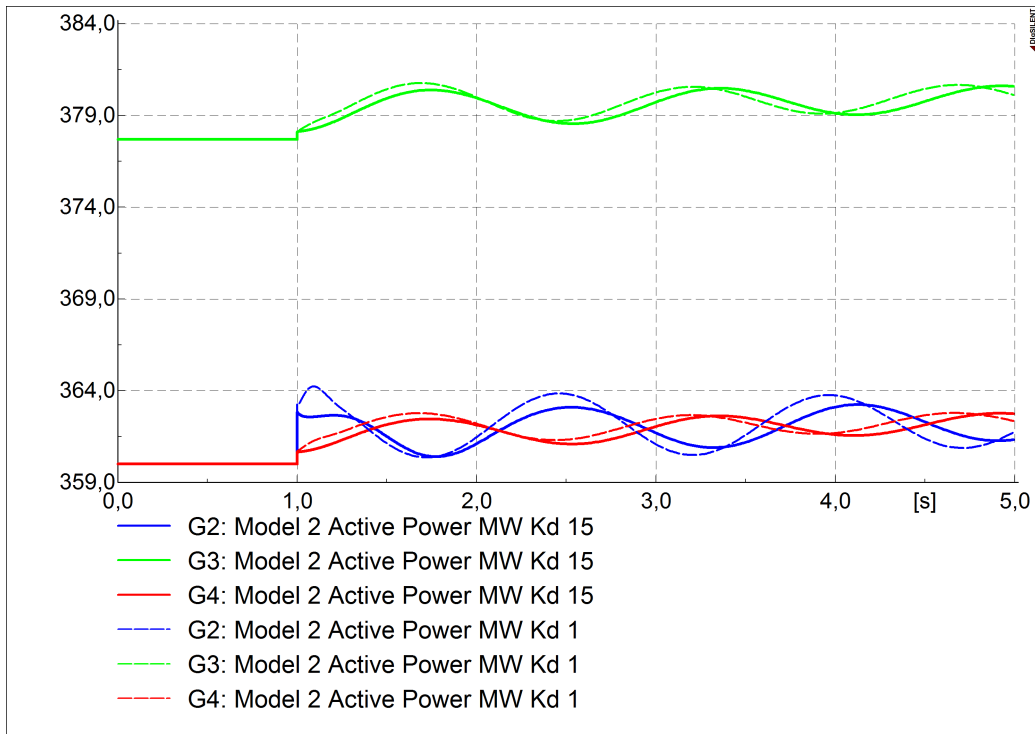


Figure 5.22: Comparison of reduced model small signal response with $K_d = 15$ and $K_d = 1$

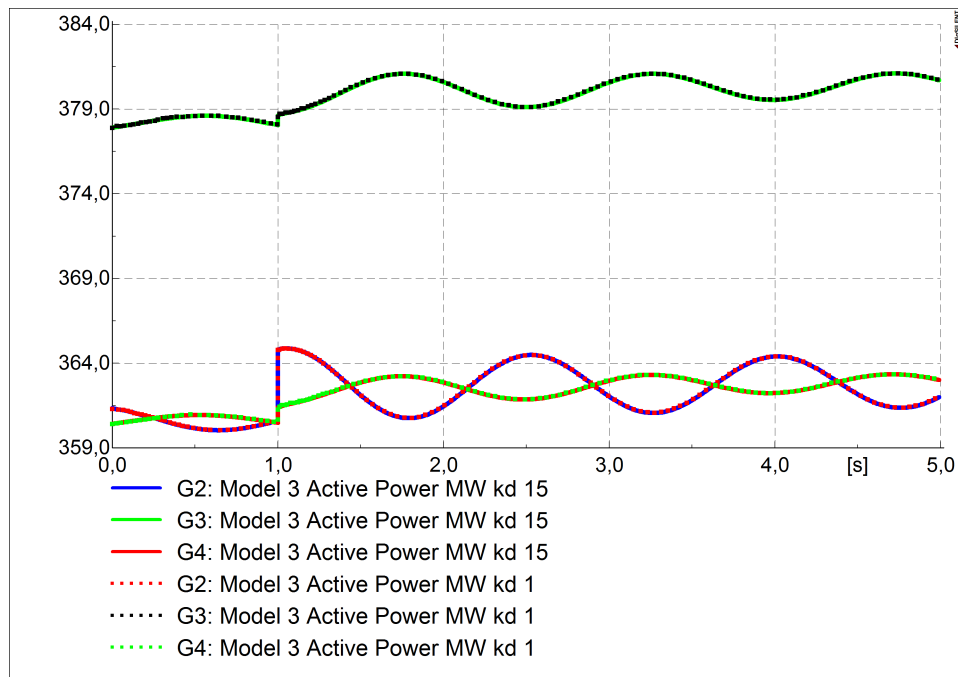


Figure 5.23: Comparison of full model small signal response with $K_d = 15$ and $K_d = 1$

full decoupled from the grid via the DC link, this result is justified.

5.5.4 Modelling of small signal response

The above results indicate that the small signal response is slightly influenced by the type of model used. The response from the reduced model is changing for different values of K_d whereas ideally it should stay constant. Therefore when modelling the small signal stability response of a system, which includes a PMSG based FRC wind farm with with frequency control, better accuracy can be gained by using a full order model.

5.6 Discussion

The two wind farm models achieve the control objectives and follow the expected operational characteristics. Both models demonstrate identical response with respect to each and every parameter when applied with the same wind sequence. This suggests that the reduced order model represents the system response as well as the full order model. However, the PMSG characteristics, the DC link characteristics and the generator side converter characteristics are lost. Therefore if the WTG internal characteristics are needed to be analysed within the system dynamic studies, then a full model will needed. This is specially important if the objective of the analysis is to find the effect of the system disturbance on the wind farm. A real wind farm, will need to protect its generator side power converter, DC capacitor, as well as the Generator. These protection measures will limit the possible operation region of the wind farm.

The results show the salient features of applying frequency control. In the case study, ROCOF is decreased from 0.5 Hz/s to 0.2 Hz/s. The importance of ROCOF is because it is an input to the load shedding scheme [80], to shed loads more intelligently and is widely used in modern power systems. Thus if the ROCOF is high, then the system loads will be shed causing brownouts. By implementing frequency control in wind farms this can be avoided. In a system similar to [80], 0.2 Hz/s will not operate to shed any loads, but 0.5 Hz/s will lead to load shedding. The primary support functionality, will however lead to a loss of production in the wind farm in both over frequency and under frequency events. This loss of energy is significant in an over frequency event, as close to 50% of the available energy is lost. However after the frequency is

stabilised, if the hydro governor set points are increased at a gradual gradient then this problem can be solved. This indicates that automatic generation controller will have a major role to play when wind farms have integrated frequency control. System stability is increased with inertial response since it acts as a damper to the oscillations. The response of both both models overlap for over frequency and under frequency events. Therefore the reduced model order model is sufficient to model the transient response of the wind farm.

Without frequency control, the small signal response of the two models do not have any significant difference. However when frequency control is integrated, wind farm small signal response presents slightly different characteristics. The full order model small signal response is unaffected by variations in K_d , whereas the reduced order model is affected. This can be explained by the decoupling effect due to the DC link in the full model. Further the frequency control auxiliary loop is augmented at the generator side de-alienating the frequency control auxiliary control loop from the grid. Though the deviation is small, this leads to the conclusion that the accuracy of the small signal study will be improve when a full order model is used. The results of this study closely matches with similar research conducted in [14][44][42][41] and [45].

Chapter 6

Conclusions

This chapter summarises the work done, presents the main contributions and describes the possibilities for future work.

6.1 Summary and Conclusions

This dissertation presents an analytical study on modelling wind farm with frequency response for power system dynamic studies. Recent trends indicate that wind energy penetration in the power system will keep on increasing. This study models a permanent magnet synchronous generator, fully rated converter based wind farm, since this is one of the state of art technologies that services this growing demand. Due to the variability in the wind resource, a high demand will be placed on the frequency stability of the power system. This necessitates the requirement of providing both inertial and governor support by the wind farm to the power system. High wind penetration will have a significant impact on the power system stability. These impacts needs to be investigated by conducting power system dynamic studies.

6.1.1 System Modelling

The main challenge is in identifying an appropriate level of complexity of the models to represent power system electro-mechanical dynamics, while keeping the models as simple as possible, to reduce the computational requirements. Taking this into consideration, the main contribution of the modelling work, is identifying a full order model and a reduced order model of a

wind farm with frequency response.

The dissertation, presents the dynamic models of the main components of a wind turbine and shows how the component models are combined to generate a full order and reduced order model. Comprehensive theoretical study is conducted for modelling permanent magnet synchronous generator based, back to back voltage source converter interfaced, wind turbine generators with frequency support. All main subsystems of a PMSG wind turbine system are presented. The mechanical subsystems include wind turbine, drive train and pitch system. The electrical subsystem include generator, power converter and DC link. The network model includes synchronous generators with turbine governor and AVR, transformers, transmission lines and capacitor banks.

6.1.2 Controller Design

The wind farm is interfaced to the utility grid by a back to back voltage source converter system. Therefore, selection of robust control structures and identification of control parameters constitutes an important study element. Both generator converter controller and grid converter controller is given special attention. From the possible multitude of control structures, appropriate control structures are chosen and applied in the two models. A theoretical approach is used to determine the controller parameters. Further a common auxiliary control loop for implementing frequency response is identified and integrated to the models. Identification of these control structures and methods for determination of controller parameters is another contribution of this work.

6.1.3 Simulation Results

The power system under study is the Kundur's two area network. One synchronous generator is substituted by the wind farm and contributes to 25% of the system capacity. The dynamic system study investigates aspects of both frequency and small signal response. The main focus of this work is on frequency and small signal response.

The full order and reduced order model dynamic response for a variable wind speed sequence shows a high degree of correspondence both with and without frequency control. There-

fore the results of this work indicate that a reduced order model is sufficient to model power system electro-mechanical dynamics without significant loss in accuracy.

The full order and reduced order model small signal response, for constant wind speed and without frequency control shows a high degree of correspondence. However the full order and reduced order model response shows deviation when wind farm is supported with frequency control. Therefore the full order model provides a more accurate small signal response for wind farms with frequency control. The studied network reveals a poorly damped inter area mode. Substitution of a synchronous generator by the wind farm, increases the damping of this mode, decreasing inter area oscillations and enhancing system small signal stability.

The simulations of an over frequency event in a system with a wind farm supporting frequency control, clearly shows superior frequency response, in comparison to a wind farm without frequency control. The salient performance is reflected in rate of change of frequency, temporary maximum frequency, steady state frequency and settling time of the frequency response.

6.2 Recommendations for Further Work

This work is focused on presenting simple models of wind turbines with integrated frequency response. All subsystem models and controllers were implemented to the extent of getting a realistic response. This opens up many possibilities of extending this study for future work.

6.2.1 Modelling

In order to accurately model the rotor angle response of the PMSG, it is important to model the drive train as a two mass model instead of the single mass model, that has been used in this study. Similarly the simple model used for pitch system can be improved to a more realistic model. Power system modelling can be extended to include full models for transmission lines, transformers and capacitor banks. The applied wind speed sequence has a resolution of 10 s. The extension of the wind model to include a wind speed sequence with higher resolution, and comparison of the resulting dynamics is another interesting extension of this work.

The wind turbine model is only valid for normal operation. It would be interesting to extend the model to analyse wind turbine low voltage ride through response. The controllers were imple-

mented to the extent of getting realistic response. This work can be extended by replacing the simple control structures by more advanced control structures.

Another possible aspect that can be investigated is to compare the simulated response with the response of a real wind turbine. This would provide a thorough and comprehensive validation of the models and methods used.

6.2.2 Controllers

All the controllers used in this study are PI controllers. Another possibility of further work is to analyse and compare output response for different types of controllers such as P controller and fuzzy controllers. The performance analysis of the wind farm when applied with alternative generator control schemes such as maximum torque control or zero d-axis control is another idea that is worth pursuing.

6.2.3 Frequency Response

In this study a simple and basic frequency response scheme is applied to the wind farm. It would be interesting to analyse the response of this hydro dominated system, when the applied frequency response scheme is made more sophisticated to include different delays, dead bands and memory. Integration of frequency control in a wind farm does not affect the inter-area mode. Therefore another interesting extension of work is to propose a method to extend the frequency response to include a power system stabiliser, which damps the inter area mode. Dynamic system studies for difference wind speed scenarios and different wind penetration ratios are another possible extension to this work. The work can be extended to include voltage stability studies. Implementing control strategy to support low voltage ride through is another possibility for further work.

Acronyms

AGC Automatic Generation Control

ENTSO-E European Network of Transmission System Operators for Electricity

FRC Fully Rated Converter

i_d Direct axis current

i_q Quadrature axis current

K_d Wind Farm synthetic inertia constant

MPT Maximum Point Tracking

PLL Phase Locked Loop

PMSG Permanent Magnet Synchronous Generator

PU Per Unit

PWM Pulse Width Modulation

R Wind farm droop constant

rms root mean square

ROCOF Rate Of Change Of Frequency

RRF Rotor Reference Frame

SRF Stator Reference Frame

VSC Voltage Source Converter

VSWT Variable Speed Wind Turbine

WTG Wind Turbine Generator

WF Wind Farm

WPR Wind Penetration Ratio

Bibliography

- [1] P. UNION, “Directive 2009/28/ec of the european parliament and of the council of 23âapril 2009 on the promotion of the use of energy from renewable sources and amending and subsequently repealing directives 2001/77/ec andâ2003/30/ec,” 2009.
- [2] P. Meibom, K. Hilger, H. Madsen, and D. Vinther, “Energy comes together in Denmark: The key to a future fossil-free danish power system,” vol. 11, no. 5, pp. 46–55, 2013.
- [3] Z. Chen and F. Blaabjerg, “Wind energy: the world’s fastest growing energy source,” *IEEE Power Electronics Society Newsletter*, vol. 18, no. 3, pp. 15–19, 2006.
- [4] A. Orths, A. Hiorns, R. van Houtert, L. Fisher, and C. Fourment, “The European north seas countries’ offshore grid initiative — the way forward,” in *Power and Energy Society General Meeting, 2012 IEEE*, pp. 1–8, 2012.
- [5] S. Wang, J. Hu, and X. Yuan, “Virtual synchronous control for grid-connected dfig-based wind turbines,”
- [6] C. P. Steinmetz, “Power control and stability of electric generating stations,” *Transactions of the American Institute of Electrical Engineers*, no. 2, pp. 1215–1287, 1920.
- [7] K. Uhlen, “Modeling and robust control of autonomous hybrid power systems,” *Doktor ingeniøravhandling, Norges tekniske høgskole, Institutt for teknisk kybernetikk, Trondheim*, 1994.
- [8] Siemens, “Siemens d6 platform 6.0-mw direct drive wind turbine answers for energy the new standard for offshore,” 2014.

- [9] N. Miller, K. Clark, and R. Walling, "Windinertia: controlled inertial response from ge wind turbine generators," in *45th annual Minnesota power systems conference, Minneapolis, Minnesota*, 2009.
- [10] M. Altin, Ö. Göksu, R. Teodorescu, P. Rodriguez, B.-B. Jensen, and L. Helle, "Overview of recent grid codes for wind power integration," in *Optimization of Electrical and Electronic Equipment (OPTIM), 2010 12th International Conference on*, pp. 1152–1160, IEEE, 2010.
- [11] P. Kundur, N. J. Balu, and M. G. Lauby, *Power system stability and control*, vol. 7. McGraw-hill New York, 1994.
- [12] M. Klein, G. Rogers, P. Kundur, *et al.*, "A fundamental study of inter-area oscillations in power systems," *IEEE Transactions on Power Systems*, vol. 6, no. 3, pp. 914–921, 1991.
- [13] Z. Chen and E. Spooner, "A modular, permanent-magnet generator for variable speed wind turbines," 1995.
- [14] J. Eek, *Power System Integration and Control of Variable Speed Wind Turbines*. PhD thesis, Department of Electrical Power Engineering, Norwegian University of Science and Technology, 2009.
- [15] S. Achilles and M. Pöller, "Direct drive synchronous machine models for stability assessment of wind farms," in *4th International Workshop on Large-scale Integration of Wind Power and Transmission Networks for Offshore Wind Farms*, pp. 1–9, 2003.
- [16] A. D. Hansen and G. Michalke, "Modelling and control of variable-speed multi-pole permanent magnet synchronous generator wind turbine," *Wind Energy*, vol. 11, no. 5, pp. 537–554, 2008.
- [17] V. Akhmatov, "Modelling and ride-through capability of variable speed wind turbines with permanent magnet generators," *Wind Energy*, vol. 9, no. 4, pp. 313–326, 2006.
- [18] A. D. Hansen, C. Jauch, P. E. Sørensen, F. Iov, and F. Blaabjerg, *Dynamic wind turbine models in power system simulation tool DIgSILENT*. 2004.

- [19] M. Yin, G. Li, M. Zhou, and C. Zhao, "Modeling of the wind turbine with a permanent magnet synchronous generator for integration," in *Power Engineering Society General Meeting, 2007. IEEE*, pp. 1–6, IEEE, 2007.
- [20] G. Ramtharan, A. Arulampalam, J. B. Ekanayake, F. Hughes, and N. Jenkins, "Fault ride through of fully rated converter wind turbines with ac and dc transmission systems," *IET Renewable Power Generation*, vol. 3, no. 4, pp. 426–438, 2009.
- [21] A. Rolan, A. Luna, G. Vazquez, D. Aguilar, and G. Azevedo, "Modeling of a variable speed wind turbine with a permanent magnet synchronous generator," in *Industrial Electronics, 2009. ISIE 2009. IEEE International Symposium on*, pp. 734–739, IEEE, 2009.
- [22] M. Pöller and S. Achilles, "Aggregated wind park models for analyzing power system dynamics," 2003.
- [23] K. Elkington, J. G. H. Slootweg, M. Ghandhari, and W. L. Kling, *Reduced-Order Modelling of Wind Turbines*, pp. 821–847. John Wiley & Sons, Ltd, 2012.
- [24] J. Slootweg, H. Polinder, and W. Kling, "Representing wind turbine electrical generating systems in fundamental frequency simulations," *Energy conversion, iee transactions on*, vol. 18, no. 4, pp. 516–524, 2003.
- [25] M. Elizondo, S. Lu, N. Zhou, N. Samaan, *et al.*, "Model reduction, validation, and calibration of wind power plants for dynamic studies," in *Power and Energy Society General Meeting, 2011 IEEE*, pp. 1–8, IEEE, 2011.
- [26] G. Michalke, A. D. Hansen, and T. Hartkopf, "Control strategy of a variable speed wind turbine with multipole permanent magnet synchronous generator," in *2007 European Wind Energy Conference and Exhibition, 2007*.
- [27] J. Machowski, J. Bialek, and J. Bumby, *Power system dynamics: stability and control*. John Wiley & Sons, 2011.
- [28] V. Akhmatov, *Analysis of dynamic behaviour of electric power systems with large amount of wind power*. PhD thesis, Electric Power Engineering, ørsted-DTU, Technical University of Denmark, 2003.

- [29] O. Anaya-Lara, D. Campos-Gaona, E. Moreno-Goytia, and G. Adam, *Offshore Wind Energy Generation: Control, Protection, and Integration to Electrical Systems*. John Wiley & Sons, 2014.
- [30] O. Anaya-Lara, N. Jenkins, J. Ekanayake, P. Cartwright, and M. Hughes, *Wind energy generation: modelling and control*. John Wiley & Sons, 2011.
- [31] S. Li, T. Haskew, R. P. Swatloski, W. Gathings, *et al.*, “Optimal and direct-current vector control of direct-driven pmsg wind turbines,” *Power Electronics, IEEE Transactions on*, vol. 27, no. 5, pp. 2325–2337, 2012.
- [32] M. Chinchilla, S. Arnaltes, and J. C. Burgos, “Control of permanent-magnet generators applied to variable-speed wind-energy systems connected to the grid,” *Energy Conversion, IEEE Transactions on*, vol. 21, no. 1, pp. 130–135, 2006.
- [33] B. Wu, Y. Lang, N. Zargari, and S. Kouro, *Power conversion and control of wind energy systems*. John Wiley & Sons, 2011.
- [34] S. Muyeen, R. Takahashi, T. Murata, and J. Tamura, “Transient stability enhancement of variable speed wind turbine driven pmsg with rectifier-boost converter-inverter,” in *Electrical Machines, 2008. ICEM 2008. 18th International Conference on*, pp. 1–6, IEEE, 2008.
- [35] L. Barote and C. Marinescu, “Pmsg wind turbine system for residential applications,” in *Power Electronics Electrical Drives Automation and Motion (SPEEDAM), 2010 International Symposium on*, pp. 772–777, IEEE, 2010.
- [36] Z. Qiu, K. Zhou, and Y. Li, “Modeling and control of diode rectifier fed pmsg based wind turbine,” in *Electric Utility Deregulation and Restructuring and Power Technologies (DRPT), 2011 4th International Conference on*, pp. 1384–1388, IEEE, 2011.
- [37] D. A. Collier and M. L. Heldwein, “Modeling and design of a micro wind energy system with a variable-speed wind turbine connected to a permanent magnet synchronous generator and a pwm rectifier,” in *Power Electronics Conference (COBEP), 2011 Brazilian*, pp. 292–299, IEEE, 2011.

- [38] F. M. Gonzalez-Longatt, P. Wall, and V. Terzija, "A simplified model for dynamic behavior of permanent magnet synchronous generator for direct drive wind turbines," in *PowerTech, 2011 IEEE Trondheim*, pp. 1–7, IEEE, 2011.
- [39] F. Gonzalez-Longatt, "Dynamical model of variable speed wecs: Attend of simplification," in *Proceeding of Fifth International Workshop on Large Scale Integration of Wind Power and Transmission Networks for Offshore Wind Farms, Glasgow, Scotland, 2006*.
- [40] M. Persson, "Frequency response by wind farms in islanded power systems with high wind power penetration," 2015.
- [41] J. Morren, S. W. De Haan, W. L. Kling, J. Ferreira, *et al.*, "Wind turbines emulating inertia and supporting primary frequency control," *IEEE Transactions on Power Systems*, 21 (1), 2006.
- [42] F. Gonzalez-Longatt, E. Chikuni, and E. Rashayi, "Effects of the synthetic inertia from wind power on the total system inertia after a frequency disturbance," in *Industrial Technology (ICIT), 2013 IEEE International Conference on*, pp. 826–832, IEEE, 2013.
- [43] W. Hu, C. Su, J. Fang, Z. Chen, and Y. Hu, "Ancillary frequency control of direct drive full-scale converter based wind power plants," in *PowerTech (POWERTECH), 2013 IEEE Grenoble*, pp. 1–6, IEEE, 2013.
- [44] A. Wickramasinghe, L. Meegahapola, A. P. Agalgaonkar, and S. Perera, "Design considerations for inertia emulating controllers used in variable speed wind turbines," in *PES General Meeting| Conference & Exposition, 2014 IEEE*, pp. 1–5, IEEE, 2014.
- [45] M. Altin, R. Teodorescu, B. Jensen, U. Annakkage, F. Iov, and P. Kjaer, "Methodology for assessment of inertial response from wind power plants," in *Power and Energy Society General Meeting, 2012 IEEE*, pp. 1–8, IEEE, 2012.
- [46] M. Tsili and S. Papathanassiou, "A review of grid code technical requirements for wind farms," *IET Renewable Power Generation*, vol. 3, no. 3, pp. 308–332, 2009.

- [47] M. Jamil, R. Gupta, and M. Singh, "A review of power converter topology used with pmsg based wind power generation," in *Power India Conference, 2012 IEEE Fifth*, pp. 1–6, IEEE, 2012.
- [48] K. Li, S. LiBao, N. YiXin, Y. Liangzhong, and M. Bazargan, "Small signal stability analysis with penetration of grid-connected wind farm of pmsg type," in *Advanced Power System Automation and Protection (APAP), 2011 International Conference on*, vol. 1, pp. 147–151, IEEE, 2011.
- [49] P. Kundur, J. Paserba, V. Ajjarapu, G. Andersson, A. Bose, C. Canizares, N. Hatziargyriou, D. Hill, A. Stankovic, C. Taylor, *et al.*, "Definition and classification of power system stability ieeecigre joint task force on stability terms and definitions," *Power Systems, IEEE Transactions on*, vol. 19, no. 3, pp. 1387–1401, 2004.
- [50] V. I. i. Vorotnikov, *Partial stability and control*. Springer Science & Business Media, 2012.
- [51] O. F. Kjetil Uhlen, "Power system operation and frequency control," in *TET 4180 Lecture Notes*, Department of Electrical Engineering, Norwegian University of Science and Technology, 2014.
- [52] E.-E. E.-E. AISBL, "Entso-e draft network code for requirements for grid connection applicable to all generators," 2012.
- [53] R. Nelson, "Active power control in siemens wind turbines," *Presentation, Siemens Energy*, 2011.
- [54] B. Fox, *Wind power integration: connection and system operational aspects*, vol. 50. Iet, 2007.
- [55] E. Camm, M. Behnke, O. Bolado, M. Bollen, M. Bradt, C. Brooks, W. Dilling, M. Edds, W. Hejdak, D. Houseman, S. Klein, F. Li, J. Li, P. Maibach, T. Nicolai, J. Patino, S. Pasupulati, N. Samaan, S. Saylor, T. Siebert, T. Smith, M. Starke, and R. Walling, "Characteristics of wind turbine generators for wind power plants," in *Power & Energy Society General Meeting, 2009. PES '09. IEEE*, pp. 1–5, 2009.

- [56] Y. Lang, N. Zargari, and S. Kouro, *Power conversion and control of wind energy systems*, vol. 74. John Wiley & Sons, 2011.
- [57] S. Zhang, K.-J. Tseng, D. M. Vilathgamuwa, T. D. Nguyen, and X.-Y. Wang, "Design of a robust grid interface system for pmsg-based wind turbine generators," *Industrial Electronics, IEEE Transactions on*, vol. 58, no. 1, pp. 316–328, 2011.
- [58] T. Ackermann *et al.*, *Wind power in power systems*, vol. 140. Wiley Online Library, 2005.
- [59] A. D. Hansen, *Generators and power electronics for wind turbines*. John Wiley and Sons, England, 2005.
- [60] A. D. Hansen, M. Altin, and N. A. Cutululis, "Modelling of wind power plant controller, wind speed time series, aggregation and sample results," tech. rep., DTU Wind Energy, 2015.
- [61] J. J. Grainger and W. D. Stevenson, *Power system analysis*. McGraw-Hill, 1994.
- [62] N. Mohan, *Advanced electric drives*. Wiley, 2014.
- [63] R. H. Park, "Two-reaction theory of synchronous machines generalized method of analysis-part i," *American Institute of Electrical Engineers, Transactions of the*, vol. 48, no. 3, pp. 716–727, 1929.
- [64] N. Mohan and T. M. Undeland, *Power electronics: converters, applications, and design*. John Wiley & Sons, 2007.
- [65] J. Feltes, V. Koritarov, L. Guzowski, Y. Kazachkov, B. Lam, C. Grande-Moran, G. Thomann, L. Eng, B. Trouille, P. Donalek, *et al.*, "Review of existing hydroelectric turbine-governor simulation models," tech. rep., Argonne National Laboratory (ANL), 2013.
- [66] P. M. Anderson and A. A. Fouad, *Power system control and stability*. John Wiley & Sons, 2008.
- [67] R. Hunter and G. Elliot, *Wind-diesel systems: a guide to the technology and its implementation*. Cambridge University Press, 1994.

- [68] K. O. Merz, "Conceptual design of a stall-regulated rotor for a deepwater offshore wind turbine," 2011.
- [69] S. Heier, *Grid integration of wind energy conversion systems*. Wiley, 1998.
- [70] A. D. Hansen and G. Michalke, "Modelling and control of variable-speed multi-pole permanent magnet synchronous generator wind turbine," *Wind Energy*, vol. 11, no. 5, pp. 537–554, 2008.
- [71] P. Anderson and A. Bose, "Stability simulation of wind turbine systems," *Power Apparatus and Systems, IEEE transactions on*, no. 12, pp. 3791–3795, 1983.
- [72] F. Gonzalez-Longatt and J. L. Rueda, *PowerFactory Applications for Power System Analysis*. Springer, 2015.
- [73] V. Okulov and G. A. van Kuik, "The betz-joukowski limit for the maximum power coefficient of wind turbines," *International scientific journal for alternative energy and ecology*, no. 9, pp. 106–111, 2009.
- [74] V. L. Okulov and G. A. van Kuik, "The betz-joukowski limit: on the contribution to rotor aerodynamics by the british, german and russian scientific schools," *Wind Energy*, vol. 15, no. 2, pp. 335–344, 2012.
- [75] N. Mohan, *Advanced Electric Drives: Analysis, Control, and Modeling Using MATLAB/Simulink*. John Wiley & Sons, 2014.
- [76] E. Spooner and A. Williamson, "Direct coupled, permanent magnet generators for wind turbine applications," *IEE Proceedings-Electric Power Applications*, vol. 143, no. 1, pp. 1–8, 1996.
- [77] C. Bajracharya, "Control of vsc-hvdc for wind power," Master's thesis, Department of Electrical Power Engineering, Norwegian University of Science and Technology, 2008.
- [78] DigSilent, "Manuals digsilent powerfactory 14.0 edition," 2007.

- [79] N. Martins, "Efficient eigenvalue and frequency response methods applied to power system small-signal stability studies," *Power Systems, IEEE Transactions on*, vol. 1, no. 1, pp. 217–224, 1986.
- [80] G. S. Grewal, J. W. Konowalec, and M. Hakim, "Optimization of a load shedding scheme," *Industry Applications Magazine, IEEE*, vol. 4, no. 4, pp. 25–30, 1998.

List of Figures

1.1	Power system under study - Kundur's two area network [11]	3
2.1	Power system stability classification [49]	9
2.2	Typical frequency response for under frequency event [51]; Frequency (Hz) vs time response for an under frequency event	10
2.3	Ideal steady state Frequency - power characteristics of governor with speed droop[11]	13
2.4	Type-4 WTG [55]	16
2.5	DC/DC Boost interfaced PMSG wind turbine	17
2.6	DC/DC Boost interfaced PMSG wind turbine [57]	18
2.7	Back to back VSC interfaced wind turbine	18
2.8	Overview of Wind farm controller	19
3.1	Synchronous generator cross section	21
3.2	Physical scheme for voltage source converter	23
3.3	block diagram for voltage source converter [30]	24
3.4	Equivalent circuit of a transformer	25
3.5	Equivalent circuit of a transmission line	25
3.6	Control Block Diagram for the Hydro Governor	26
3.7	Control Block Diagram for the AVR	27
3.8	Coordinate transformation from local rotor reference frame to system reference frame	28
4.1	Wind farm single line diagram	30
4.2	Functional structure of wind turbine	30

4.3 Full Model : Full order model functional structure of mechanical system	31
4.4 Full Model : Electrical system structure	31
4.5 Reduced order model functional structure	32
4.6 Wind aerodynamic block diagram	34
4.7 C_p as function of λ for different pitch angles	34
4.8 Wind turbine output power variation as a function of turbine rotational speed . . .	35
4.9 MPT scheme block diagram	36
4.10 Pitch angle Controller block diagram	36
4.11 Output power control by blade pitch control	37
4.12 Mechanical drive train block diagram	38
4.13 Rectifier controller reference frame	38
4.14 Inverter controller reference frame	39
4.15 Rectifier controller configuration diagram	40
4.16 Rectifier controller active power control loop	41
4.17 Rectifier Controller reactive power control loop	41
4.18 Block diagram for rectifier inner current control loop	43
4.19 Transfer function for inner current control loop	44
4.20 Generator current controller open loop bode plot	45
4.21 Generator current controller step response plot	45
4.22 Rectifier controller outer active power loop	46
4.23 Generator current controller open loop bode plot	47
4.24 Generator current controller step response plot	47
4.25 Stator voltage control loop block diagram	48
4.26 Generator stator voltage controller open loop bode plot	49
4.27 Generator stator voltage controller step response plot	49
4.28 Inverter controller configuration diagram	50
4.29 Inverter DC voltage control loop	50
4.30 Inverter reactive power control loop	51
4.31 Control block diagram for inner current control loop	51
4.32 SLD for grid side converter interface	51

4.33 Transfer function for inner current control loop	52
4.34 Inverter current controller open loop bode plot	54
4.35 Inverter current controller step response plot	54
4.36 DC voltage control loop block diagram	55
4.37 DC voltage outer control open loop bode plot	56
4.38 DC voltage outer control loop step response plot	57
4.39 Reactive power control block diagram	58
4.40 Grid reactive power open loop bode plot	59
4.41 Grid reactive power step response	59
4.42 Reduced Model Electrical control structure	60
4.43 Reduced order model active power control loop	60
4.44 Reduced order model active power loop block diagram	61
4.45 Auxiliary control loop for frequency control	61
5.1 Single line diagram of power system under study - Kundur's two area network [12]	63
5.2 Validation of the full model mechanical system response, subplot A - wind speed(ms^{-1}) variation, subplot B - wind turbine speed ($rads^{-1}$) variation, subplot C - pitch an- gle (β - degrees) variation, subplot D - wind farm electrical output (MW) variation	66
5.3 Validation of the reduced model electrical system response, subplot A - reference power set point (MW) generated by the maximum power point tracking scheme, subplot B - system frequency measured at bus 7 in Hz, subplot C - wind farm elec- trical output (MW), subplot D - all generator active power output (MW) variation .	66
5.4 Validation of the reduced model mechanical system response, subplot A - wind speed(ms^{-1}) variation, subplot B - wind turbine speed ($rads^{-1}$) variation, subplot C - pitch angle (β - degrees) variation, subplot D - wind farm electrical output (MW) variation	67
5.5 Validation of the reduced model electrical system response, subplot A - reference power set point (pu) generated by the maximum power point tracking scheme, subplot B - system frequency measured at bus 7 in Hz, subplot C - wind farm elec- trical output (MW), subplot D - all generator active power output (MW) variation .	68

5.6	Reduced Model and full model output power comparison	69
5.7	Comparison of Mechanical response between full model and the reduced model, subplot A - wind speed(ms^{-1}) variation, subplot B - wind turbine speed ($rads^{-1}$) variation, subplot C - pitch angle (β - degrees) variation, subplot D - wind farm electrical output (MW) variation	69
5.8	Reduced Model and full model generator active power (MW) comparison	70
5.9	Reduced Model and full model system frequency (Hz) response comparison	70
5.10	Comparison of Small Signal Response	72
5.11	Wind farm mechanical system response for over frequency event : Case Study; subplot A - wind speed(ms^{-1}) variation, subplot B - wind turbine speed ($rads^{-1}$) variation, subplot C - pitch angle (β - degrees) variation, subplot D - wind farm electrical output (MW) variation	73
5.12	Primary response emulation control loop for over frequency event : Case Study	74
5.13	System frequency comparison	74
5.14	Comparison of Mechanical response between reduced model with primary support and without primary support, subplot A - wind speed(ms^{-1}) variation, subplot B - wind turbine speed ($rads^{-1}$) variation, subplot C - pitch angle (β - degrees) variation, subplot D - wind farm electrical output (MW) variation	75
5.15	Comparison of generator active power response with and without frequency control	76
5.16	Over frequency event - Comparison of Mechanical response between reduced order model and full order model, subplot A - wind speed(ms^{-1}) variation, subplot B - wind turbine speed ($rads^{-1}$) variation, subplot C - pitch angle (β - degrees) variation, subplot D - wind farm electrical output (MW) variation	77
5.17	Over frequency event - Comparison of reduced order model and full order model generator active power	78
5.18	Over frequency event - Comparison of reduced order model and full order model system frequency response	78

5.19 Under frequency event - Comparison of Mechanical response between reduced model and full, subplot A - wind speed(ms^{-1}) variation, subplot B - wind turbine speed ($rads^{-1}$) variation, subplot C - pitch angle (β - degrees) variation, subplot D - wind farm electrical output (MW) variation	79
5.20 Under frequency event - Comparison of reduced model and full model generator active power	80
5.21 Under frequency event - Comparison of reduced model and full model system frequency response	80
5.22 Comparison of reduced model small signal response with $K_d = 15$ and $K_d = 1$. . .	82
5.23 Comparison of full model small signal response with $K_d = 15$ and $K_d = 1$	82

List of Tables

4.1	Generator Parameters for controller tuning	44
4.2	Rectifier inner current controller parameters	45
4.3	Rectifier active power loop controller parameters	46
4.4	Calculated parameters of the outer loop controller	49
4.5	Grid Parameters for controller tuning	53
4.6	Parameters for inverter current controller	53
4.7	DC voltage control loop parameters	56
4.8	Grid reactive power controller parameters	58
5.1	Initial state of the power system	64
5.2	Comparison of poorly damped eigen values (without frequency control)	71
5.3	Comparison of poorly damped eigen values : changing k_d from 1 to 15	81
A.1	Synchronous generator parameters	107
A.2	Main transformer parameters	108
A.3	Wind turbine generator transformer parameters	108
A.4	Transmission line parameters	108
A.5	Capacitor parameters	108
A.6	Hydro governor parameters	109
A.7	Simple Excitation System (SEXS) parameters	109
B.1	Generator parameters	110
B.2	Wind turbine parameters	111
B.3	Pitch Control system parameters	111

B.4 Per unit system 112

Appendix A

Power System Model - Parameters

A.1 Synchronous generators

Table A.1: Synchronous generator parameters

Parameter	Value
T''_{do}	0.03 s
T'_{do}	8.0 s
T''_{qo}	0.05 s
T'_{qo}	0.4 s
X''_q	0.25
X'_q	0.55
X''_d	0.25
X'_d	0.3
X_d	1.8
X_q	1.7
H (for G1 and G2)	6.5 s
H (for G3 and G4)	6.75 s

A.2 Transformer

A.3 Transmission line

Same set of parameters apply to all the transmission lines.

Table A.2: Main transformer parameters

Parameter	Value
Voltage ratio	20/230 kV
Capacity	900 MVA
Type	YNyn0
Impedance	0.15 pu

Table A.3: Wind turbine generator transformer parameters

Parameter	Value
Voltage ratio	0.4/20 kV
Capacity	400 MVA
Type	Dyn5
Impedance	0.06 pu

Table A.4: Transmission line parameters

Parameter	Value
Resistance	0.0529 Ω /km
Reactance	0.529 Ω /km

A.4 Capacitor

Same set of parameters apply to all the transmission lines.

Table A.5: Capacitor parameters

Capacitor	Reactive Power
Bus 7	200 MVar
Bus 9	350 MVar

A.5 Turbine Governor

Same set of parameters apply to all the hydro governors of the synchronous generators.

A.6 Automatic voltage regulator

Same parameters apply to all the AVR of the synchronous generators.

Table A.6: Hydro governor parameters

Parameter	value
r	0.1
T_r	5
T_f	0.1
T_g	0.5
T_w	1
A_t	1
R	0.04
D_{turb}	0.01
q_{nl}	0.01

Table A.7: Simple Excitation System (SEXS) parameters

Parameter	value
T_a	2
T_b	10
T_e	0.5
K	100

Appendix B

WTG parameters

B.1 Generator Model

Table B.1: Generator parameters

Parameter	value
X	1.5
R	0.0001
H	2
Number of pole	26
Rated Power	1.5 MW
Number of wind turbines	240
Wind farm rated power	360 MW
Rated LV Voltage	0.4 kV
Rated frequency	50 Hz
Rated speed	38 rpm(50 Hz)

B.2 Wind turbine Model

Table B.2: Wind turbine parameters

Parameter	value
R	25.375 m
ρ	1.225 kg/m ³
H (including generator)	6.5 s
H (excluding generator)	4.5 s
rated speed	38 rpm
Rated wind speed	14 m/s
T	0.5

B.3 Pitch Model

Table B.3: Pitch Control system parameters

Parameter	value
K_a	100
T_r	5
T_a	1
ω_{ref}	1
T	0.5
$\dot{\beta}$	5

B.4 Per Unit System

Table B.4: Per unit system

Parameter	value
Base voltage U_b	U_{rated}
Base apparent power S_b	P_{rated}
Base current I_b	$S_b/\sqrt{3}U_b$
Base impedance Z_b	U_b^2/S_b
Base inductance L_b	Z_b/ω_b
Base capacitance C_b	$1/R_b\omega_b$
Base mechanical speed ω_b	ω_{rated}